EVALUATION OF MMFX STEEL FOR NCDOT CONCRETE BRIDGES

By

Sami Rizkalla

Paul Zia

Principal Investigators

Hatem Seliem

Gregory Lucier

Graduate Research Assistants

Research Project 2004-27

Final Report

In cooperation with the

North Carolina Department of Transportation

And

Federal Highway Administration

United States Department of Transportation

Department of Civil Engineering

North Carolina State University

Raleigh, NC 27695-7908

December 2005

Technical Report Documentation Page

1. Report No.	2. Government Accession No.	3. Recipient's Catalog No.
FHWA/NC/2006-31		

4. Title and Subtitle	5. Report Date
Evaluation of MMFX Steel for NCDOT Concrete Bridges	**December 2005**
	6. Performing Organization Code
7. Author(s) **Sami Rizkalla, Paul Zia, Hatem Seliem, and Gregory Lucier**	8. Performing Organization Report No.
9. Performing Organization Name and Address **Department of Civil Engineering** **North Carolina State University** **Campus Box 7908** **Raleigh, NC 27695-7908**	10. Work Unit No. (TRAIS) 11. Contract or Grant No.
12. Sponsoring Agency Name and Address **North Carolina Department of Transportation** **Research and Analysis Group** **1 South Wilmington Street** **Raleigh, North Carolina 27601**	13. Type of Report and Period Covered **Final Report,** **7/1/2004 – 12/31/2005** 14. Sponsoring Agency Code **2004-27**

15. Supplementary Notes

16. Abstract

The new commercially available Micro-Composite Multi-Structural Formable (MMFX) steel is a high strength and highly corrosion-resistant steel. Use of MMFX steel could lead to potential savings due to its unique characteristics. Many state transportation departments have begun to use MMFX steel as a direct replacement for conventional Grade 60 steel. However, the higher strength and lack of well-defined yield point of MMFX steel alter the structural behavior of bridge decks reinforced with MMFX steel bars. Therefore, three concrete bridge decks with a span-to-depth ratio of 12.5 were tested up to failure using concentrated loads intended to simulate the effects of truck wheel loadings. The first and second bridge decks were reinforced with the same amount of MMFX and conventional Grade 60 steel, respectively. The third bridge deck was reinforced with MMFX steel reduced by 33 percent in an attempt to utilize its high strength characteristics. The results of the experimental program and the analytical modeling demonstrated that bridge decks reinforced with 33 percent less MMFX steel developed the same ultimate load-carrying capacity and deflection at service load as those reinforced with Grade 60 steel.
In addition, the effect of bending on the tensile strength of MMFX steel bars was experimentally investigated. Experimental results demonstrated that debonded MMFX bent bars have a reduced ultimate strength by 6 percent. However, bonded bent bars developed the full strength as those of straight bars.
The high corrosion-resistance of MMFX steel bars claimed by the manufacturer was validated by using very severe test conditions. The corrosion test results confirmed that that MMFX steel has a lower corrosion rate compared to conventional Grade 60 steel.

17. Key Words	18. Distribution Statement
Bridge Decks, Concrete, Corrosion, High-Strength Steel, MMFX, Bar Bending, Reinforcement, Flexure, Punching, Shear	

19. Security Classif. (of this report)	20. Security Classif. (of this page)	21. No. of Pages	22. Price
Unclassified	Unclassified	128	

Form DOT F 1700.7 (8-72) **Reproduction of completed page authorized**

DISCLAIMER

ACKNOWLEDGMENT

The authors gratefully acknowledge the support of North Carolina Department of Transportation (NCDOT) for sponsoring this research project. MMFX Technologies Corporation supplied the MMFX steel and CC Mangum Inc. of Raleigh helped casting the three bridge decks. SteelFab of Charlotte donated the steel sections for the testing frames. Special thanks are extended to Catrina Walter for taking part in the bent bars experimental study. The authors would like also to thank Jerry Atkinson and Bill Dunleavy, technicians at the Constructed Facilities Laboratory at North Carolina State University, for their invaluable help.

SUMMARY

The new commercially available Micro-Composite Multi-Structural Formable (MMFX) steel is a high strength and highly corrosion-resistant steel. Use of MMFX steel could lead to potential savings due to its unique characteristics. Many state transportation departments have begun to use MMFX steel as a direct replacement for conventional Grade 60 steel. However, the higher strength and lack of well-defined yield point of MMFX steel alter the structural behavior of bridge decks reinforced with MMFX steel bars. Therefore, three concrete bridge decks with a span-to-depth ratio of 12.5 were tested up to failure using concentrated loads to simulate the effect of truck wheel load. The first and second bridge decks were reinforced with the same amount of MMFX and conventional Grade 60 steel, respectively. The third bridge deck was reinforced with MMFX steel reduced by 33 percent in an attempt to utilize its high strength characteristics. The results of the experimental program and the analytical modeling demonstrated that bridge decks reinforced with 33 percent less MMFX steel developed the same ultimate load-carrying capacity and deflection at service load as those reinforced with Grade 60 steel.

In addition, the effect of bending on the tensile strength of MMFX steel bars was experimentally investigated. Experimental results demonstrated that debonded MMFX bent bars have a reduced ultimate strength by 6 percent. However, bonded bent bars developed the full strength as those of straight bars.

The high corrosion-resistance of MMFX steel bars claimed by the manufacturer was validated by using very severe test conditions. The corrosion test results confirmed that that MMFX steel has a lower corrosion rate compared to conventional Grade 60 steel.

Table of Contents

List of Tables

List of Figures

1. INTRODUCTION

Corrosion of steel reinforcement has been identified as one of the leading causes of deterioration of concrete bridges. Bridge decks are bridge components typically subjected to severe environmental conditions, and in some states, the use of de-icing compounds. A Corroded reinforcing steel bar occupies a larger volume than its original volume, causing internal pressure, which leads to cracking and spalling of concrete cover and, ultimately, failure of the structure. Over the last few decades, this phenomenon has led to the development of various technologies that attempt to mitigate this expensive problem. Such technologies include cathodic protection systems, chemical corrosion inhibitors, high-performance concretes, epoxy-coated bars, non-metallic reinforcement, and corrosion-resistant steels. However, there are drawbacks associated with some of these technologies. For instance the use of Fiber Reinforced Polymers (FRP) bars is limited due to the lack of information on the long term performance of those materials under field conditions. Also, the use of Epoxy-coated bars has been restricted by several states and some countries due to their unsatisfactory behavior.

The recent development of high strength, highly corrosion-resistant steel commercially known as Micro-composite Multi-Structural Formable (MMFX) steel is a promising technology. According to the manufacturer, MMFX steel offers corrosion resistance approaching that of stainless steel (but at a much lower cost), superior strength and mechanical properties over other high-strength steels. It offers the advantage of high corrosion resistance without the use of the coating technologies. This characteristic was achieved by proprietary alteration of the steel composition and microstructure. The control of the morphology of MMFX steel microstructure has resulted in higher strength in comparison to conventional steel. Use of MMFX steel could lead to potential savings by reducing reinforcement ratios based on its higher strength characteristics and longer service life of structures because of its high corrosion resistance.

Recently, many state transportation departments have begun to use MMFX steel as a direct replacement for conventional Grade 60 steel in concrete bridge decks. MMFX steel has been used as reinforcement in new bridge deck projects by the Iowa DOT, the Kentucky DOT, and the Pennsylvania DOT. Also, it has been used as shear reinforcement in bridge girders by the Oklahoma DOT. However, the behavior of MMFX steel as main reinforcement for flexural members and more specifically as reinforcement for bridge deck slabs is limited. In addition, the effect of bending on the tensile strength of the MMFX bars is not well defined and, therefore, must be evaluated. The high corrosion-resistant claimed by the manufacturer need to be validated using more severe environmental conditions.

2. RESEARCH OBJECTIVES AND SCOPE

The objectives of this research are two-fold: (1) to examine the performance and evaluate the effectiveness of the MMFX steel bars as main flexural reinforcement for concrete bridge decks, and (2) to develop an approach to take advantage of the higher strength of the product to provide a more economical and safer design for bridge decks in North Carolina. To meet the objectives the following tasks were pursued:

1. Conduct a comprehensive state-of-the-art literature review on the MMFX steel reinforcement. The review will include all published reports and articles on the completed research and use of MMFX steel.

2. Validate the fundamental mechanical properties of the MMFX steel bars.

3. Determine the design requirements for the use of MMFX steel bars as reinforcement for concrete bridge decks and assess their structural performance. Study the behavior of bridge decks reinforced with lower reinforcement ratio based on the inherited high strength of MMFX steel.

4. Study the various flexural limit state behaviors of typical bridge decks reinforced with MMFX steel bars including the behavior prior to cracking, post-cracking, yielding of steel, ultimate strength, and mode of failure.

5. Conduct analytical modeling to develop in-depth and full understanding of the behavior of concrete bridge decks reinforced with MMFX steel bars and compare the behavior to decks reinforced with Grade 60 steel.

6. Compare and correlate the experimental results of the MMFX reinforced concrete bridge decks with prediction of the flexural behavior using the AASHTO LRFD

Specifications. Check the validity of the AASHTO LRFD equations for predictions of the strength and deformations.

7. Examine the effect of bending of MMFX steel bars on their tensile strength.

8. Establish the rate of corrosion of MMFX steel bars in comparison to conventional Grade 60 steel.

9. Develop and provide detailing information, design guidelines and construction specifications for using MMFX steel bars as main flexural reinforcement for concrete bridge decks.

10. Recommend means for technology transfer which will focus primarily on disseminating the information to the NCDOT as well as future field applications.

3. LITERATURE REVIEW

3.1. Overview

This chapter provides general review of the behavior of concrete bridge decks and the punching shear capacity of bridge deck slabs. Review of the current code provisions for predicting shear capacity of concrete slabs will be also included. In addition, corrosion of steel reinforcement and properties of Micro-composite Multi-Structural Formable (MMFX) steel will be summarized. It should be noted that concrete bridge decks, concrete deck slabs, and concrete slabs will be used interchangeably throughout this section, because of the different notation used in the literature.

3.2. Behavior of Bridge Decks

In general, the behavior of concrete bridge decks is governed by three important parameters, amount of steel reinforcement, span-to-depth ratio, and the lateral restrain of the edges of the deck. Consequently their failure modes can be classified into three categories: pure flexural failure, pure punching failure, and ductile shear failure, Marzouk and Hussein (1991). Bridge decks with small span-to-depth ratio (< 18) primarily fail due to punching shear under the truck wheel load with small deflections prior to failure. While for bridge decks with large span-to-depth ratio they mainly behave in flexural, exhibits large deflections before failure, and ultimately fail at a less load. In addition, laterally restraining the edges of the bridge deck significantly enhances its punching shear strength due to the formation of compressive membrane forces, which is referred to as “arch action”. Each of the three parameters will be discussed in detail in the following sections.

3.2.1. Effect of Reinforcement ratio

As would be expected, the load-carrying capacity or the punching shear strength of concrete bridge decks or concrete slabs in general increases with the addition of steel reinforcement. Therefore many researchers, especially between the 1930’s and 1970’s included the reinforcement ratio as a variable in their research programs, Dilger et al. (2005).

Marzouk and Hussein (1991) examined the behavior of two-way slabs through experimental testing. Based on their experimental results a mechanical model was adopted and developed for high-strength concrete slabs. They reported that the ultimate punching shear load increased as the reinforcement ratio was increased. They also concluded that the degree to which yielding spread in the reinforcement varied with the reinforcement ratio. For slabs with high reinforcement ratio, yielding of the reinforcement occurred at a high load and was localized at the loaded area. On the other hand, for lightly reinforced slabs, yielding was initiated at the column stub and gradually progressed throughout the whole tension reinforcement.

Kuang and Morely (1992) experimentally tested 12 concrete slabs with different reinforcement ratio, different span-to-depth ratio, and different degree of edge restraint. With respect to the influence of steel reinforcement they concluded that steel reinforcement has an important effect on the punching shear strength for the lightly reinforced slabs, but little effect for those that are heavily reinforced.

Khanna et al. (2000) tested a full-scale bridge deck supported on girders which was divided into four segments. The first segment was reinforced with isotropic steel reinforcement in two layers. The second segment contained only the bottom layer of steel reinforcement. The third segment contained only the bottom transverse steel bars. The fourth segment contained only bottom transverse Glass Fiber Reinforced Polymer (GFRP) bars. It was concluded that only the bottom transverse reinforcement affects the load-carrying capacity of deck slabs supported on girders.

Moreover, they concluded that the stiffness of the bottom transverse reinforcement affects the load-carrying capacity more than its strength.

Hassan et al. (2000) investigated the effect of reinforcement ratio on bridge decks capacity using an analytical model that was verified using two-way slab model tested at Ghent University, Belgium. The analytical results indicated that the failure load increased as the reinforcement ratio increase. Based on the arch action mechanism introduced by the bottom transverse reinforcement, the study also concluded that the use of top reinforcement does not affect the ultimate capacity of the bridge deck slabs. This finding is in agreement with the conclusion of Khanna et al. (2000) and Kuang and Morely (1992).

Dilger et al. (2005) conducted a statistical evaluation of the experimental results obtained by many researchers to demonstrate the effect of reinforcement ratio on the punching shear strength of concrete slabs. From the test series of Vanderbilt (1972), Marzouk and Hussien (1991), and Hallgren (1996), they concluded that with an increase in the flexural reinforcement ratio the stresses along the punching cone and hence the load-carrying capacity of the concrete slabs is increased. They also reported that an explanation of this behavior was given by Richart (1948) who found that significant yielding of the flexural reinforcement produces large cracks, which reduces the effective area resisting shear. Since the crack width and depth are controlled by the amount of flexural reinforcement, it was concluded that the reinforcement ratio significantly influences the punching shear strength of concrete slabs.

3.2.2. Effect of Lateral Restraint

Due to the lateral restraint of the bridge deck it is capable of forming in-plane compressive forces due to the arching action that develops. Lateral restraint in bridge decks exists in the form of the longitudinal beams, the adjacent slab, and the surrounding slab area, Hon et al (2005).

Taylor and Hayes (1965) tested 22 plain and reinforced concrete simply supported square slabs. The effect of lateral restraint on punching shear strength was obtained by testing pairs of slabs. One of each pair was unrestrained while the other was restrained by means of a surrounding steel frame. Direct comparison of the failure loads of the slabs leaded to the extent of the effect of restraint. Although the plain slabs were un-reinforced the edge restraint prevented collapse of the slabs and the load was carried to the supports by arching action. Restraint of the edges of slabs with low reinforcement ratio (1.57 percent) had little effect on the early behavior, where the crack widths and deflections of unrestrained slabs were similar to the restrained ones. However, the edge restraint affected the subsequent behavior and increased the punching failure load by 16-60 percent. For slabs with high reinforcement ratio (3.14 percent) the punching failure load was increased by 15 percent only.

Kuang and Morely (1992) reported an increase in the punching shear capacity of 46 percent for thin concrete slabs and 64 percent for thick concrete slabs due to edge restraint. This increase in the load-carrying capacity reveals that the edge restraint has a significant effect on the ultimate punching load of reinforced concrete slabs, resulting from enhancement of shear resistance, and effectively increasing the load-carrying capacity.

Hassan et al. (2000) experimentally tested two full-scale models in addition to their analytical model. Their test results revealed that restraining the bridge deck laterally increased the load-carrying capacity by 20 percent. Also, edge stiffening increased the capacity of the slab by an additional 12 percent.

Hon, et al. (2005) presented a design method, taking into account the restraint stiffness and the strength enhancement due to compressive membrane action. The method was developed based on experimental testing of concrete slabs and the use of non-linear finite element modeling. They found that the strength of the slabs in both flexure and punching shear was higher due to edge restraint.

Appreciation of the internal arching system that develops in bridge decks led to the development of fibre-reinforced concrete (FRC) deck slabs without internal tensile reinforcement, or also known as steel-free deck slabs. Mufti et al. (1993) demonstrated through experimental testing that deck slabs void of steel reinforcement can develop the same load-carrying characteristics as conventional deck slabs provided that the supporting girders are connected with adequate and properly spaced transverse steel straps. The steel-free deck slabs utilize the transverse steel straps to laterally restraint the supporting girders, hence the deck slab develops the required arching forces. Also it utilizes the fibres to control the cracks in concrete, which may develop due to volumetric changes at the initial setting of the concrete. This concept has been used for designing cast-in-place deck slabs in five highway bridges in Canada, Mufti et al. (2004). In addition, the concept has been applied to precast steel-free deck slabs supported on girders. Furthermore, design provisions for steel-free decks slabs will be included in the forthcoming version of the Canadian Highway Bridge Design Code (CAN/CSA-S6-00).

3.3. Punching Shear of Concrete slabs

Punching shear (also known as two-way action shear) in most cases is the mode of failure of concrete slabs when they are subjected to concentrated loads such as slab-column connection in flat-slab buildings and bridge decks having a certain range of span-to-depth ratio. Review of the various rational models that have been proposed by researchers to describe and quantify punching shear failure of slabs when subjected to concentrated loads is given in the following section. In addition, current code provisions for predicting the punching shear strength are presented.

3.3.1. Rational Models

Kinnunen and Nylander (1960) conducted an experimental and theoretical study dealing with the punching of slabs without shear reinforcement from which their model was derived. They tested circular concrete slabs uniformly loaded along the circumference and supported by a column stub at the center. Kinnunen and Nylander's model has served as the basis to many models developed thereafter by others. Marzouk and Hussein (1991) reported that the model developed by Kinnunen and Nylander still provides the best account of the punching behavior of concrete slabs. Mufti and Newhook (1998) deployed Kinnunen and Nylander model with modification to the failure strain.

3.3.2. Code Provisions

This section discusses current design code provisions used to predict the punching shear capacity of reinforced concrete slabs. Three different codes are used in this study to estimate the ultimate load-carrying capacity of the bridge decks. The values are compared to the failure loads obtained from experimental testing as shown in subsequent sections.

- *AASHTO LRFD Bridge Design Specifications (2004)*

For two-way action of sections without transverse reinforcement, the nominal shear resistance, V_c using kips and inches, of the concrete is the lesser of:

$$V_c = \left(0.063 + \frac{0.126}{\beta_c}\right)\sqrt{f_c'}\,b_o d$$

$$V_c = 0.126\sqrt{f_c'}\,b_o d$$

- *American Concrete Institute (ACI 318-05)*

For two-way action, the nominal shear resistance of concrete slabs, V_c using pounds and inches, shall be the smallest of:

$$V_c = \left(2 + \frac{4}{\beta_c}\right)\sqrt{f_c'}\,b_o d$$

$$V_c = \left(2 + \frac{\alpha_s d}{b_o}\right)\sqrt{f_c'}\,b_o d$$

$$V_c = 4\sqrt{f_c'}\,b_o d$$

- *Canadian Highway Bridge Design Code (CAN/CSA-S6-00)*

The nominal shear strength, V_c using Newton and millimeters, of concrete slabs in two-action is given by the following equation:

$$V_c = \left(0.6 f_r + 0.25 f_{pc}\right) b_o d + 0.9 V_p$$

where;

V_c = punching shear capacity of bridge deck;

β_c = ratio of long side to short side of loading plate;

f_c' = concrete compressive strength;

b_o = perimeter of critical section at a distance of d/2 from loading plate;

d = effective section depth;

α_s = constant;

f_r = concrete tensile strength;

f_{pc} = compressive stress in concrete due to prestressing; and

V_p = component of effective prestressing force in direction of applied shear.

3.4. Corrosion of MMFX Steel

There are two major causes of corrosion of steel embedded in concrete, namely carbonation of concrete and chloride-induced corrosion. Up to 1950s carbonation of concrete was the main cause of corrosion. Since then chloride-induced corrosion has become much more important for structures exposed to chloride environment (de-icing salt, a marine climate, and salt-contaminated aggregates) Hunkler (2005). The high alkalinity of the concrete pore water (pH over 12.5) leads to a passive layer forming on the steel surface that reduces corrosion attack to negligible values. As long as this layer is sustained corrosion will not occur. However, carbonation of concrete or chloride attack destroys this protective layer leading to corrosion of steel. Chromium in particular is an element that allows passivation and therefore, it is generally understood that the corrosion rate of steel is reduced when the percentage of chromium is increased in the steel.

Corrosion of metals is an electrochemical process in which an anodic metal losses electrons to a cathode in the presence of an electrolyte. In conventional steel, an electrochemical reaction takes place between ferrite (the anode) and iron-carbide (the cathode). As the reaction progresses, micro-galvanic cells are created, leading to the formation of ferrous oxide $Fe(OH)_2$, or rust. MMFX steel is virtually carbide free (less than 1% carbon content) and has high chromium content (8-10% chromium). This lack of carbide inhibits the formation of microgalvanic cells, thus accounting for the superior corrosion resistance of MMFX steel, MMFX (2002).

A comprehensive study was conducted by Trejo (2002) to evaluate the corrosion behavior of six different types of steel reinforcement including MMFX steel. Three different test methods were used in this investigation, the non-standard Accelerated Chloride Threshold (ACT), ASTM G-109 standard test method, and the solution test method. The study showed that MMFX steel reinforcement has a critical chloride threshold level 8 to 9 times that of the conventional ASTM A 615 steel, which leads to longer times-to-repair in comparison with ASTM A 615 steel, and can potentially decrease the overall life-cycle cost of reinforced concrete structures. Based on the non-standard short-term Accelerated Chloride Threshold test, the Concrete Innovations Appraisal Service (CIAS) report, (2003) supported the claim that MMFX steel offers improved corrosion resistance when compared to conventional steel. However, CIAS (2003) cautioned that this conclusion can not be extended to long-term behavior due to the lack of long-term field data.

Another major study was conducted at the University of Kansas for the South Dakota Department of Transportation (SDDOT), Darwin et al. (2002). The study investigated the corrosion resistance of MMFX steel compared to epoxy-coated reinforcement as well as estimating the life expectancy and cost effectiveness of MMFX steel, epoxy-coated reinforcement, and mild steel. The rapid macrocell, Southern Exposure, and Cracked Beam test methods were used. The study concluded that the corrosion rate of MMFX steel is between one-third and two-thirds that of conventional reinforcement. The study also showed that epoxy-coated reinforcement provides superior corrosion performance to MMFX steel. Therefore, the study recommended that MMFX steel should not be used as a direct replacement for epoxy-coated reinforcement without the use of a supplementary corrosion protection system. In addition, it was concluded that bridge decks containing MMFX steel do not appear to be cost-effective when compared to bridge decks containing epoxy-coated reinforcement. However, CIAS report (2003) questioned the conclusions made by the SDDOT report due to the shortcomings of the test methods and the data interpretation, including unjustifiable data selection. Moreover, two independent reviewers, Thomas (2002), who are considered to be corrosion experts, expressed many areas of concerns in their independent reviews to the report. The two reviewers are Dr. Michael Thomas, University of Toronto, Toronto, Ontario, Canada and Dr. David Trejo, University of Texas A&M, Texas, USA. Both reviewers expressed their incomplete agreement with the authors' interpretation of the corrosion data and their use of these data in predicting the service life and life cycle costs of concrete bridge decks exposed to chlorides attack.

4. EXPERIMENTAL PROGRAM

Despite the advanced computing techniques, experimental testing remains the most reliable tool to understand and evaluate the inelastic structural behavior. In order for MMFX steel to be accepted by the engineering community, it has to be experimentally validated prior to its usage. The following sections describe the experimental testing conducted at the Constructed Facilities Laboratory (CFL), North Carolina State University (NCSU) to determine tensile characteristics of MMFX steel, the behavior of bridge decks reinforced with MMFX steel, effect of bending on the tensile strength of MMFX steel bars, and its corrosion rate.

4.1. Mechanical Properties

4.1.1. Tensile Strength

Tension coupons of #4 (No. 13), and #5 (No. 16) MMFX bars were tested according to ASTM-A370 specification. Five coupons were tested for each bar size and 8-in gage lengths were marked on the specimens over which the elongation measurements were made. An MTS axial mechanical extensometer that measures the change in length over a 2-in gage length was attached to each test specimen at mid-height to measure the deformation during loading, as shown in Figure 4.1. The measured stress-strain characteristics of the #4 (No. 13) and #5 (No. 16) bars are shown in Figure 4.2 and Figure 4.3, respectively. In general, the MMFX reinforcing bars exhibit a linear behavior initially, followed by a nonlinear stress-strain relationship up to failure without a well-defined yield point. The initial modulus of elasticity was determined to be 29,000 ksi (200 GPa), followed by a nonlinear behavior and reduction in the modulus of elasticity after the stress exceeded 100 ksi (689 MPa). It should be noted that the obtained stress-strain curves are the engineering stress-strain curves not the true stress-strain curves since the actual instantaneous cross-sectional area was not measured at each load increment. The stress-strain relationship for the MMFX steel can be approximately modeled by the following equation: $f_s(ksi) = 177\left(1 - e^{-185\varepsilon_s}\right)$

Figure 4.1: MTS axial extensometer attached to #5 MMFX bar

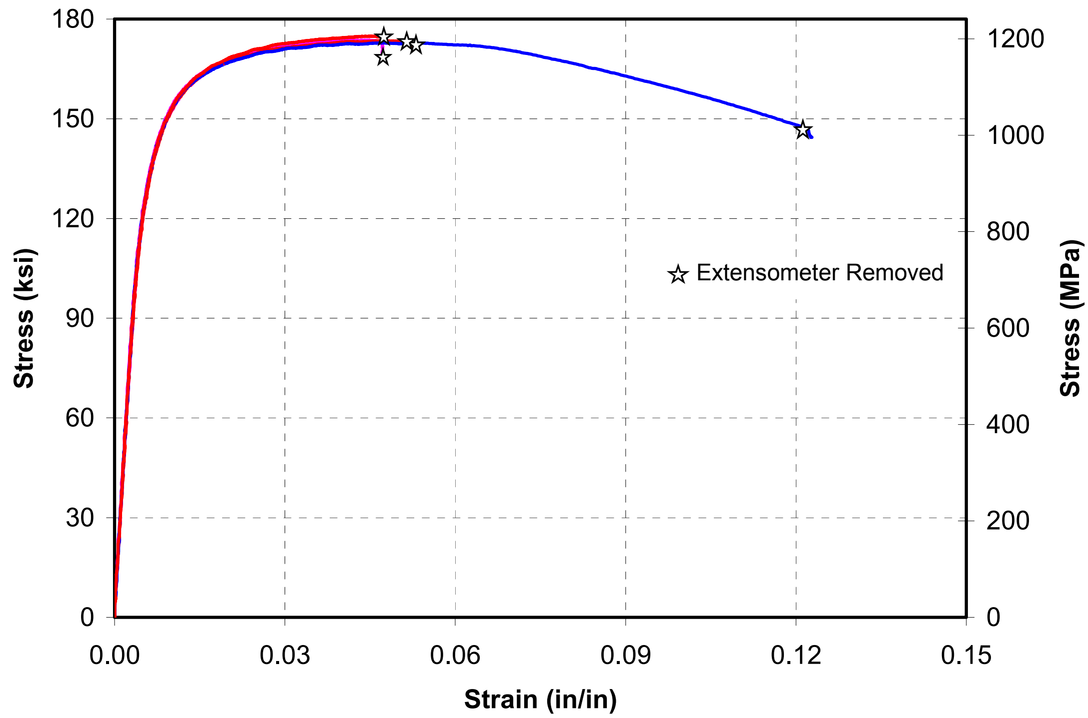

Figure 4.2: Stress-strain relationship for #4 (No. 13) MMFX steel bars

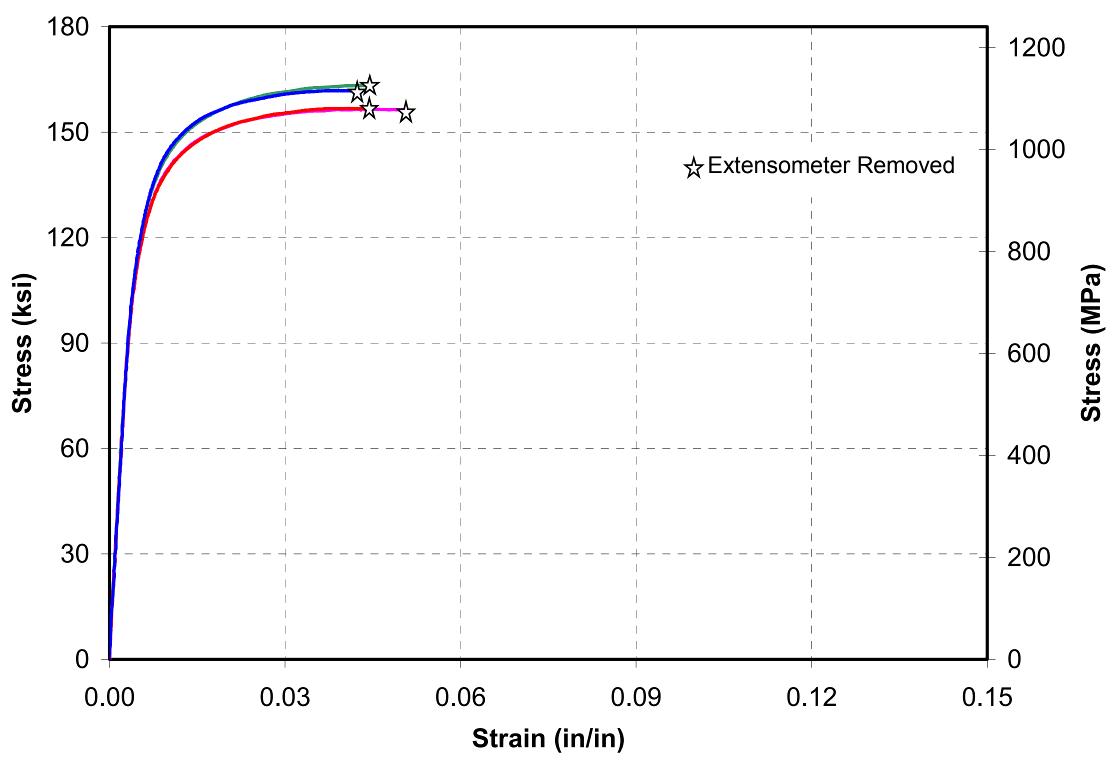

Figure 4.3: Stress-strain relationship for #5 (No. 16) MMFX steel bars

After the maximum load was reached, the diameter of the specimen started to decrease and the reduction of the area was clearly visible due to "necking", as shown in Figure 4.4. It was observed that rupture occurred along a cone-shaped surface which forms an angle of 45^{o} with the longitudinal axis of the specimen. After rupture of the specimen, the two pieces were re-aligned and the fractured ends were fit together matching the failure surfaces. Then the final gage length was measured between the gage marks using a digimatic caliper with an accuracy of 0.0005-in. and the ultimate elongation recorded. The #4 and #5 bars had an average ultimate elongation of 0.072 in/in and 0.063 in/in, respectively. It should be mentioned that necking occurred outside the extensometer 2-in. gage length for all the specimens except for one specimen of #4 (No. 13) bars, see Figure 4.5 which enabled obtaining the descending branch of the stress-strain curve as shown in Figure 4.2. For comparison purposes, the stress-strain relationship obtained for the conventional Grade 60 is plotted versus MMFX steel along with the exponential equation in Figure 4.6.

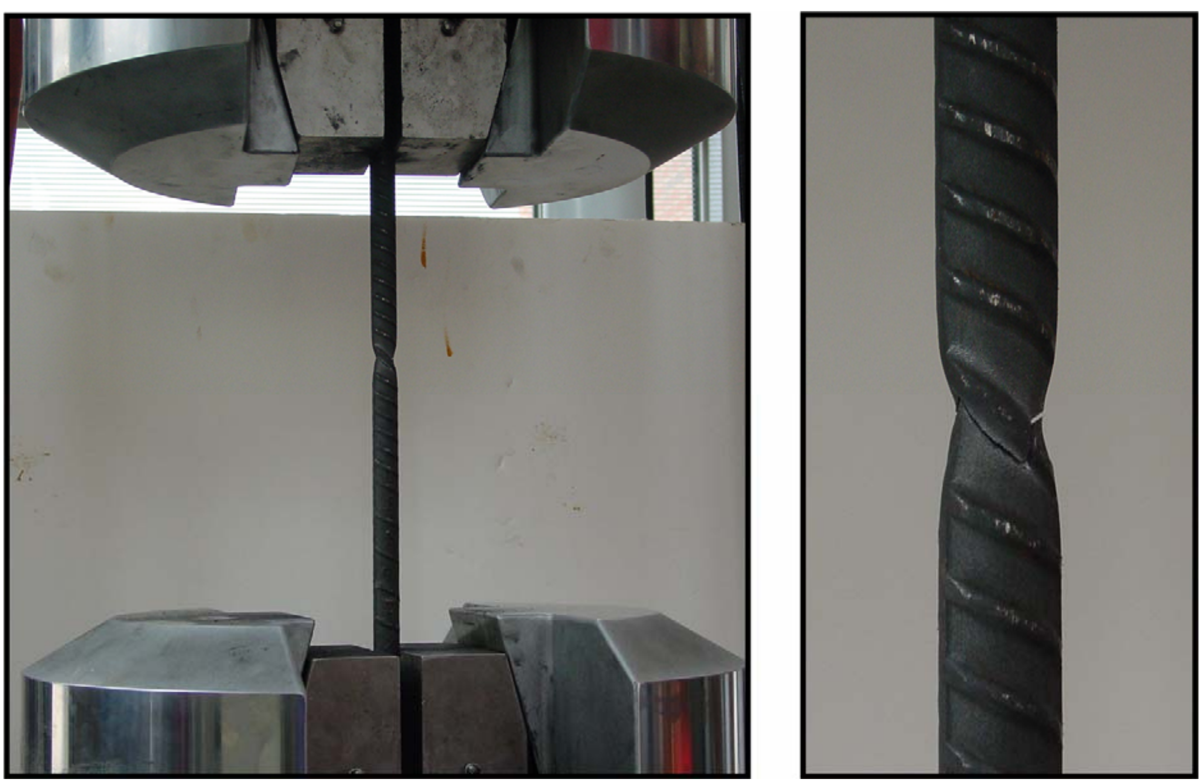

Figure 4.4: Rupture of #5 MMFX bar at the necking

Figure 4.5: Necking occurring inside the MTS extensometer 2-in gage length

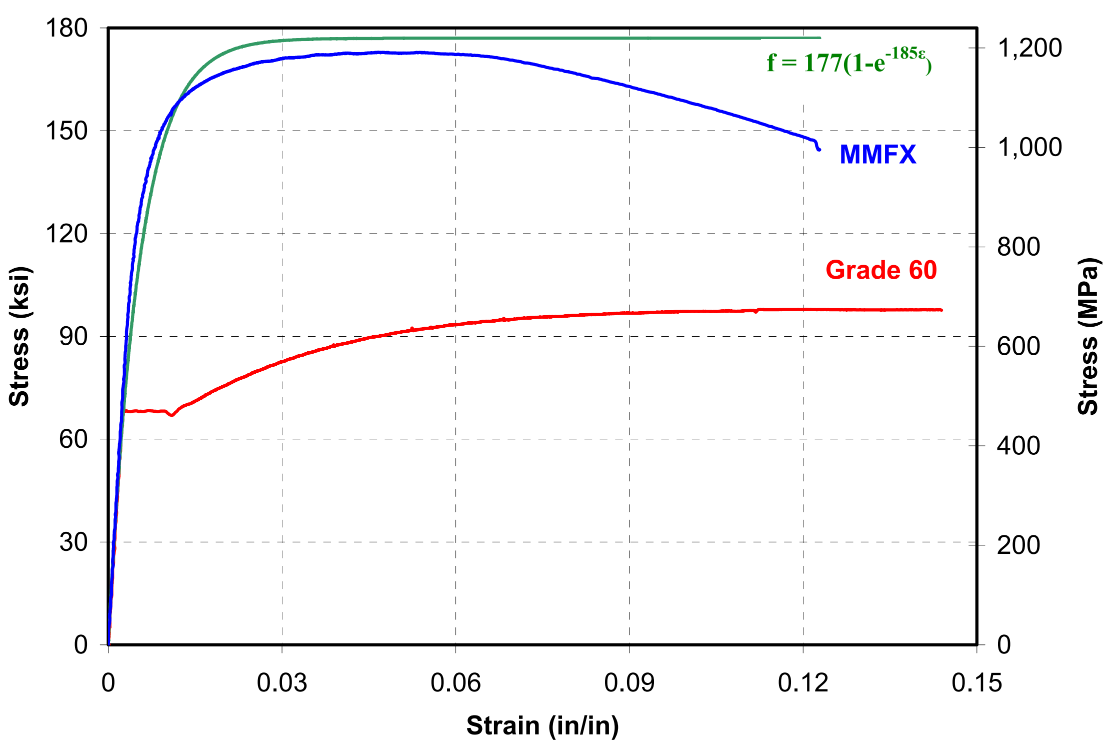

Figure 4.6: Stress-strain relationship for MMFX and Grade 60 steel

4.2. Full-Scale Bridge Deck Models

Three full-scale bridge deck slabs were constructed and tested under static loading conditions up to failure. The first and second bridge decks were reinforced with the same amount of MMFX steel, and conventional Grade 60, respectively. The third bridge deck was also reinforced with MMFX steel, using 33% less amount of steel in the transverse direction. Detailed description of the test models, test setup, and the obtained results are given in the following sections.

4.2.1. Test Models

The three bridge decks considered in this study were identical in all aspects except for the type and amount of steel used in each. Each bridge deck consisted of two spans and two cantilevers, supported in composite action by three post-tensioned concrete girders with cross-sectional dimensions of 24x10 in. (610x254 mm). The three bridge decks were designed to simulate the actual bridge that was built in Johnston County, North Carolina, USA in 2004. The three bridge decks had the same span and thickness as the actual bridge, and were supported by girders designed to have the same torsinal rigidity as the actual steel bridge girders as will be discussed below.

The bridge deck of Johnston County Bridge is supported by steel girders, while the test models were supported by prestressed concrete girders in composite action with the deck slab. The size of the concrete girders was determined to provide similar torsional stiffness of the steel girders, since the torsional stiffness of the supporting girders plays a significant role in the load-carrying capacity of the bridge deck. Both the actual bridge and the test models were analyzed by using non-linear finite element programs “ANACAP” and “SAP2000”. Several girder cross-sections and spans were considered in the analysis to match the torsional stiffness of the model to that of the bridge. A prestressed concrete girder of cross-sectional dimensions of

24x10 in (610x254 mm) and span of 96 in. (2438 mm) was found to have similar torsional stiffness as the actual bridge steel girders. In order to reduce the span of the girders from 13'-2" (4013 mm) used for the model to the required 96 in. (2438 mm) for torsion, the girders were supported by concrete blocks. The supporting girders and the concrete blocks were designed and detailed according to ACI318-02.

The design of the form required for casting the test models is shown in Figure 4.7. The form was designed to provide minimum deflection during casting of concrete and was reused for casting the other two test models. The nominal dimensions of the bridge decks were 21'-10"x13'-2"x8⅝" (6655x4013x220 mm) with a span-to-depth ratio of 12.5. The supporting girders were post-tensioned using deformed prestressing bars of 1 in. (25 mm) diameter with ultimate strength of 150 ksi (1034 MPa). Each girder was prestressed by four bars resulting in a total prestressing force of 360 kips (1601 KN) per girder. The prestressing force was applied one day before casting the deck, so the total prestressing forces was resisted by the girder only.

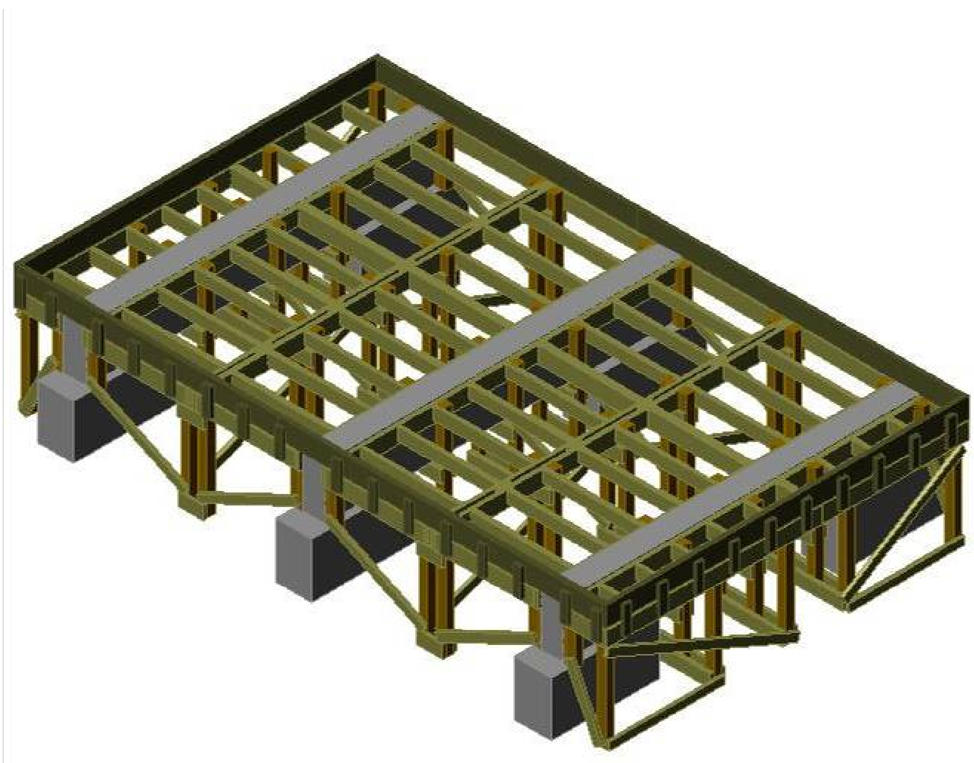

Figure 4.7: Wooden forms used for casting the three bridge decks

The first and third bridge decks were reinforced with MMFX steel, while the second bridge deck was reinforced with conventional Grade 60 steel for comparison purposes. The test matrix is given in Table 1 and the reinforcement details for the three bridge decks are shown in Figure 4.8. It should be noted that the reinforcement ratio (ρ) was calculated using the total slab thickness. The first and second bridge decks were constructed with the same reinforcement ratio using MMFX and conventional Grade 60 steel, respectively. However, the third bridge deck was reinforced with MMFX steel using only two third of the reinforcement ratio used for the first deck in an attempt to utilize the higher tensile strength of MMFX steel. It should be noted that the first bridge deck was designed to simulate the same reinforcement ratio of the actual bridge that was built in Johnston County, North Carolina in 2004. Figure 4.9 shows the first bridge deck after placing the steel and prior to casting of concrete.

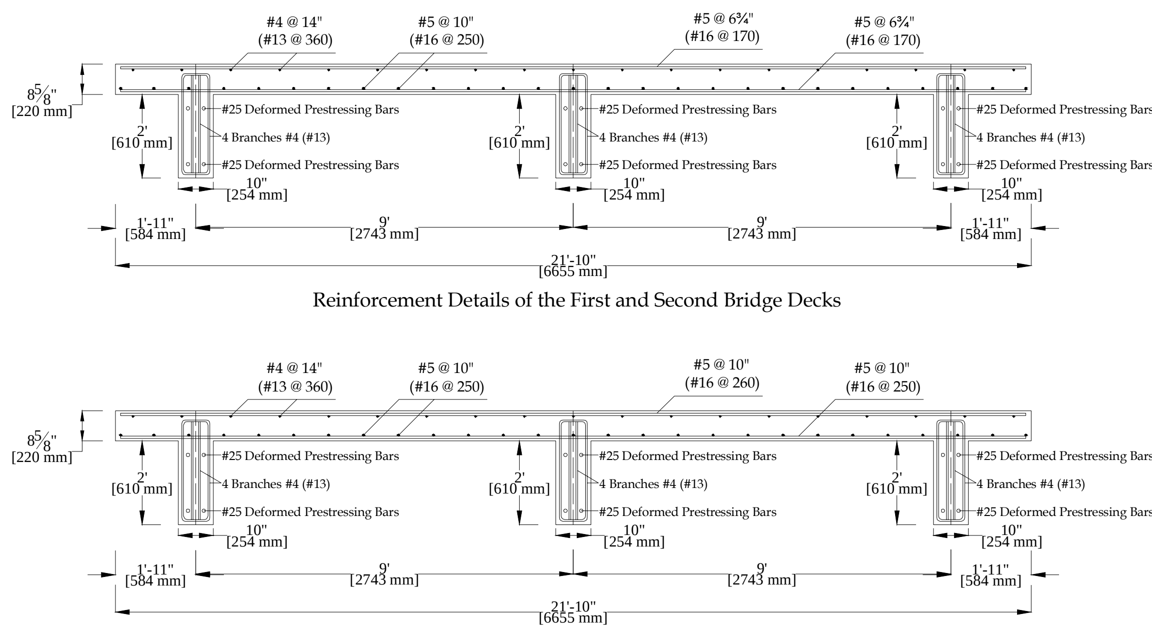

Figure 4.8: Reinforcement details of the three bridge decks

Table 1: Bridge decks test matrix

Bridge Deck	Steel Type	Bottom Reinforcement		Top Reinforcement	
		Transverse	Longitudinal	Transverse	Longitudinal
First	MMFX	#5 @ 6.75” (#16 @ 170) ρ = 0.54%	#5 @ 10” (#16 @ 250) ρ = 0.36%	#5 @ 6.75” (#16 @ 170) ρ = 0.54%	#4 @ 14” (#13 @ 360) ρ = 0.17%
Second	Grade 60	#5 @ 6.75” (#16 @ 170) ρ = 0.54%	# 5 @ 10” (#16 @ 250) ρ = 0.36%	#5 @ 6.75” (#16 @ 170) ρ = 0.54%	#4 @ 14” (#13 @ 360) ρ = 0.17%
Third	MMFX	#5 @ 10” (#16 @ 250) ρ = 0.36%	#5 @ 10” (#16 @ 250) ρ = 0.36%	#5 @ 10” (#16 @ 250) ρ = 0.36%	#4 @ 14” (#13 @ 360) ρ = 0.17%

Figure 4.9: First bridge deck prior to casting

4.2.2. Material Properties

The target concrete compressive strength for the three decks was 4500 psi (31.0 MPa). However, the measured concrete compressive strengths at the day of testing for the three bridge decks were 7000, 4500, and 5278 psi (48.2, 31.0, and 36.4 MPa), respectively. The concrete compressive strengths were determined using 4x8 in. (102x204 mm) concrete cylinders cast for each deck and cured under the same conditions as the deck. Concrete was provided by a local supplier.

Tension coupons of the MMFX and Grade 60 steels used in the three bridge decks were tested according to ASTM-A370 specifications. The measured stress-strain characteristics of the MMFX and Grade 60 steel are shown in Figure 4.10. The MMFX reinforcing bars exhibit a linear stress-strain relationship up to 100 ksi (689 MPa) followed by a nonlinear behavior with ultimate strength of 173 ksi (1193 MPa). According to the ASTM-A370 offset method (0.2% offset) the yield strength was determined to be 120 ksi (827 MPa). The initial modulus of elasticity was determined to be 29,000 ksi (200 GPa), followed by a nonlinear behavior and reduction in the modulus of elasticity after the stress exceeded 100 ksi (689 MPa). The yield strength of the Grade 60 steel was determined to be 68 ksi (469 MPa).

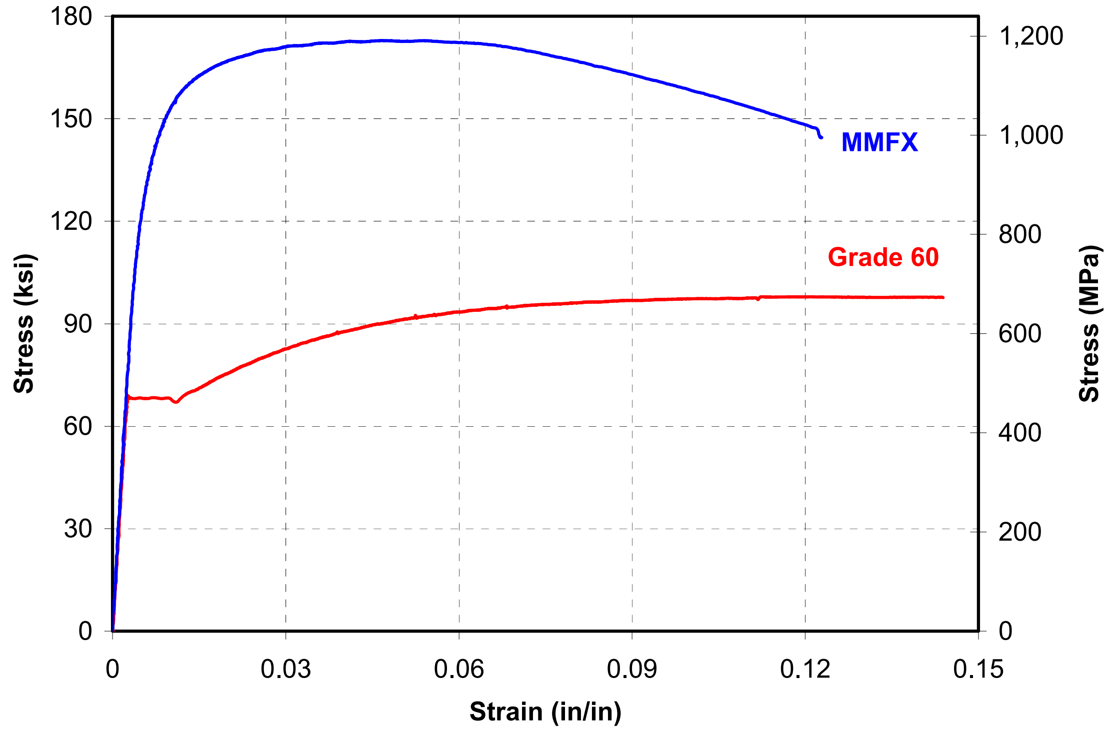

Figure 4.10: Stress-strain characteristics of Grade 60 and MMFX steel

4.2.3. Test Setup and Instrumentation

Two 440 kips (1957 KN) MTS hydraulic actuators were used to apply a concentrated load to each span simultaneously to simulate the effect of a truck wheel load. Two 10x20 in. (254x508 mm) steel plates were used to transfer the load from the actuator to comply with the AASHTO Specifications (2004) for tire contact area. A ½ in. (13 mm) thick neoprene pad was placed under each loading plate to prevent possible local crushing of the concrete. The supporting girders were supported by concrete blocks to transfer the applied load to the strong floor resulting in a clear span of 96 in. (2438 mm). The clear span of supporting girders was determined based on the equivalency of the torsional rigidity of the supporting girders to that of the steel girders used in the actual bridge as discussed above. Figure 4.11 and Figure 4.12 show an isometric view of the test setup and the first bridge deck prior to testing, respectively.

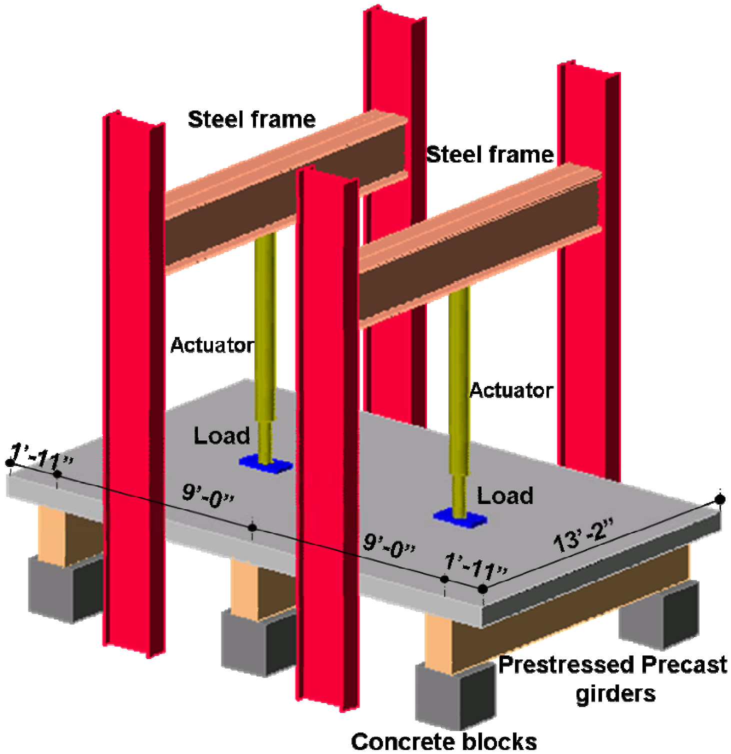

Figure 4.11: Isometric view of the bridge decks test setup

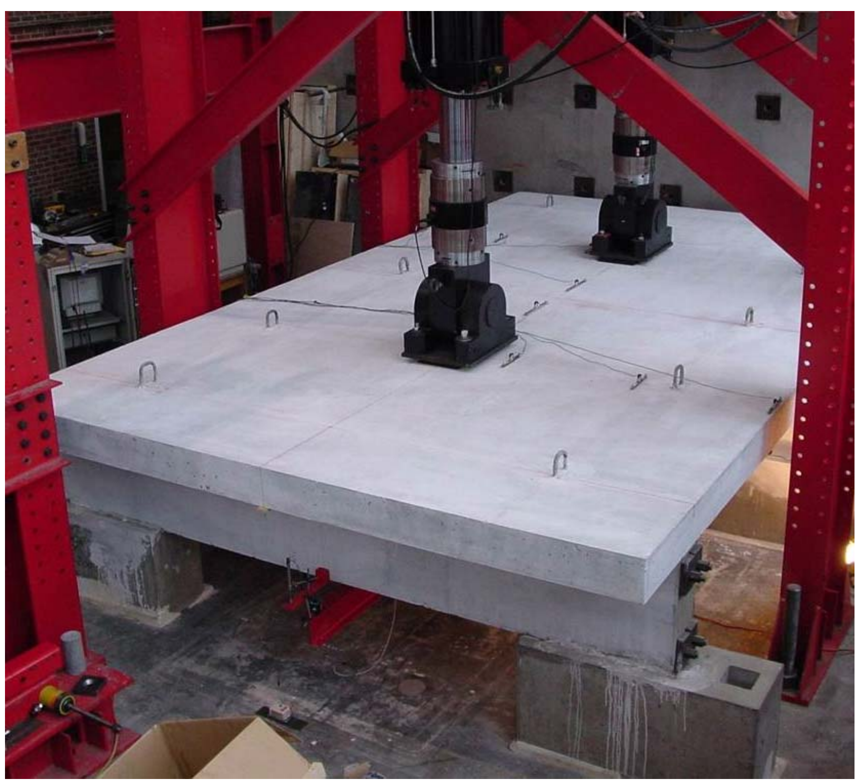

Figure 4.12: First bridge deck prior to testing

A total of 72 channels were used for instrumentation of each bridge deck. A 440 kips (1957 KN) load cell was mounted to each actuator to measure the applied load. Twenty-four string potentiometers (string pots) were used to measure the bridge deck deflection profiles along the longitudinal and transverse directions. In addition, six linear potentiometers were used to measure the girders deflections and rotations. Twenty PI gages were used to measure the concrete strain at various locations. The measured strains were used to determine the strain profiles of the sections at the measured locations. Twenty electrical resistance strain gages of 120 ohm and 6 mm gage length were attached to selected reinforcing bars to determine the strains in these bars. Data were electronically recorded by an Optim Megadac data acquisition system. Figure 4.13 establishes the references for various members and their orientations adopted hereafter. Figure 4.14 and Figure 4.15 show the locations of the PI gages and the string pots used. Figure 4.16 shows the location of the strain gages attached to the bottom transverse reinforcement and Figure 4.17 depicts one of these strain gages.

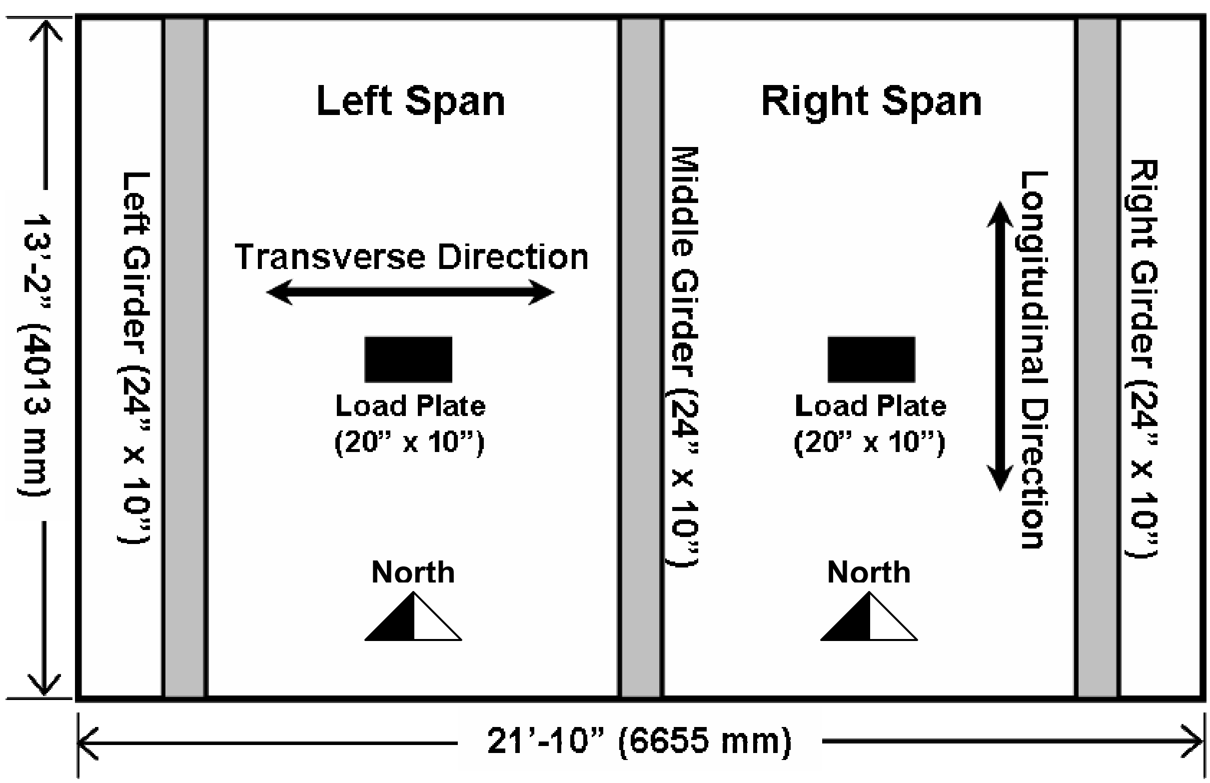

Figure 4.13: Notations for the three bridge decks

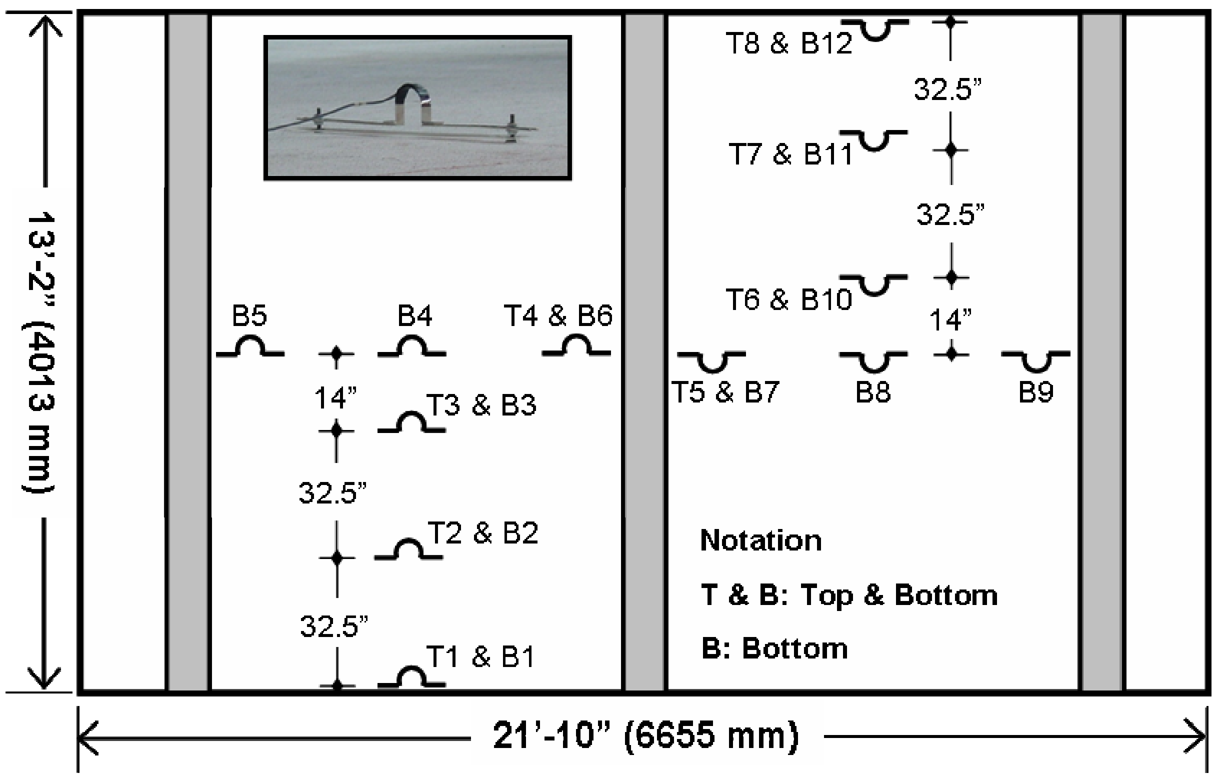

Figure 4.14: PI gages locations

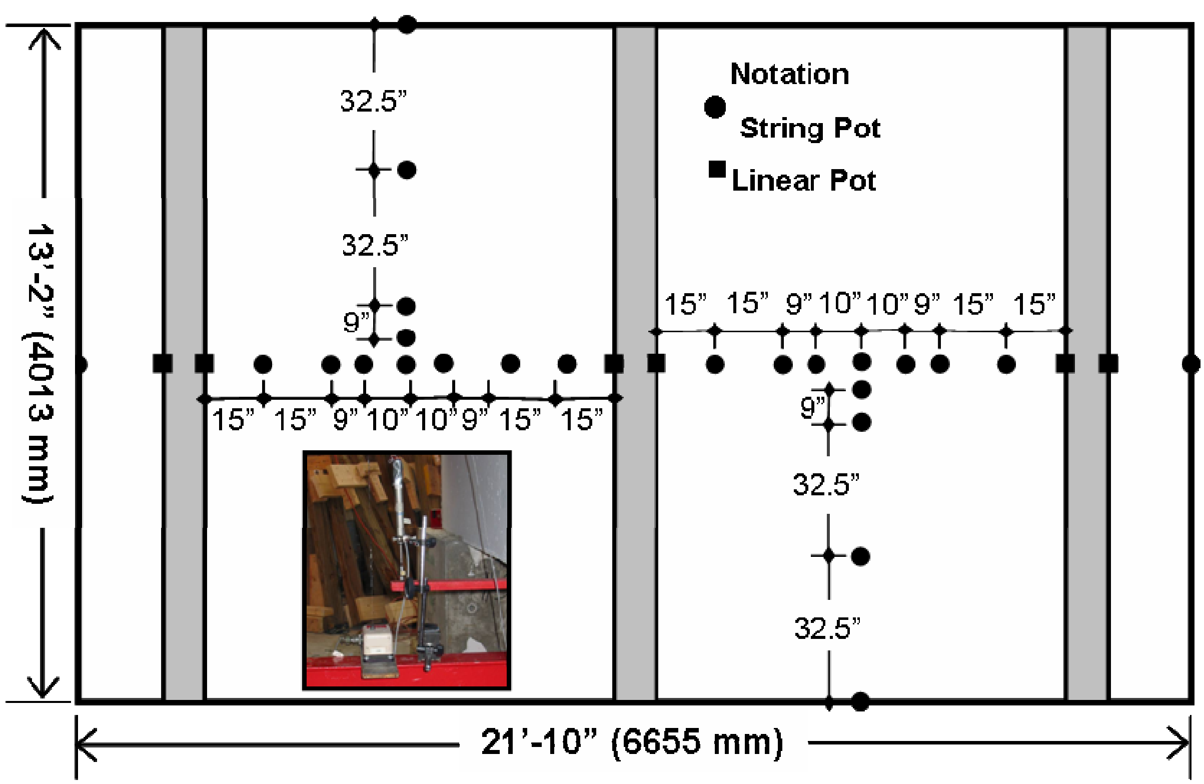

Figure 4.15: String and linear pots locations

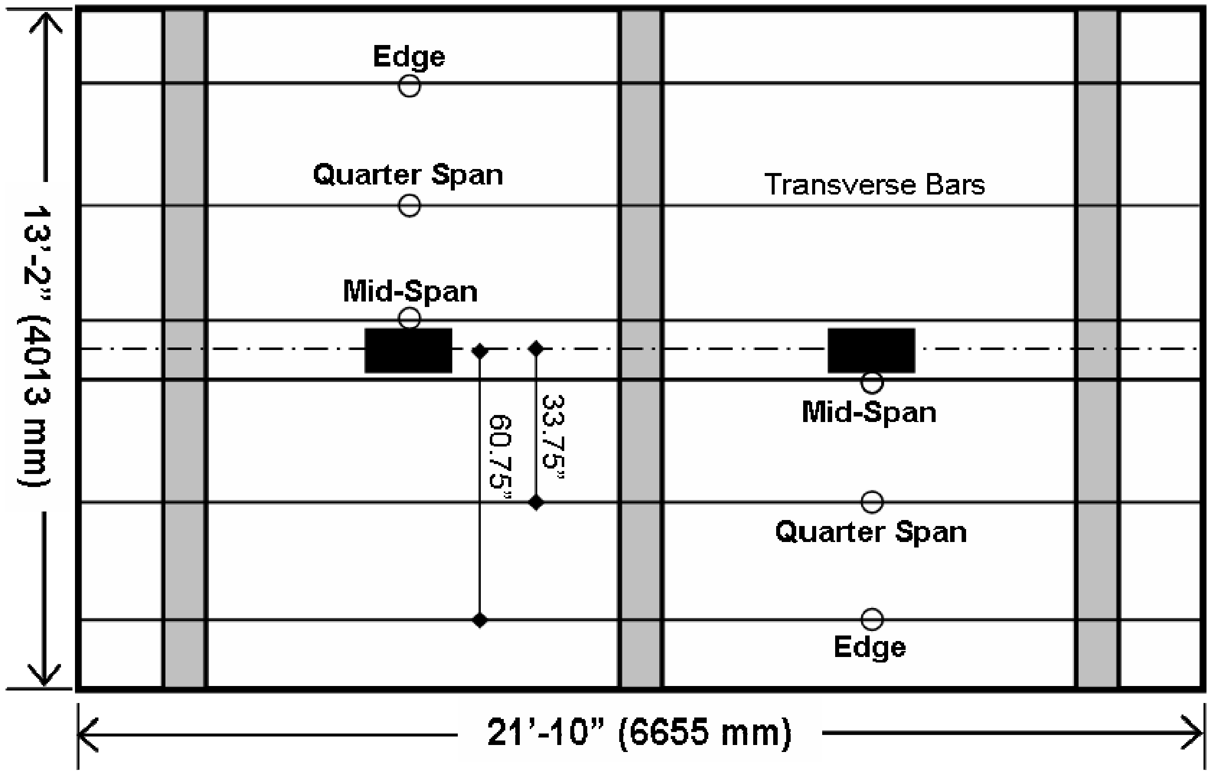

Figure 4.16: Location of strain gages attached to transverse steel bars

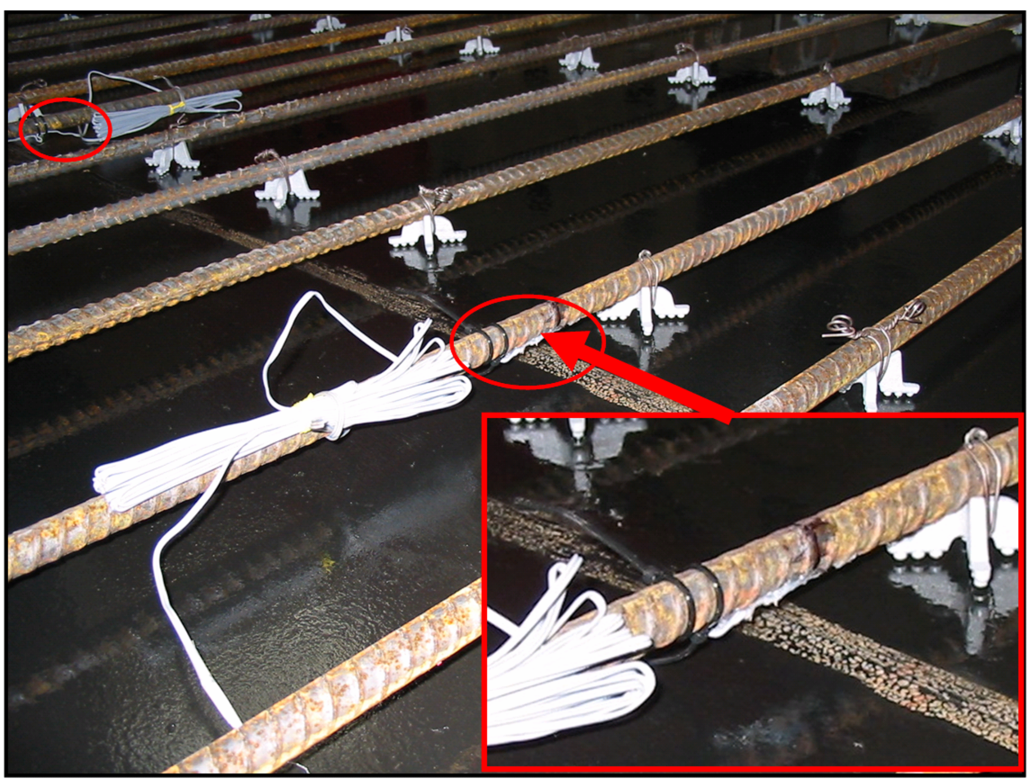

Figure 4.17: Strain gage on the bottom transverse mesh

4.2.4. Test Results

This section discusses in detail the experimental results, and the observed behavior of the three bridge decks investigated in this study. English units (kips, feet, and inches) are the primary units, in addition metric units (kN, meter, and millimeter) are shown in parentheses. The results for each test are presented in the order they were tested, and analyzed to critically examine the performance of bridge decks reinforced with MMFX steel bars in light of the following aspects of behavior:

- *Load-Deflection Behavior*

The load-deflection envelopes up to failure for the three bridge decks are given in Figure 4.18 and Figure 4.19 for the left and right spans, respectively. It should be noted that the deflection plotted in Figure 4.18 and Figure 4.19 is measured at the center of the respective deck span directly under the applied load. It is readily apparent from Figure 4.18 and Figure 4.19 that the first bridge deck reinforced with MMFX steel using the same reinforcement ratio as used for the actual bridge exhibited smaller deflection in comparison to the other two bridge decks. Due to the use of higher reinforcement ratio in the first bridge deck, stiffness was higher than the other two decks; this could also be due to the higher compressive strength of the concrete used for the first deck. Despite the lower reinforcement ratio used for the third bridge deck (33 percent less than the first two decks), it was capable of sustaining the same load as the second bridge deck of the Grade 60 steel. This behavior is attributed to the utilization of the higher tensile strength of MMFX steel. The slight increase of the deflection measured for the third bridge deck in comparison to the second deck is possibly due to the slight reduction of the modulus of elasticity of MMFX steel at high stress levels. According to the AASHTO Specifications (2004), the design tandem consists of a pair of 32 kips (111 kN) axles. Therefore, at a load level of 21 kips (93 kN), which is less than the cracking load; the deflection at service load was almost identical for the three bridge decks.

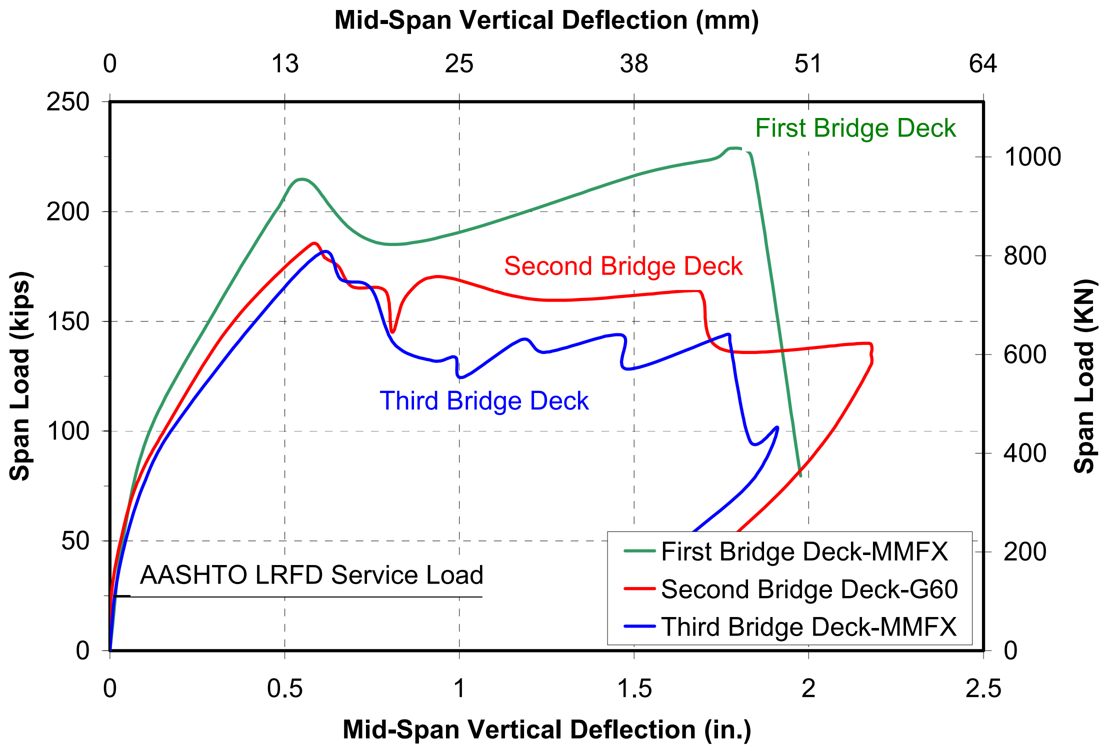

Figure 4.18: Load-deflection envelopes for the left span of the three bridge decks

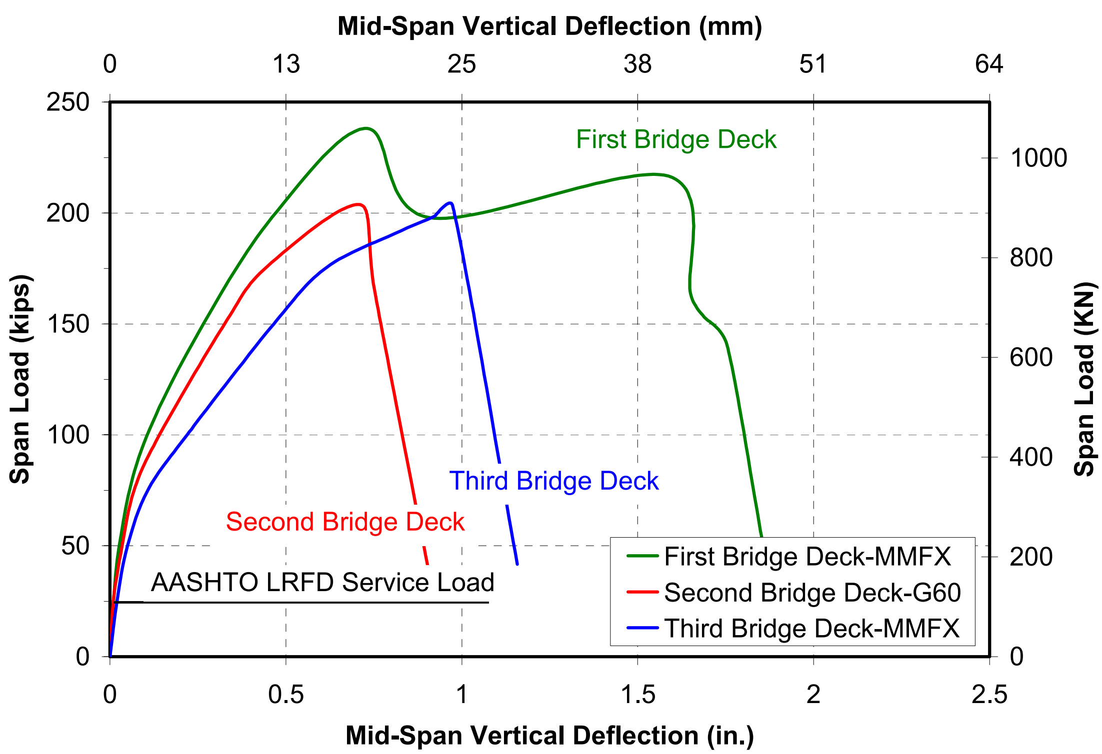

Figure 4.19: Load-deflection envelopes for the right span of the three bridge decks

- *Deflection Profiles*

The deflection profiles along the transverse direction of the three bridge decks are given in Figure 4.20 through Figure 4.25. It should again be noted that the deflection profiles are plotted for the last loading cycle only, therefore residual deflections are shown at the beginning of the loading cycle (zero load). Also, note that the figures for the right span are North-South view, while for left span they are South-North view. The deflection profiles indicate that the maximum deflection occurred at the mid-span under the applied load. Also, it is clear that the spans failed in punching shear (right span) exhibited less deflection than the spans failed due to flexural-shear as will be discussed in the following sections.

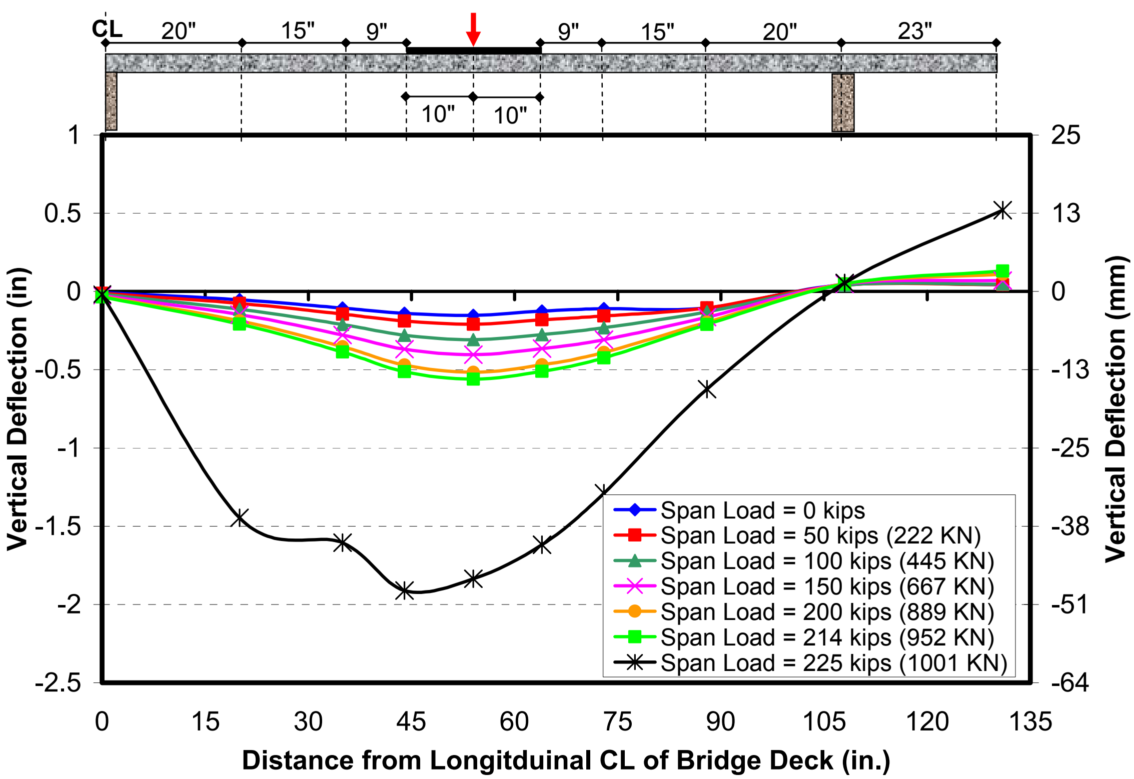

Figure 4.20: Transverse deflection profile for the left span of the first bridge deck

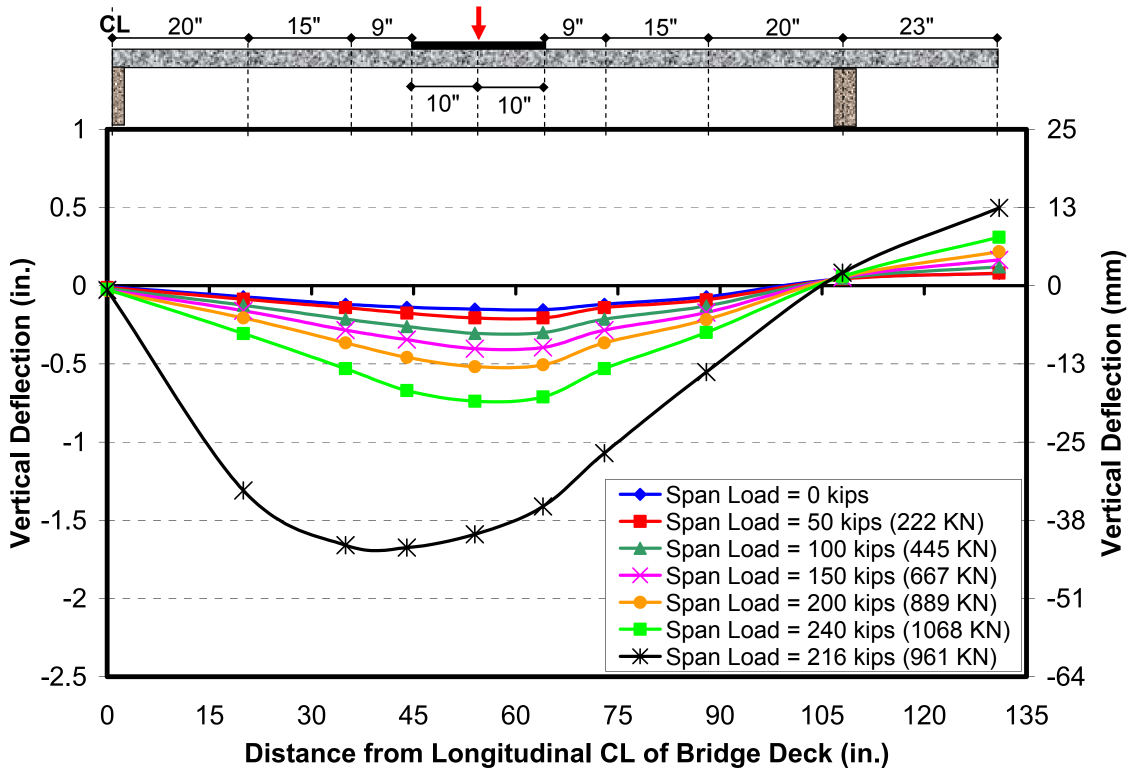

Figure 4.21: Transverse deflection profile for the right span of the first bridge deck

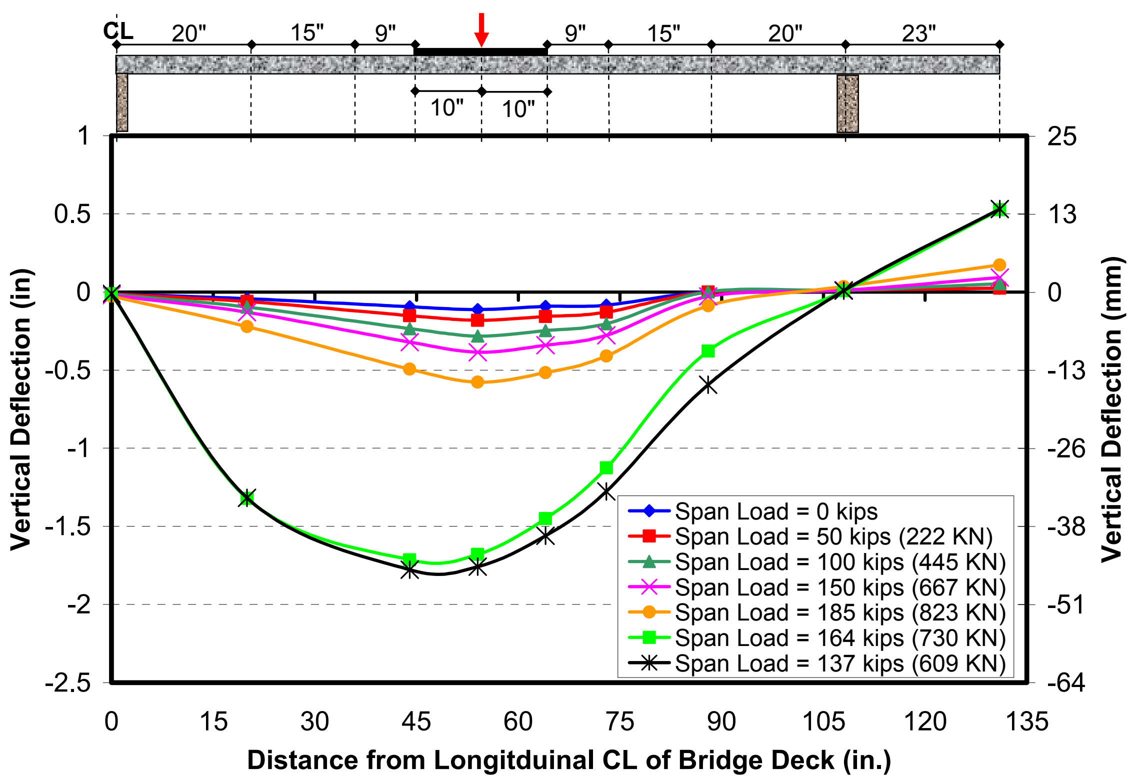

Figure 4.22: Transverse deflection profile for the left span of the second bridge deck

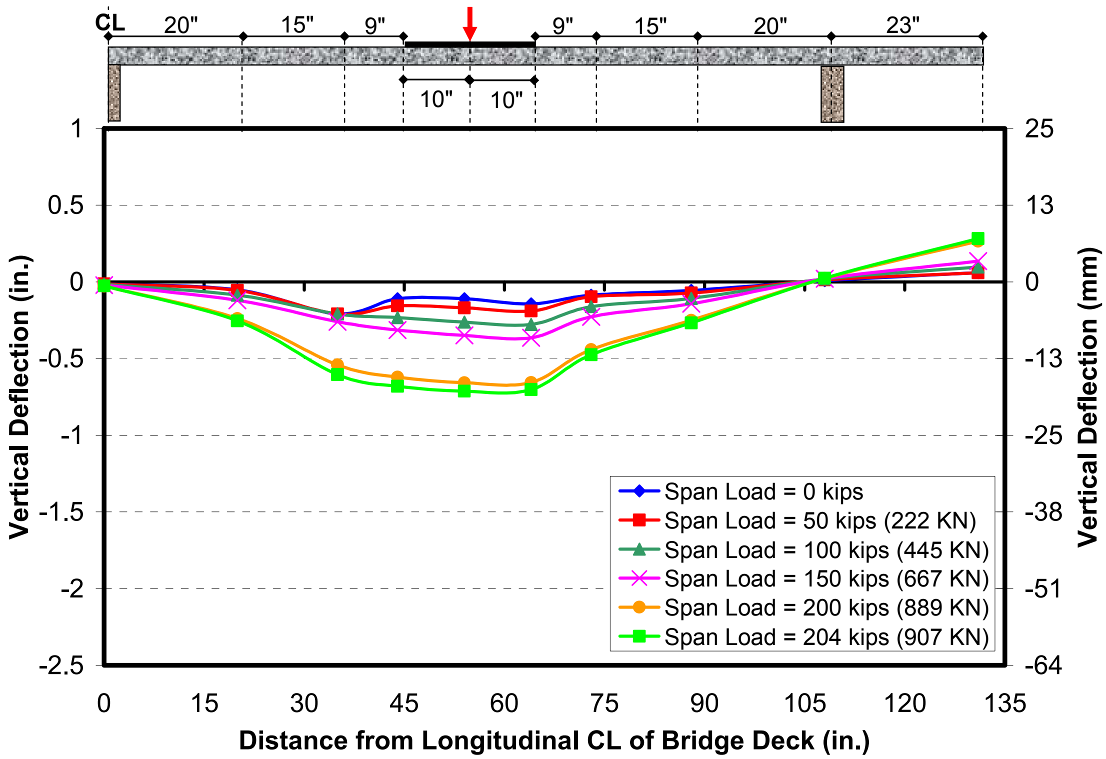

Figure 4.23: Transverse deflection profile for the right span of the second bridge deck

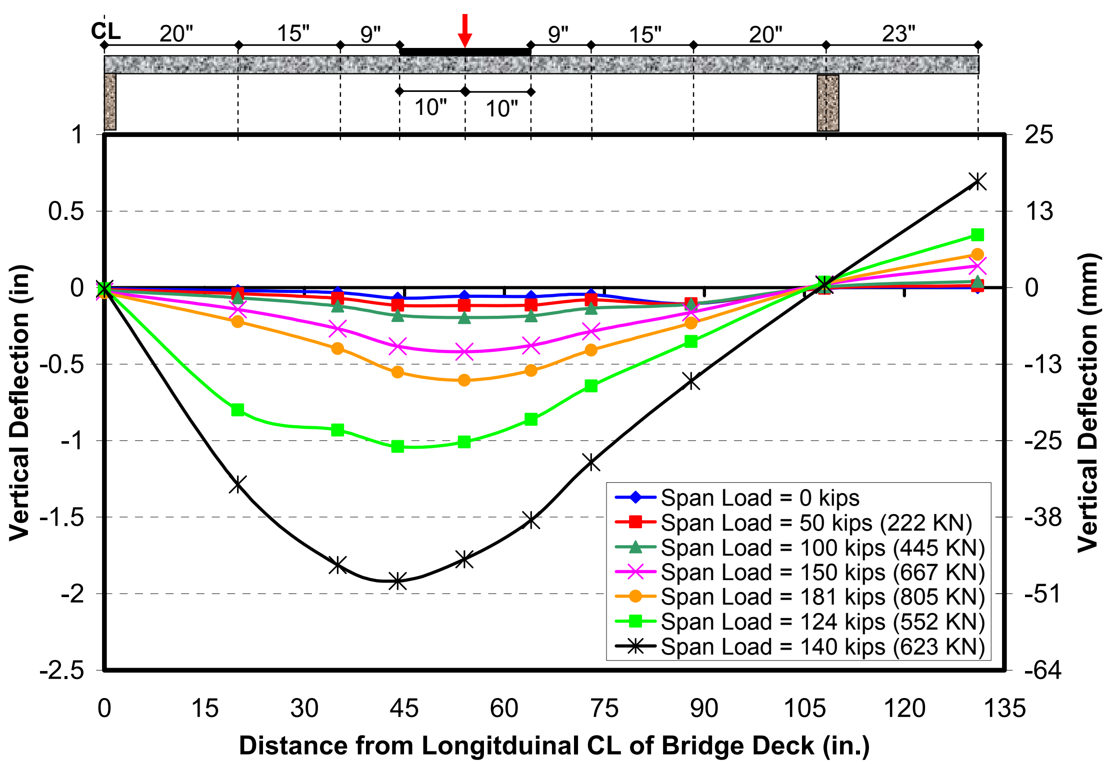

Figure 4.24: Transverse deflection profile for the left span of the third bridge deck

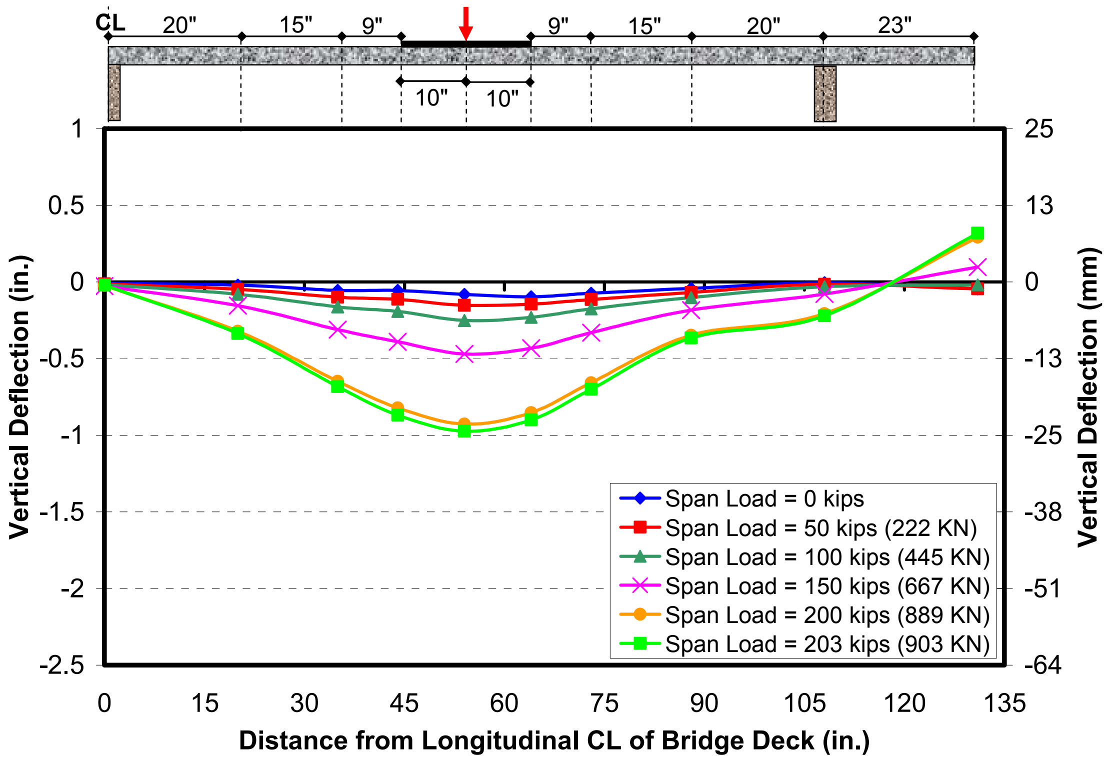

Figure 4.25: Transverse deflection profile for the right span of the third bridge deck

The deflection profiles along the longitudinal direction of the three bridge decks are given in Figure 4.26 through Figure 4.31. It should be noted that the deflection profiles are plotted for the final loading cycle only. The deflections shown for each deck represent the residual deflection from previous loading. Also, note that the figures for the right span are North-South view, while for left span they are South-North view. The deflection profiles for the three bridge decks indicate that the deflection at the edge of the bridge decks was very small. This implies that selection of the length of the model is adequate for carrying the total load, and therefore, representative to the actual bridge deck.

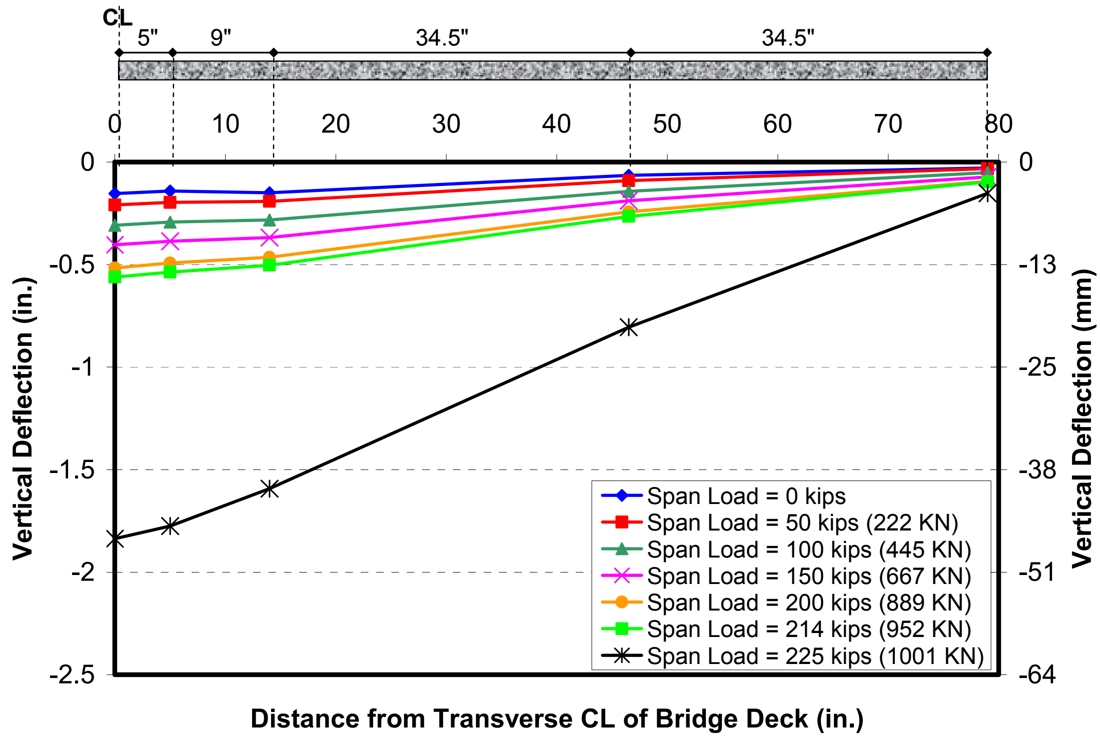

Figure 4.26: Longitudinal deflection profile for the left span of the first bridge deck

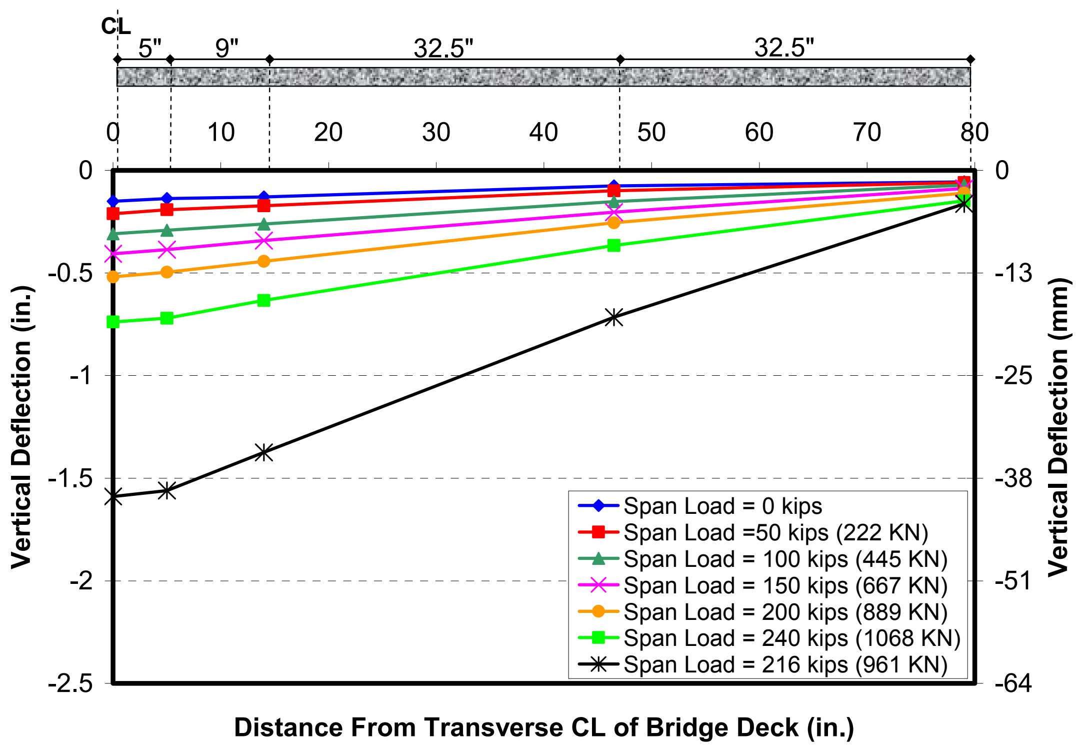

Figure 4.27: Longitudinal deflection profile for the right span of the first bridge deck

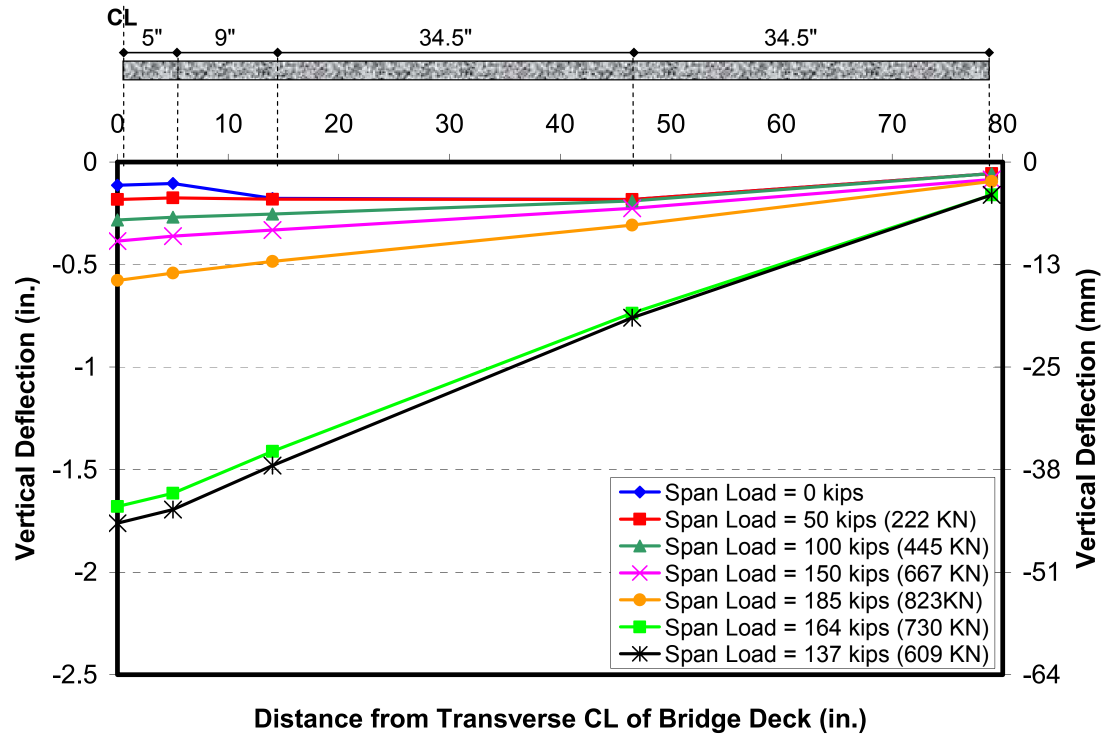

Figure 4.28: Longitudinal deflection profile for the left span of the second bridge deck

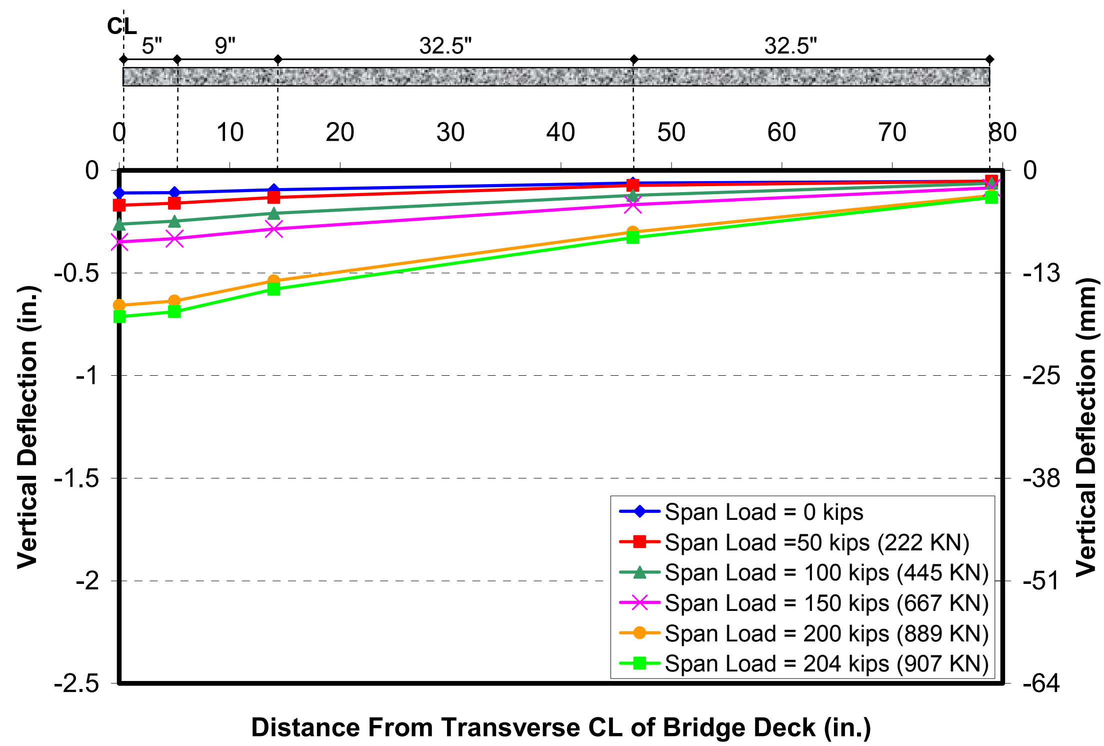

Figure 4.29: Longitudinal deflection profile for the right span of the second bridge deck

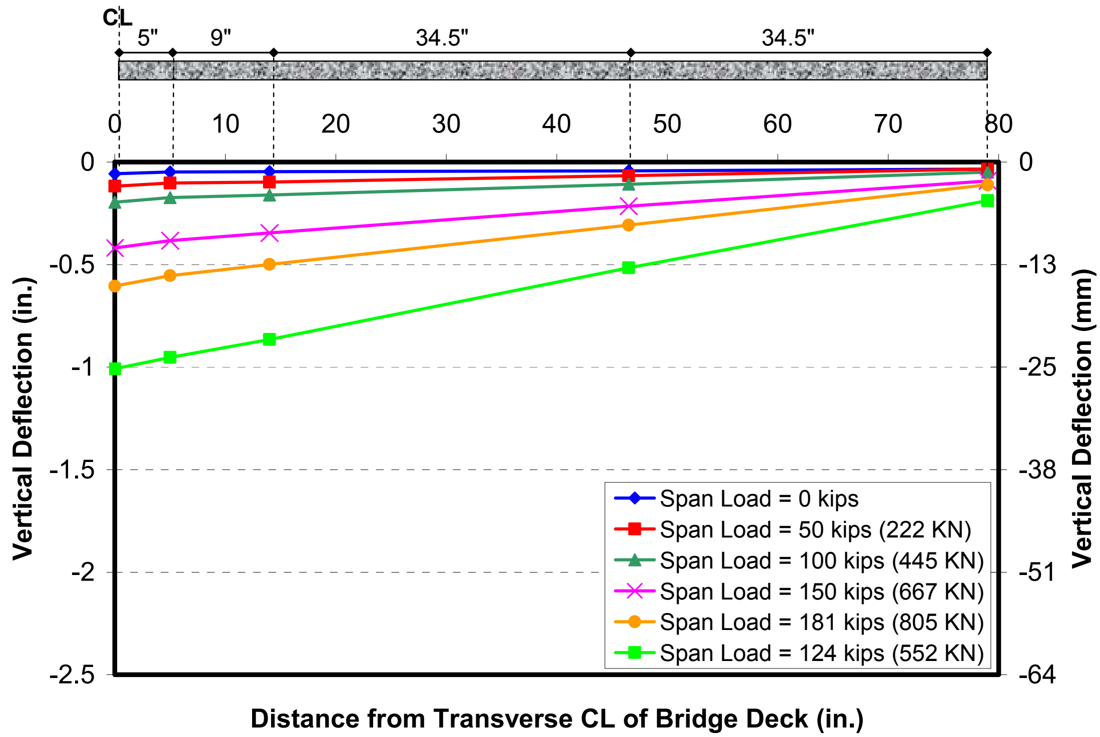

Figure 4.30: Longitudinal deflection profile for the left span of the third bridge deck

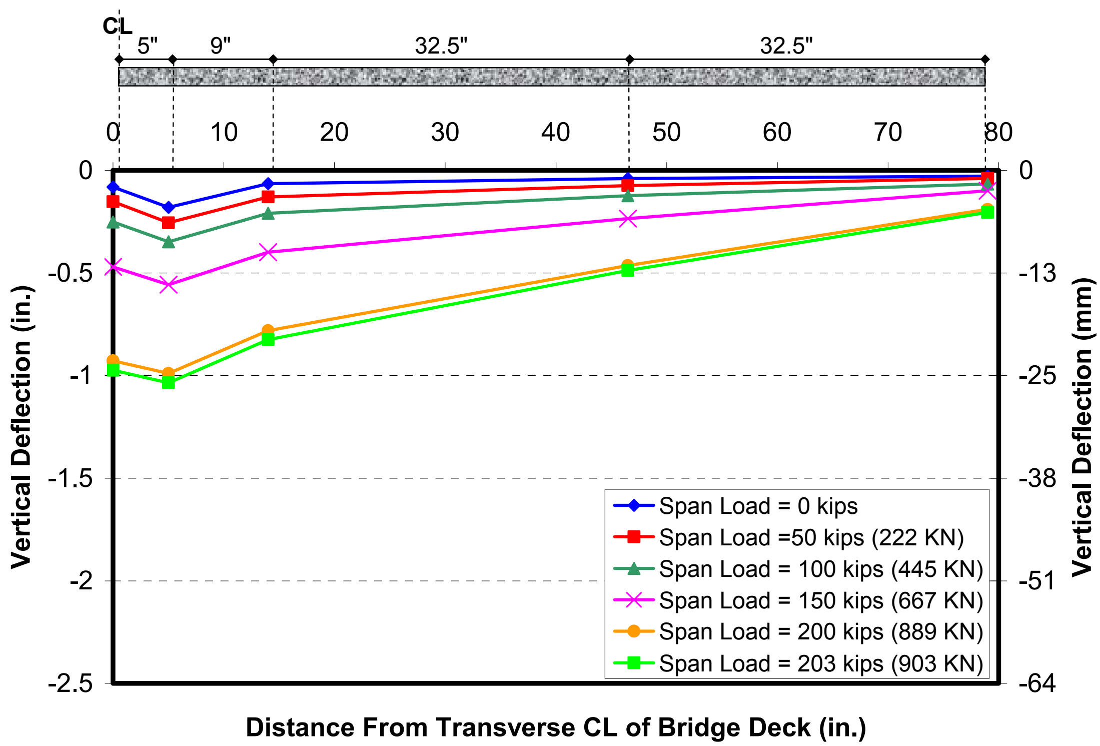

Figure 4.31: Longitudinal deflection profile for the right span of the third bridge deck

- *Mode of Failure*

In general, the behavior under concentrated load was two-way flexural mode followed by development of an arching action supported by membrane forces developed in the bottom layer of the reinforcement. At the first peak load of the first bridge deck, a sudden drop of the load occurred due to the formation of flexural-shear cracks along the top surface of the bridge deck on both sides of the middle girder. Further loading led to the widening of those cracks associated with slight increase in the load until punching failure occurred. Punching failure of both spans occurred simultaneously at a load level of 229 kips (1019 kN) and 216 kips (961 kN) for the left and right spans, respectively. Figure 4.32 and Figure 4.33 show the first bridge deck at the conclusion of the test, where the punching areas under the two loads and the shear cone at the bottom of the left span can be seen clearly.

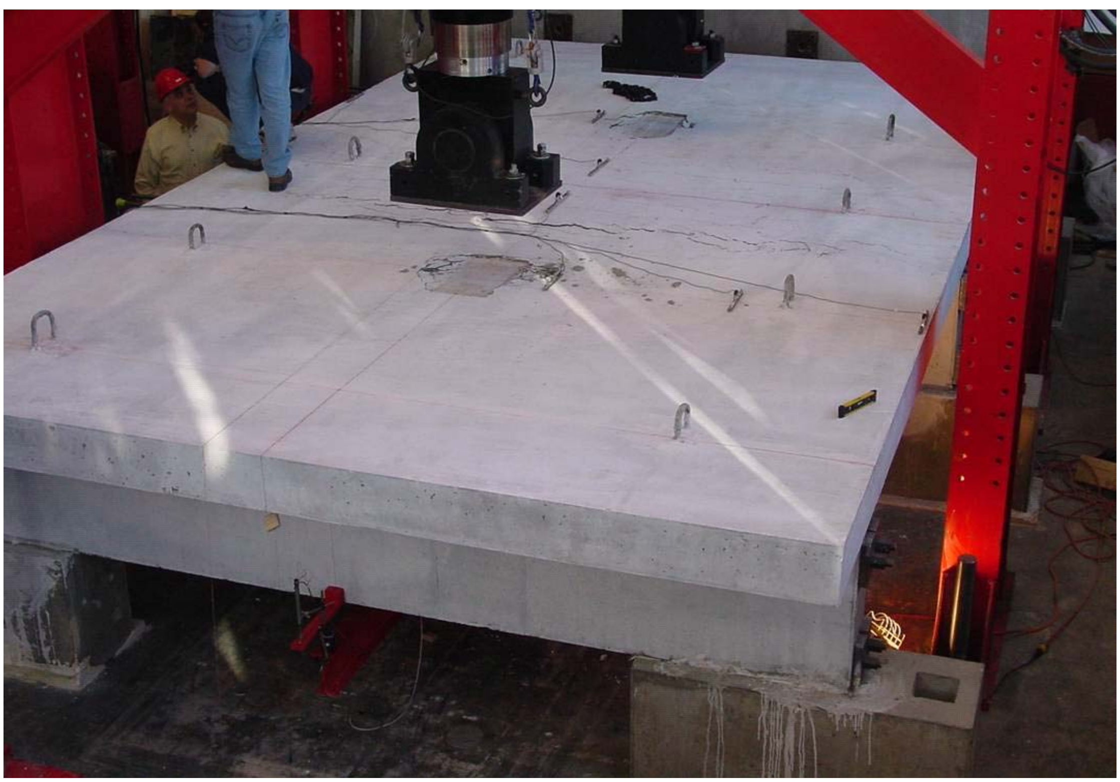

Figure 4.32: First bridge deck at the conclusion of the test

Figure 4.33: Punching cone for the left span of the first bridge deck

The behavior of the second bridge deck, reinforced with grade 60 steel using the same reinforcement ratio was similar to the first deck. At the peak load of the left span, a sudden drop in the load occurred due to the formation of a flexural-shear crack on the top surface of the bridge deck to the left of the middle girder only (left span only). This drop in the load made the left span incapable to carry higher load equivalent to the punching shear capacity of the deck. The test was terminated due to excessive deflections in the left span. The gradual decrease of the load carrying capacity of the left span indicates that flexural-shear failure was the mode of failure of the left span. The maximum measured load for the left span was 185 kips (823 kN) and a deflection of 2.2 in. (56 mm) prior to load termination. Failure of the right span was due to punching shear at a load level of 204 kips (907 kN). Figure 4.34 shows the second bridge deck at failure, where the punching area under the actuator in the right span and the flexural-shear crack formed in the left span are clearly visible.

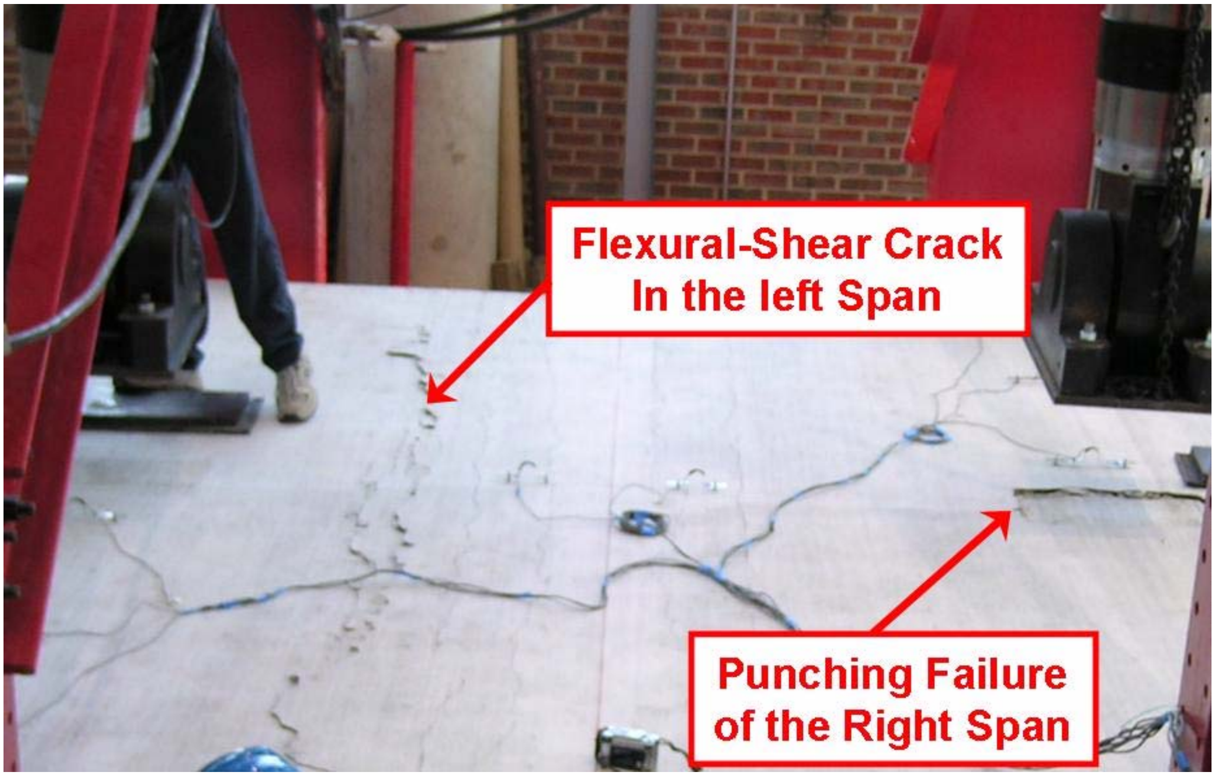

Figure 4.34: Second bridge deck at the conclusion of the test

Similar to the second bridge deck the right span of the third deck failed by punching shear prior to the failure of the left span. A flexural-shear crack formed in the left span causing a sudden drop in the load which made the left span incapable to carry more load equivalent to its punching shear resistance. Flexural-shear failure was the mode of failure of the left span as revealed by the gradual decrease in the load carrying capacity of the load, whereas the right span failed in punching shear at a load level of 203 kips (903 kN). The test terminated due to excessive deflections in the left span and the maximum recorded load for the left span was 181 kips (805 kN). Figure 4.35 shows the third bridge decks at failure, where the punching area under the actuator in the right span and the flexural-shear crack formed in the left span are clearly visible.

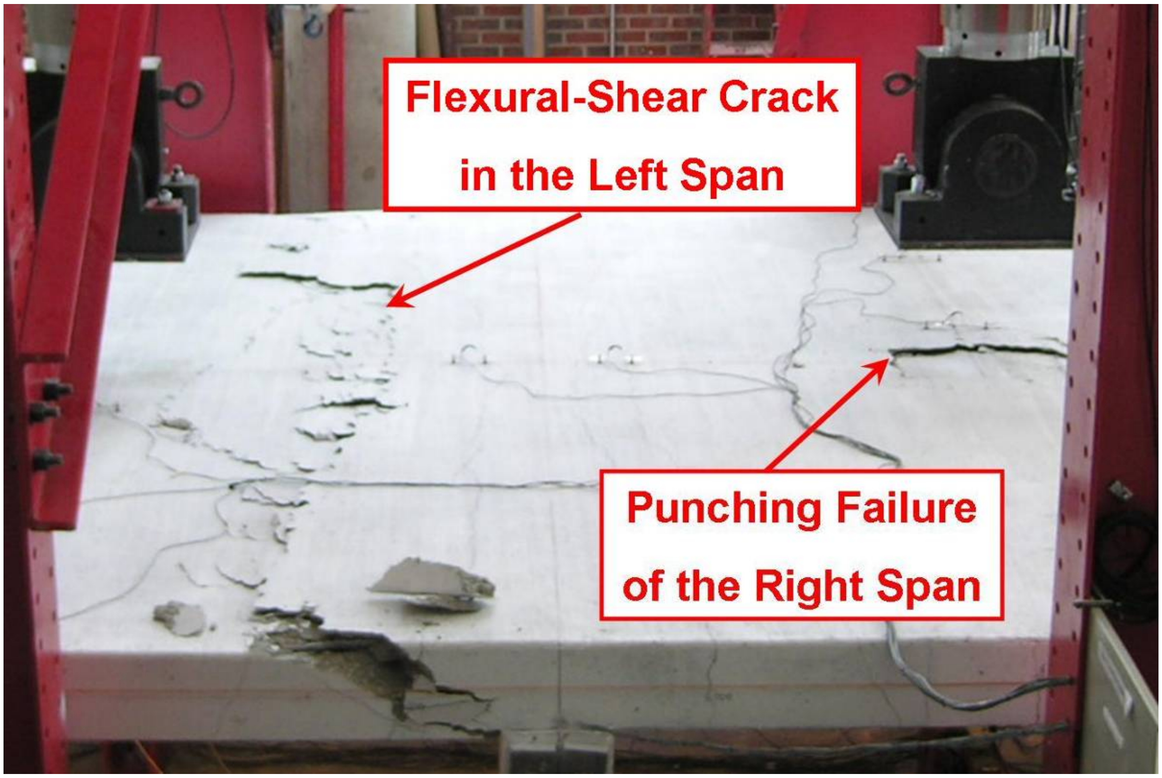

Figure 4.35: Third bridge deck at the conclusion of the test

- *Crack Pattern*

No cracks were observed up to a load level of 50 kips (222 kN) for any of the three bridge decks. However visible top cracks occurred at a load level of roughly 60 kips (267 kN) for each deck. Figure 4.36 through Figure 4.38 show the top cracks at a load level of 100 kips (445 kN) for the three bridge decks. Negative flexural cracks formed before the positive cracks due to the higher values of negative moments in comparison to the positive moments.

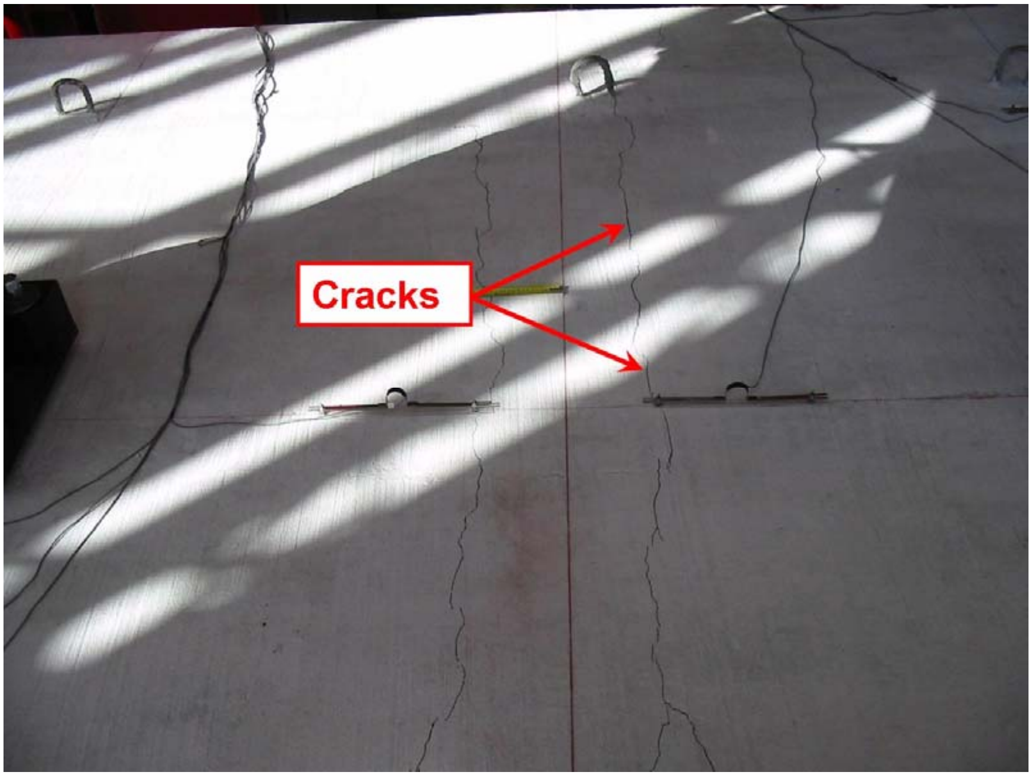

Figure 4.36: Negative flexural cracks at 100 kips (445 kN) for the first bridge deck

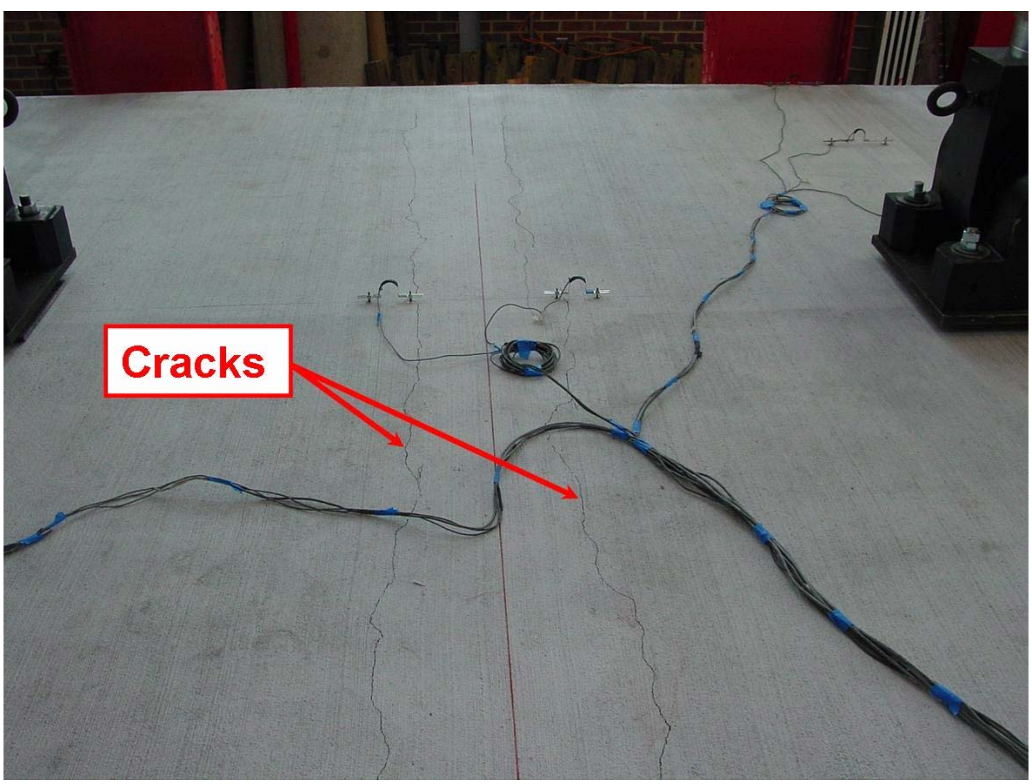

Figure 4.37: Negative flexural cracks at 100 kips (445 kN) for the second bridge deck

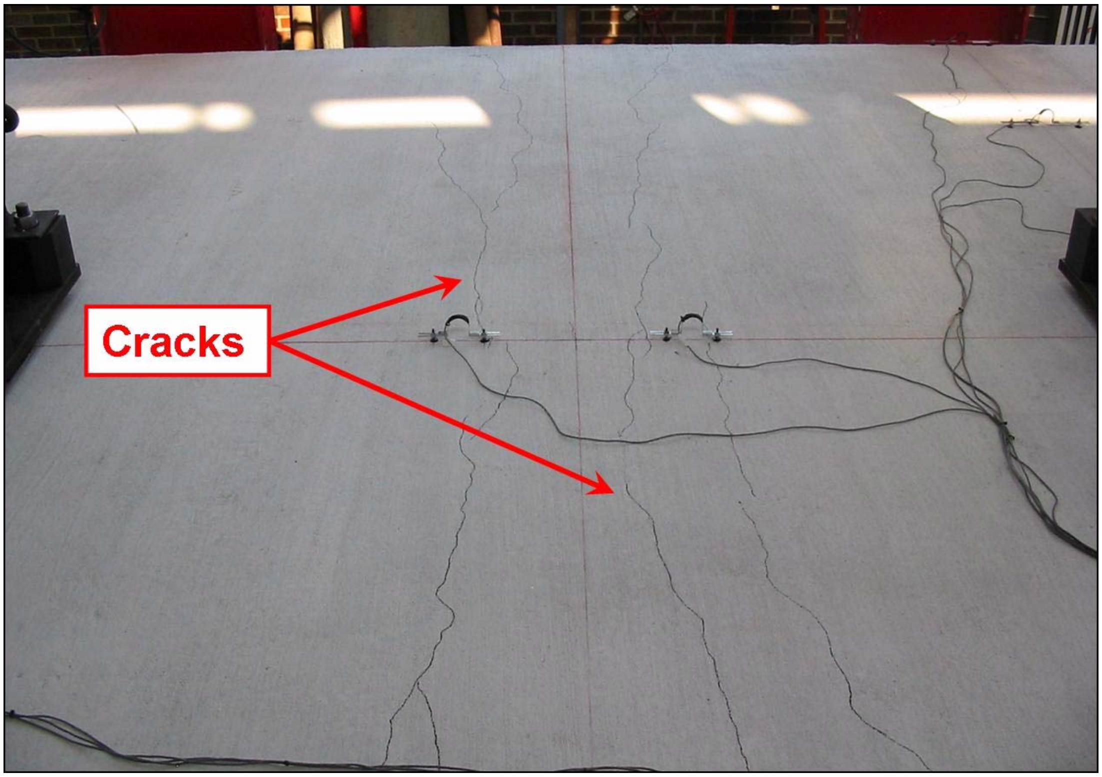

Figure 4.38: Negative flexural cracks at 100 kips (445 kN) for the third bridge deck

Positive moment flexural cracks at load levels of 100 and 150 kips (445 and 667 kN) for the first bridge deck are shown in Figure 4.39 and Figure 4.40, respectively. The crack pattern confirms the two-way distribution of the load. Further loading led to spreading and widening of the flexural cracks until the formation of the flexural-shear crack at the top surface of the deck close to the middle girder. The formation of the flexural-shear crack led to a sudden drop in the load as previously discussed. However, the flexural-shear crack formed symmetrically on both sides of the middle girder of the first bridge deck, as shown in Figure 4.41, therefore allowed increase of the load to cause punching shear of both spans. For the second and third bridge decks, the flexural-shear crack occurred on the left side of the middle girder only which allowed the load to increase in the right span causing punching shear at the right span only as shown in Figure 4.34 and Figure 4.35.

Figure 4.39: Positive flexural cracks at 100 kips (445 kN) for the first bridge deck

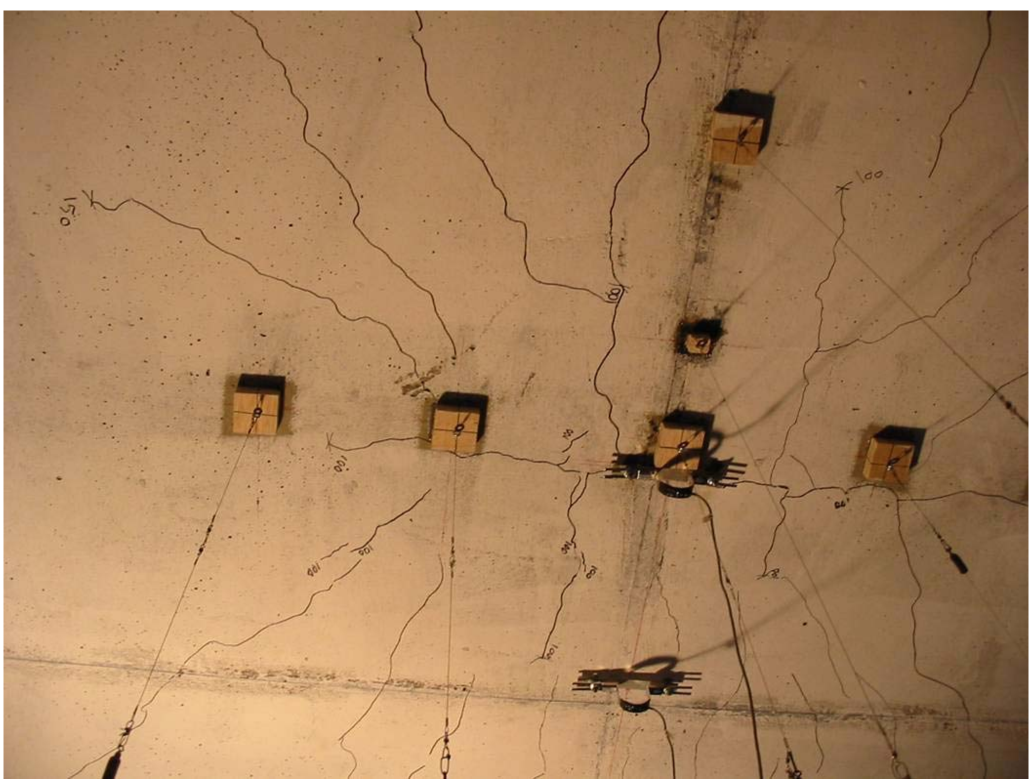

Figure 4.40: Positive flexural cracks at 150 kips (667 kN) for the first bridge deck

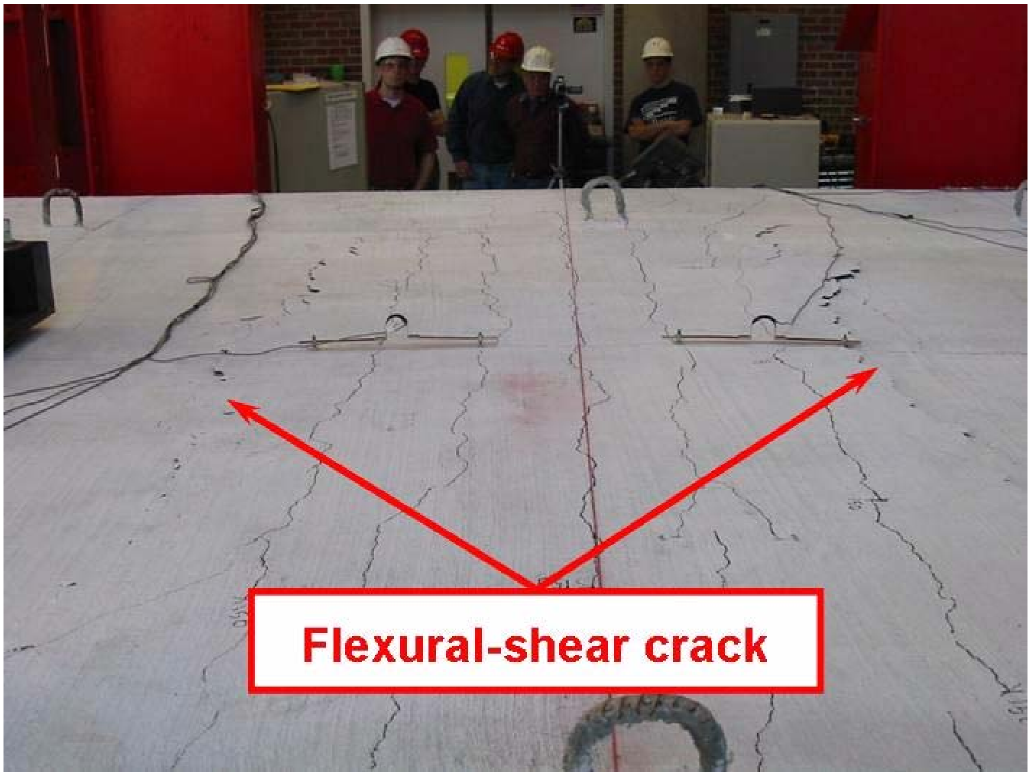

Figure 4.41: Flexural-shear cracks in the first bridge deck

- *Concrete Strain Profiles*

Based on the deformations measured by the PI gages, strain profiles were determined using the measured strain at the extreme top and bottom fibers of each bridge deck. It should be noted that all the strain profiles are plotted for the final loading cycle only, and therefore residual strains are shown at zero load. The strain profiles obtained from the two PI gages located in the right span at 14 in. (356 mm) from the centerline of the deck (T6 and B10 in Figure 4.14) are shown in Figure 4.42, through Figure 4.44, for the three bridge decks, respectively. Figure 4.45 shows the location of PI gage T6 with respect to the punching area of the first bridge deck. The strain profiles indicate that the top surface of the concrete at the vicinity of the punching area reached the limiting compressive strain value of 0.003.

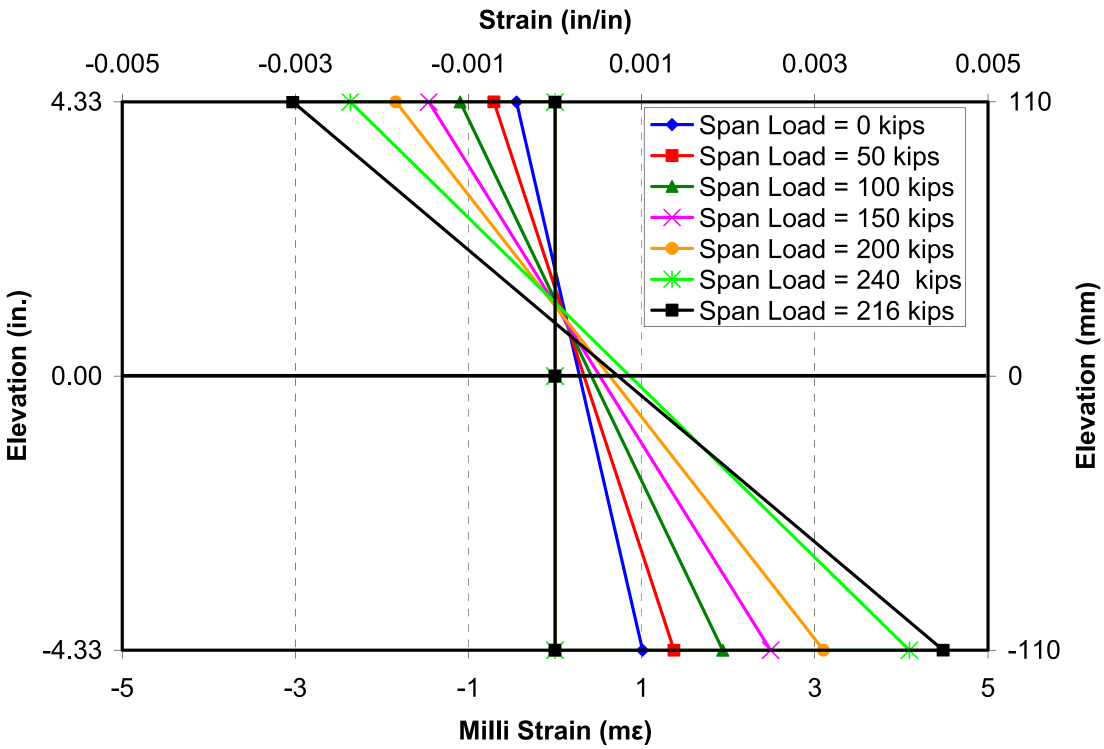

Figure 4.42: Strain profiles from T6 and B10 PI gages for the first bridge deck

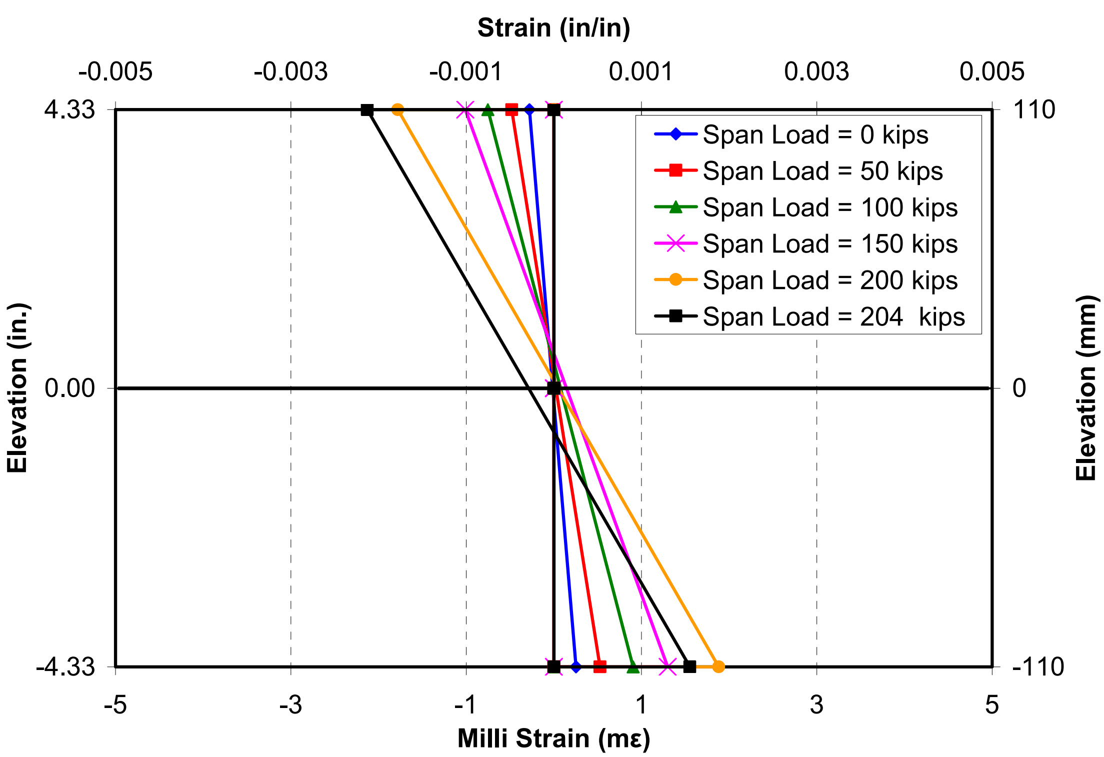

Figure 4.43: Strain profiles from T6 and B10 PI gages for the second bridge deck

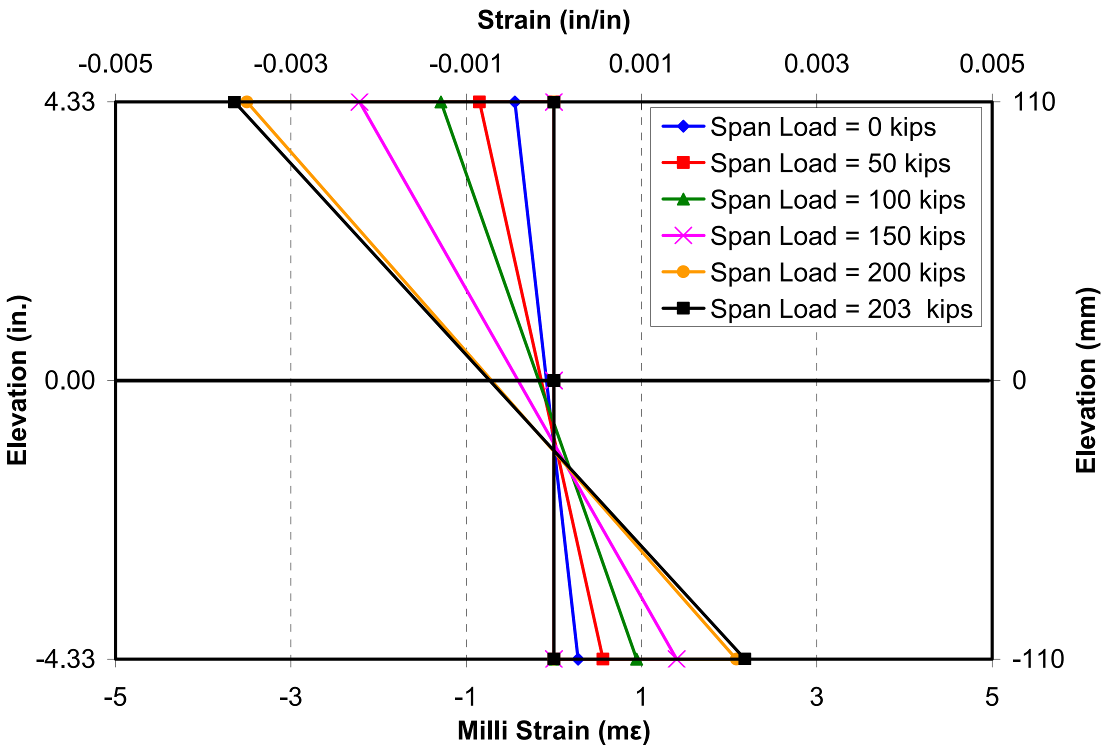

Figure 4.44: Strain profiles from T6 and B10 PI gages for the third bridge deck

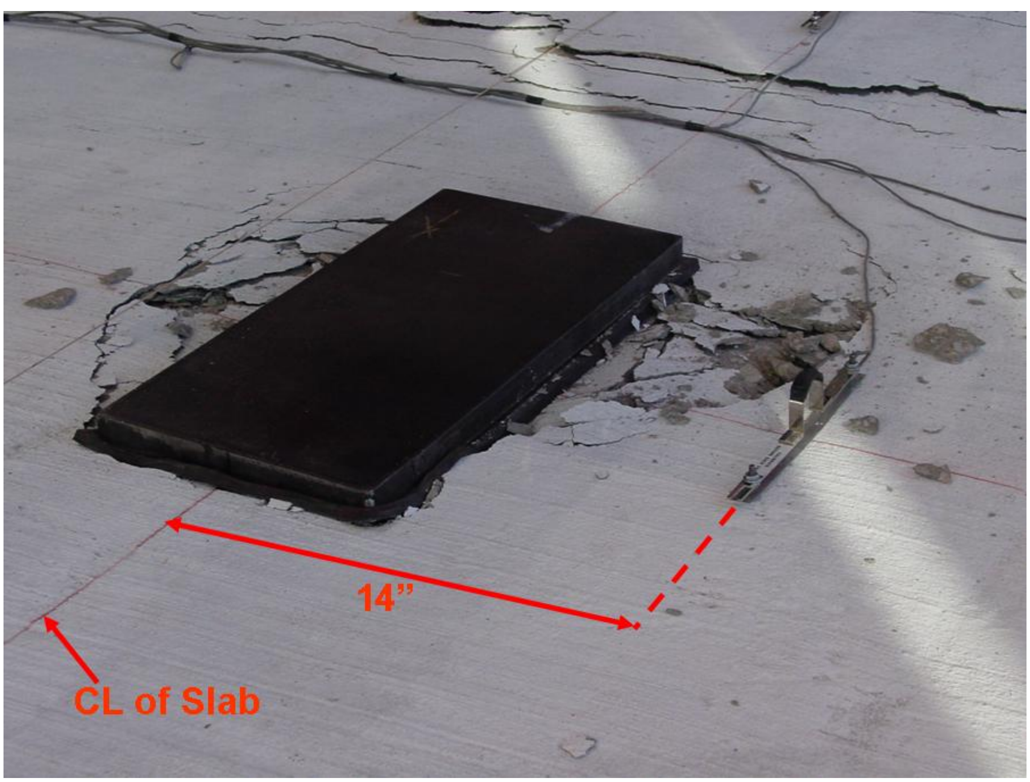

Figure 4.45: Location of PI gage T6

The strain profiles obtained from the PI gages at the edge of the right span (T8 and B12 in Figure 4.14) are shown in Figure 4.46, Figure 4.47, and Figure 4.48 for the three bridge decks, respectively. The strain profiles for the three decks show that the strain values were very small, which is another indication that the selected length of the bridge deck is effective and representative to the behavior of typical bridges.

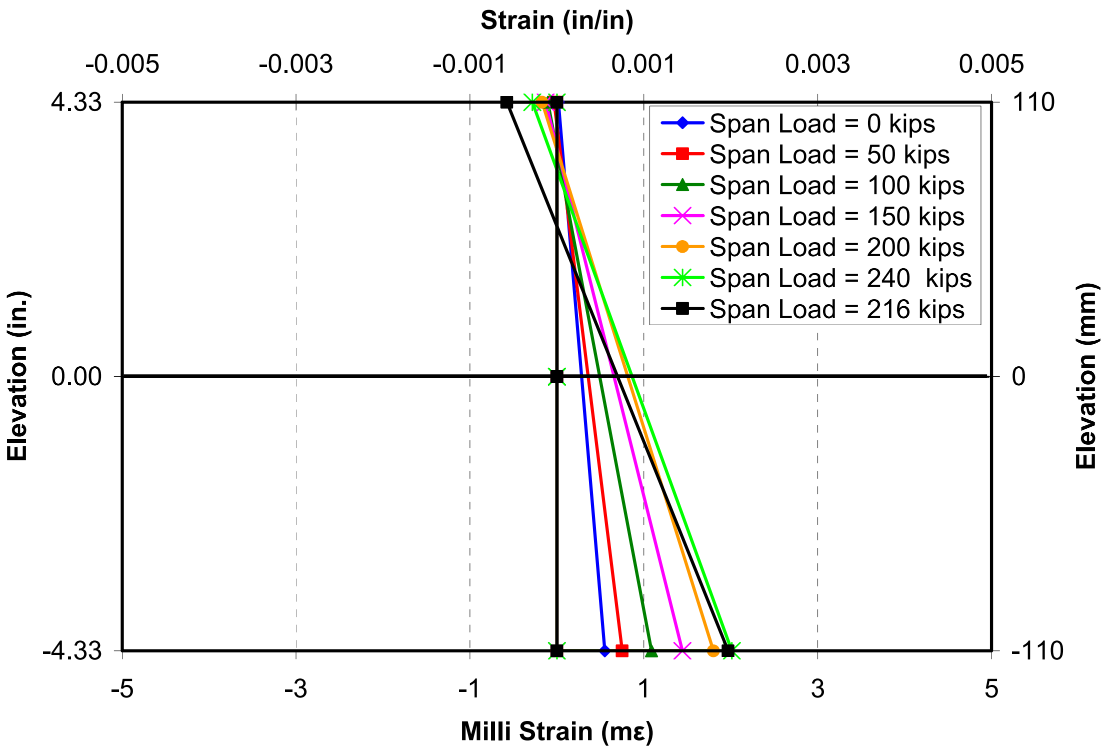

Figure 4.46: Strain profiles from T8 and B12 PI gages for the first bridge deck

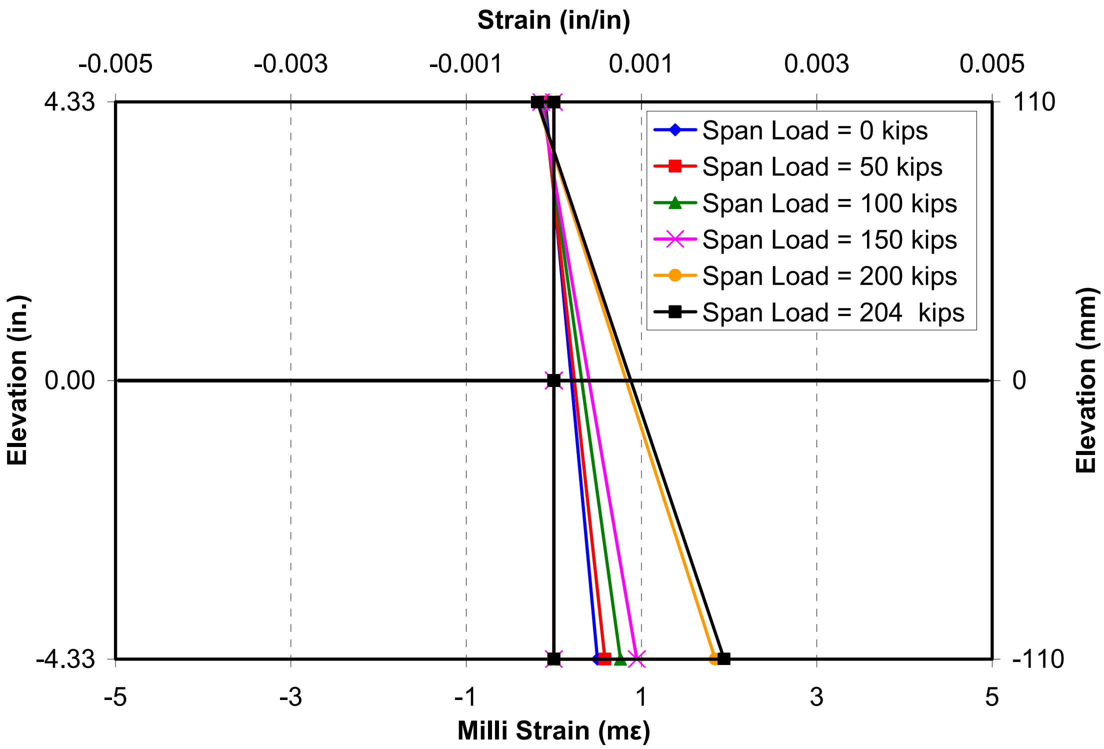

Figure 4.47: Strain profiles from T8 and B12 PI gages for the second bridge deck

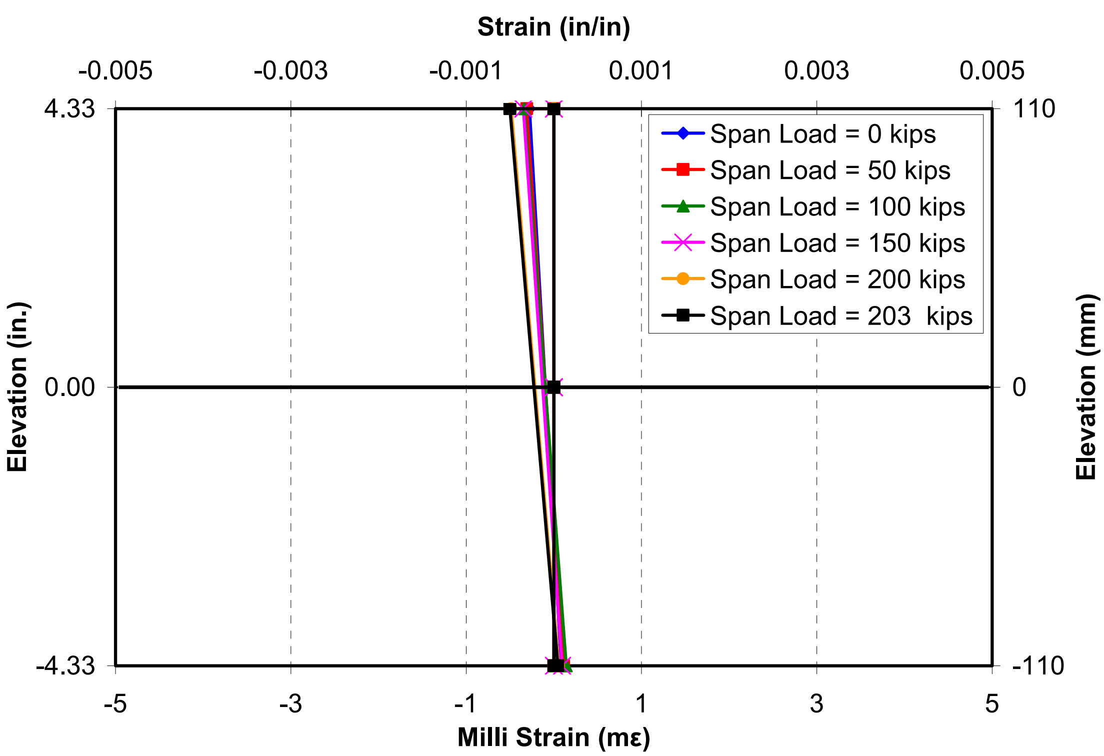

Figure 4.48: Strain profiles from T8 and B12 PI gages for the third bridge deck

- ***<u>Steel Strain</u>***

The strain in the steel was measured using conventional electrical strain gages, where twenty strain gages were used for each bridge deck. It should be noted that all the strain profiles are plotted for the final loading cycle only, and therefore residual strains are shown at zero load. The strain in the bottom transverse steel bars of the right span for the three bridge decks (see Figure 4.16) are shown in Figure 4.49 through Figure 4.51, respectively. Recalling that according to the ASTM-A370 offset method (0.2% offset) the yield strain of MMFX steel was determined to be 0.006 (6000 με) and the measured yield strength of Grade 60 steel was measured to be 68 ksi (469 MPa). It can be concluded that the steel bar next to the loading plate (approximately at mid-span) in the right span of the first bridge deck was close to yielding, but didn't yield. While for the second bridge deck the same bar yielded. However, it is also apparent that yielding of steel bars in the second bridge deck was very localized in the vicinity of the loading plate. Such conclusion is expected due to the punching shear failure mode of the right span for the bridge decks.

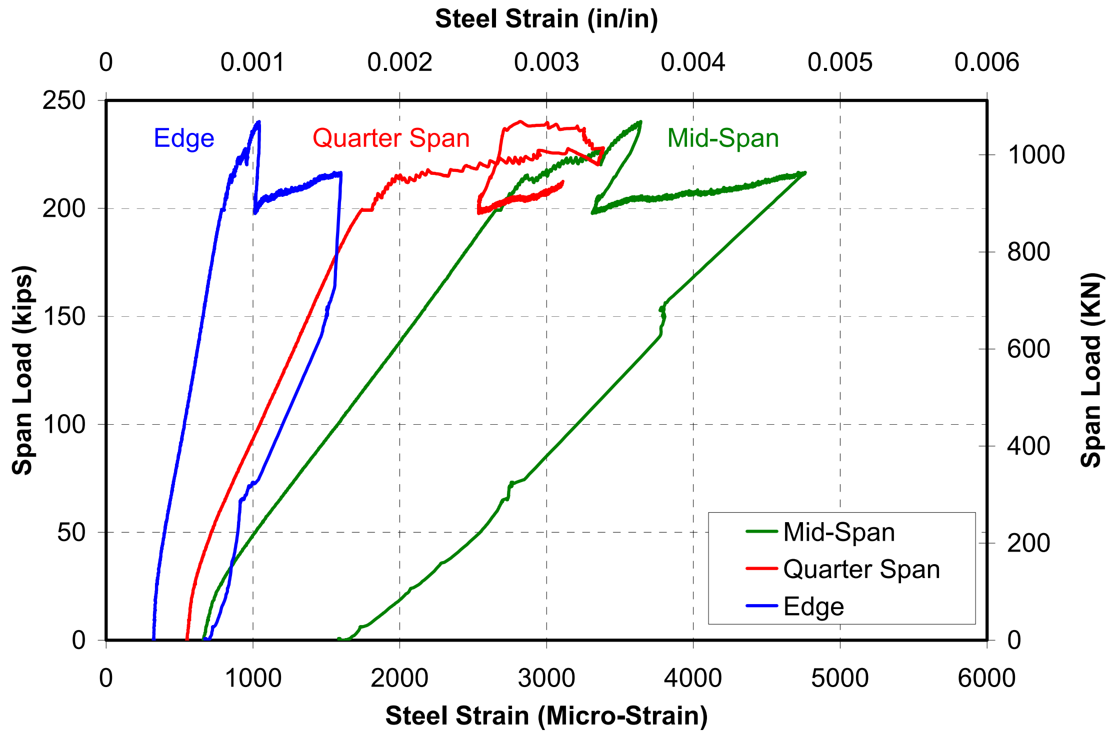

Figure 4.49: Strain in right span bottom transverse steel of the first bridge deck

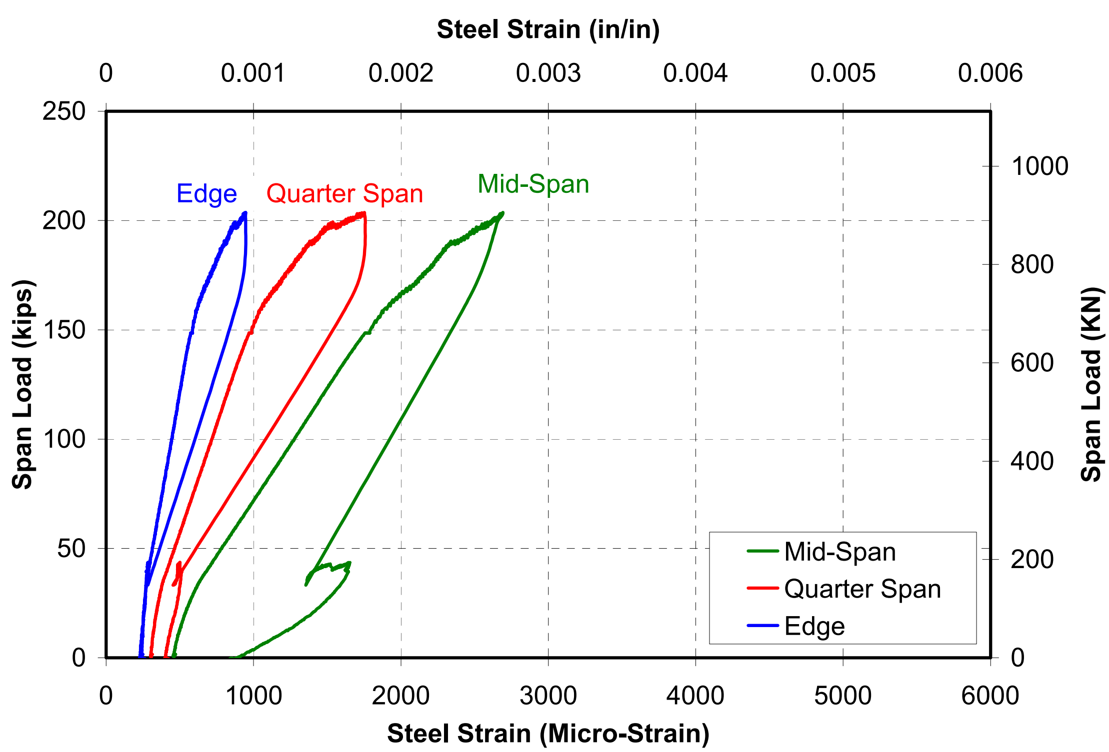

Figure 4.50: Strain in right span bottom transverse steel of the second bridge deck

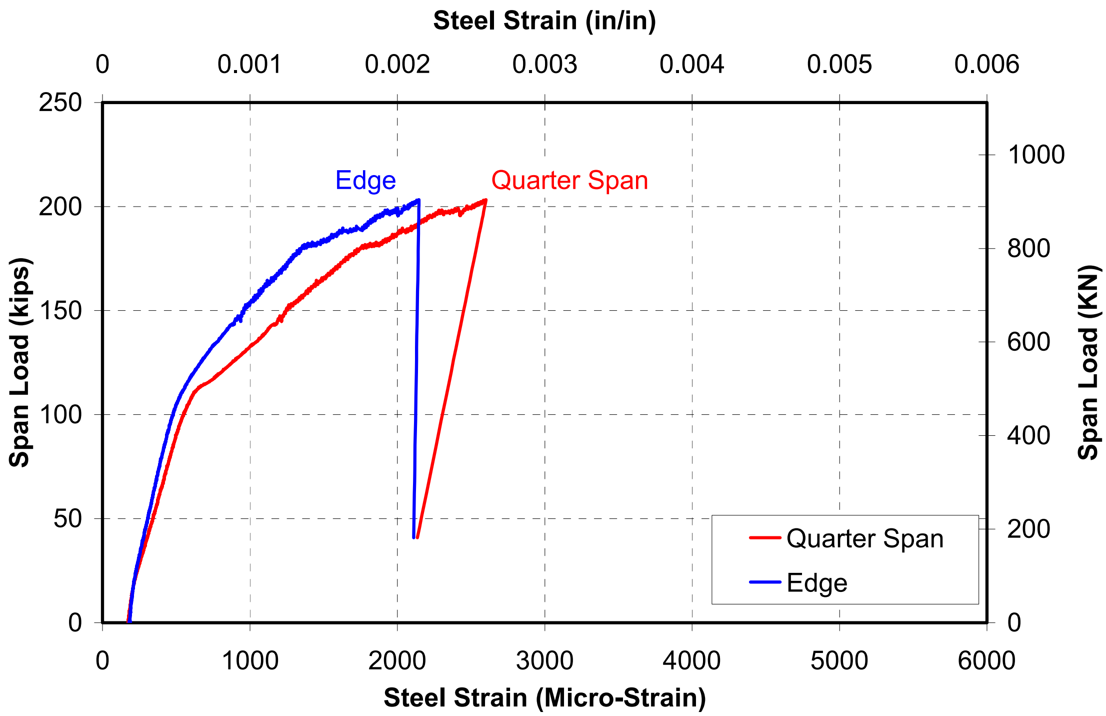

Figure 4.51: Strain in right span bottom transverse steel of the third bridge deck

The strain in the bottom transverse steel bars of the left span for the first and second bridge decks are given in Figure 4.52 and Figure 4.53, respectively. Again, from both figures it is readily apparent that central bars of the first bridge deck didn't yield, while for the second bridge deck they yielded. However, the yielding of the reinforcement was localized at the loaded area. The strain gages in the left span of the third bridge deck were lost, therefore, the results from the third bridge deck were not considered in this comparison.

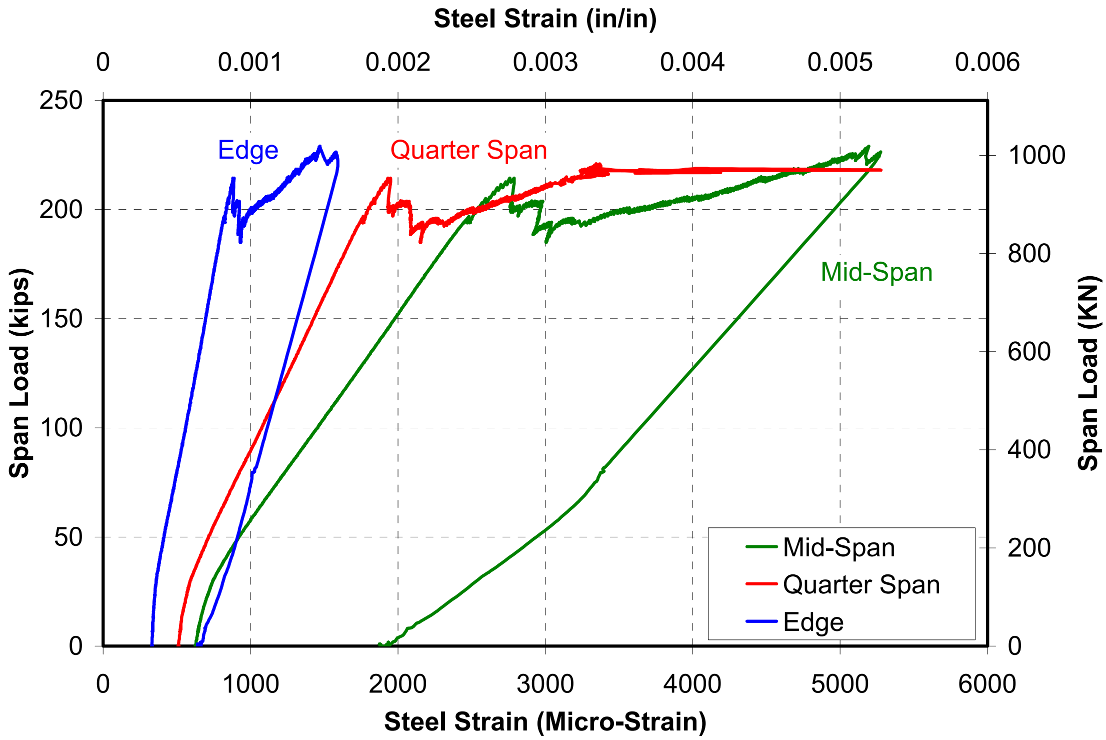

Figure 4.52: Strain in left span bottom transverse steel of the first bridge deck

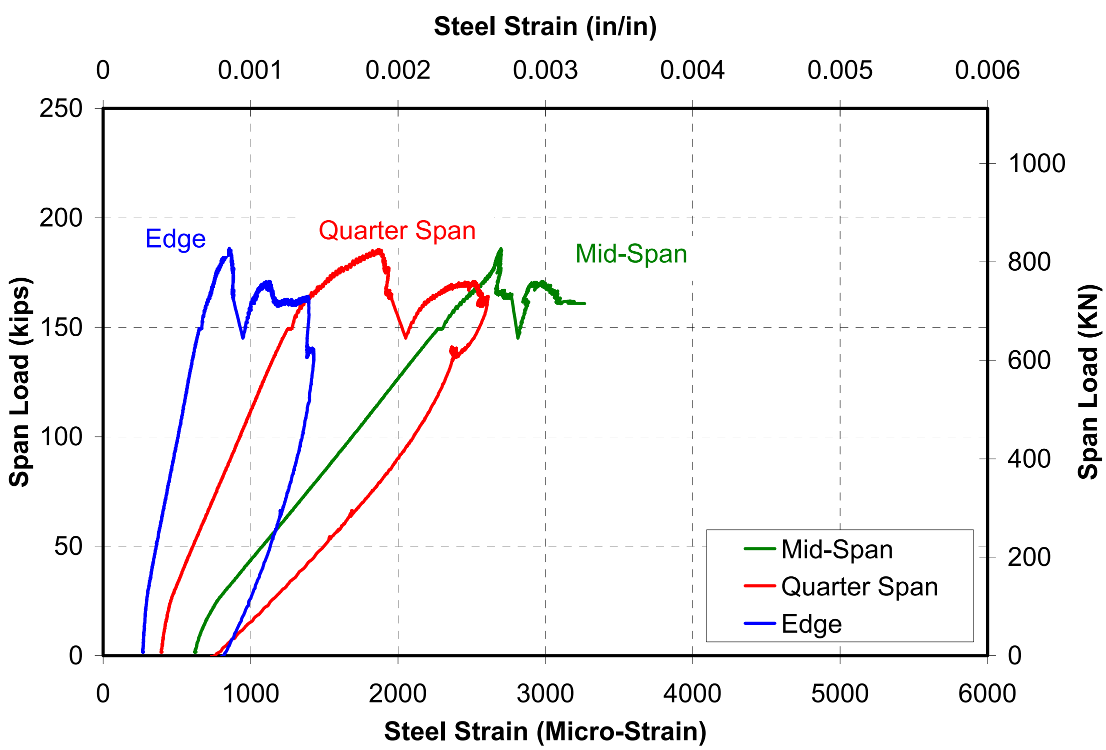

Figure 4.53: Strain in left span bottom transverse steel of the second bridge deck

- *Girders Rotation*

Rotation of the three supporting girders was monitored throughout the test of the three bridge decks as shown in Figure 4.54, through Figure 4.56 for the three decks, respectively. For all three decks the two outside girders exhibited larger rotations in comparison to the middle girder due to the unbalanced moment effect. In addition, the outside girders of the first bridge deck underwent more rotations due to the higher failure load than the other two decks.

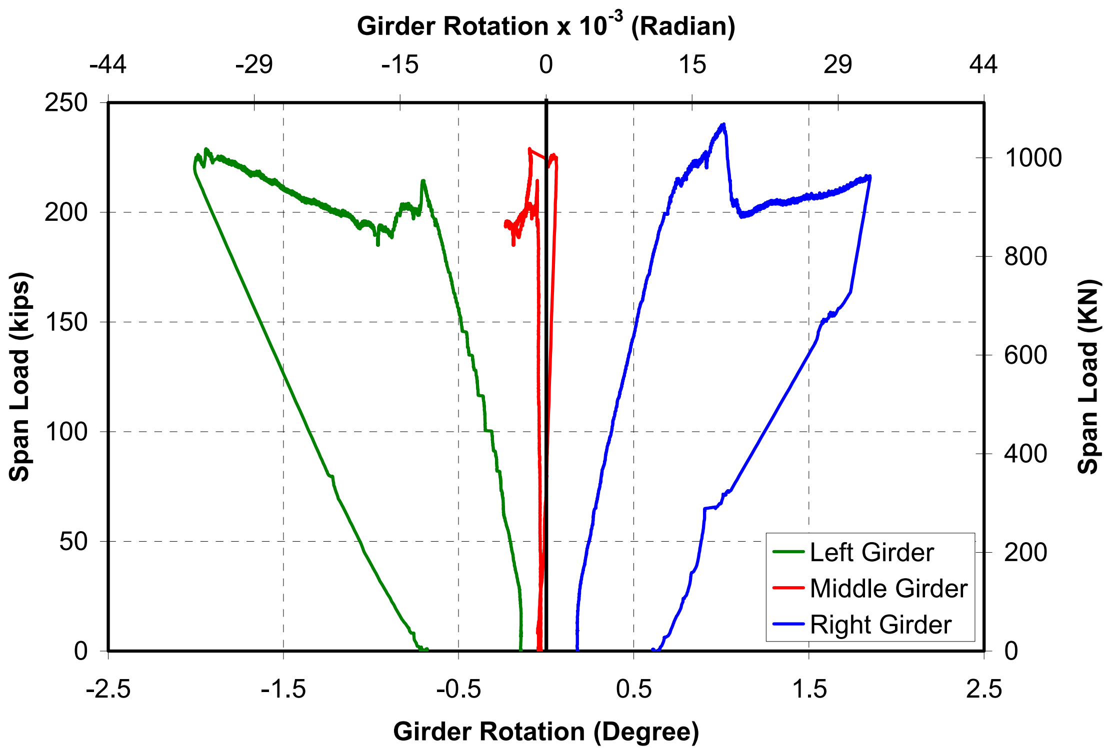

Figure 4.54: Girders rotation of the first bridge deck

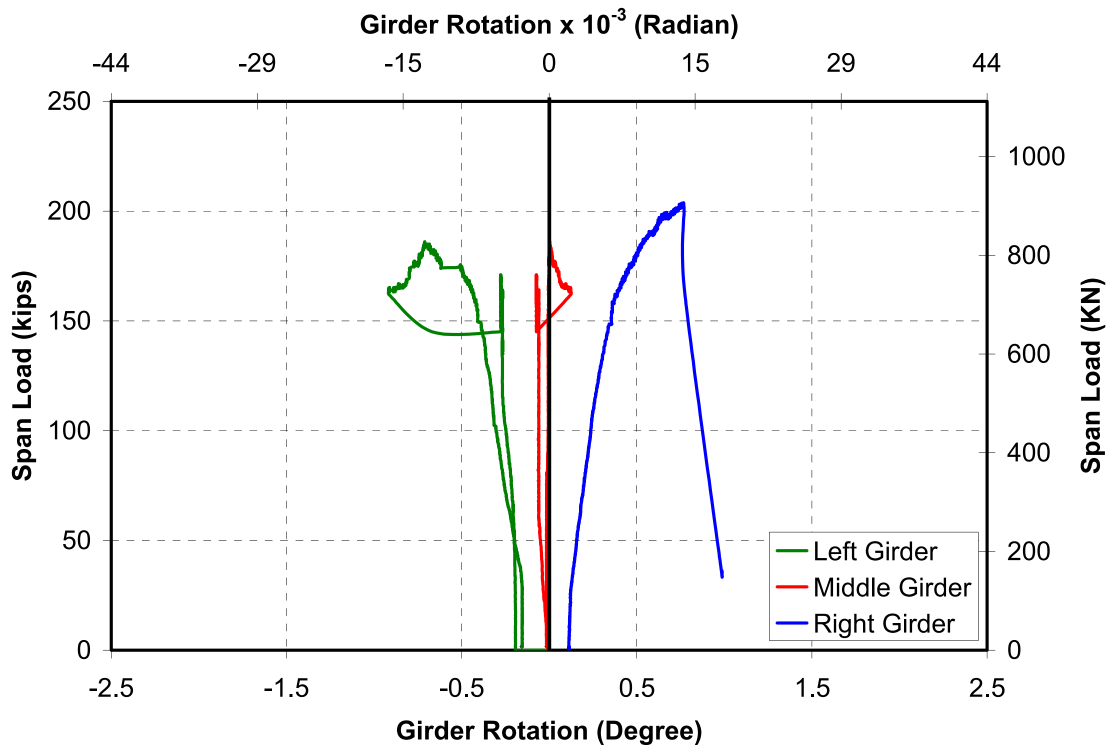

Figure 4.55: Girders rotation of the second bridge deck

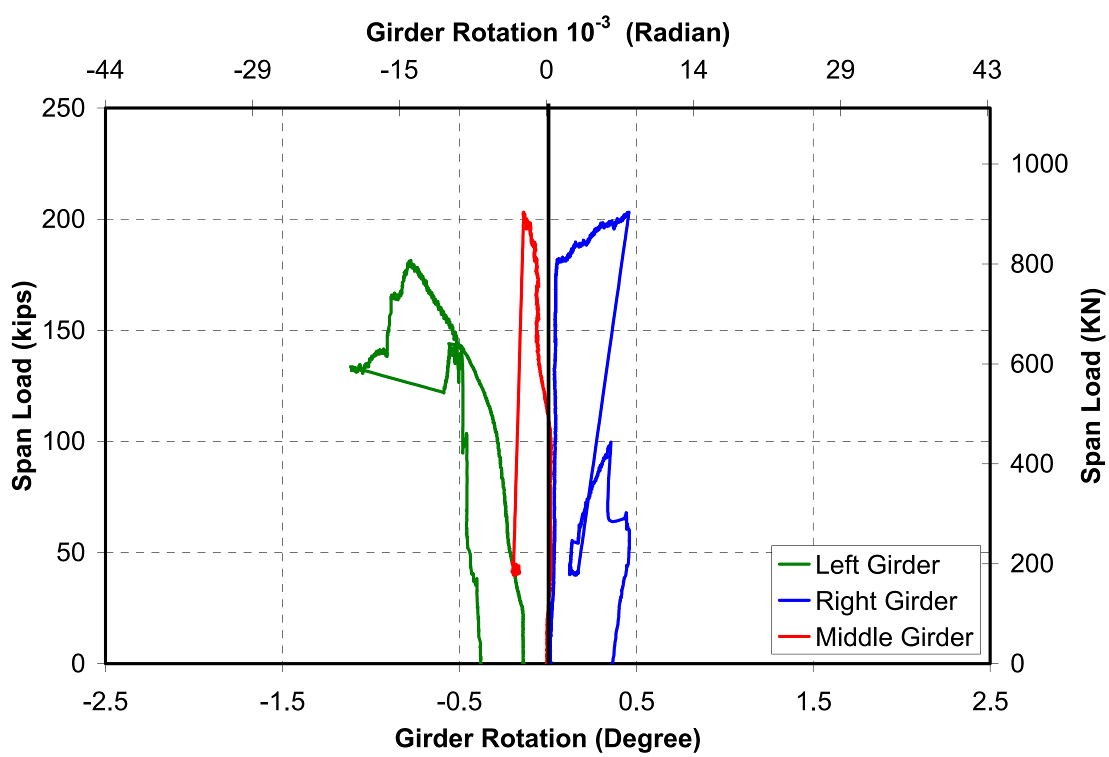

Figure 4.56: Girders rotation of the third bridge deck

- *Predicted strength*

The predicted shear strengths for the three bridge decks according to the different design codes are given in Figure 4.57 as well as the experimental values. The design codes included are: AASHTO LRFD Bridge Design Specifications (2004), American Concrete Institute (ACI 318-05), and Canadian Highway Bridge Design Code (CAN/CSA-S6-00). The equations used are as follow:

AASHTO 2004: $V_c = \min\left[0.063 + \frac{0.126}{\beta_c}; 0.126\right]\sqrt{f_c^{'}}\,b_o d$; units: kips & in.

ACI 318-05: $V_c = \min\left[2 + \frac{4}{\beta_c}; 4; \frac{\alpha_s d}{b_o} + 2\right]\sqrt{f_c^{'}}\,b_o d$; units: lbs & in.

CAN/CSA-S6-00: $V_c = \left[0.6 f_r + 0.25 f_{pc}\right] b_o d + 0.9 V_p$; units: N & mm

where;

V_c = punching shear capacity of bridge deck;

β_c = ratio of long side to short side of loading plate;

f_c' = concrete compressive strength;

b_o = perimeter of critical section at a distance of d/2 from loading plate;

d = effective section depth;

α_s = constant;

f_r = concrete tensile strength;

f_{pc} = compressive stress in concrete due to prestressing; and

V_p = component of effective prestressing force in direction of applied shear.

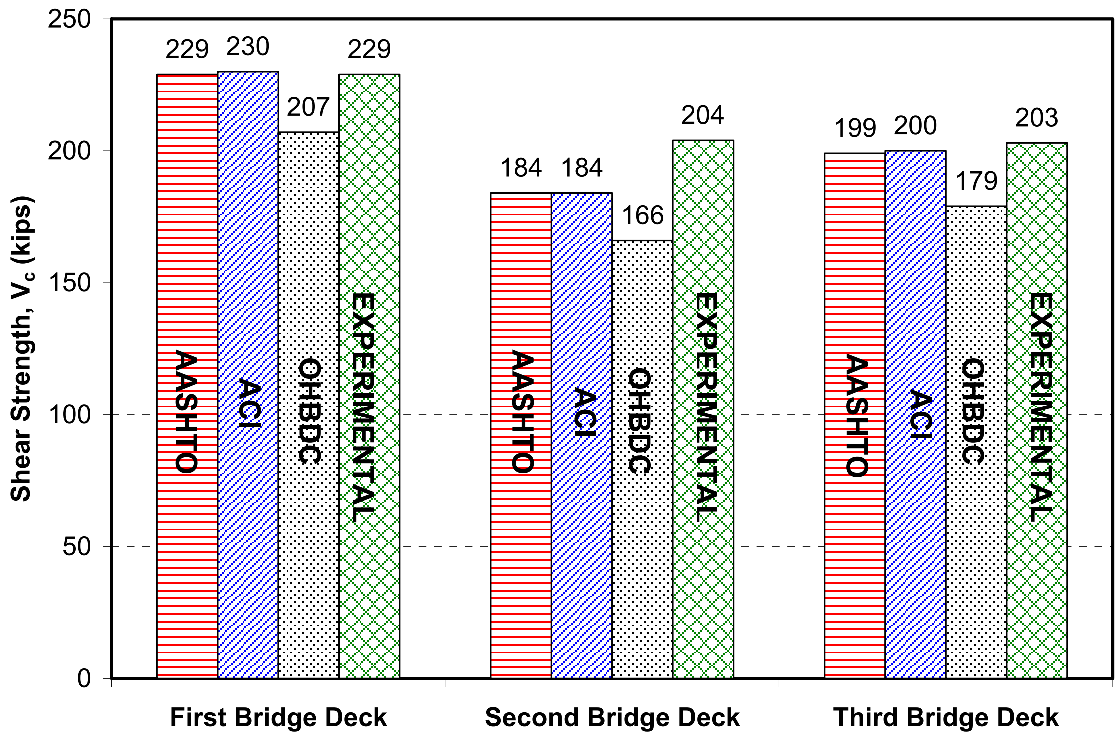

Figure 4.57: Predicted and experimental shear strength of the three bridge decks

It is clear from Figure 4.57 that the predicted values according to the AASHTO and ACI design codes predict very well the measured values for the bridge decks using MMFX and Grade 60 steel.

4.3. Effect of Bending on Tensile Strength

Since transverse reinforcement usually requires bending of bars and because of the strain hardening characteristics of MMFX steel, the effect of bending on the tensile strength of MMFX bars need to be evaluated, if MMFX bars are to be used for transverse reinforcement.

4.3.1. Specimens and Test Setup

The typical specimen used to evaluate the effect of bending of MMFX steel on its tensile strength consisted of two concrete blocks to anchor the two ends of the bent bar in the shape of a stirrup as shown in Figure 4.58. Two specimens were tested for each bar size, #4 (No.13) and #5 (No.16). The bend was 90^{o} according to ACI 318-05, as shown in Figure 4.58. The lengths of the MMFX stirrups were selected based on the dimensions of the concrete blocks, dimensions of the hydraulic jack, and the load cell placed between the concrete blocks. The total embedded part (straight and curved portions) of one end (left) of the stirrups was totally debonded from the concrete using a thick rubber tape, while on the other end (right) the straight portion only was debonded. The schematic details of the test setup layout for #5 (No.16) specimens are shown in Figure 4.59. The concrete blocks were heavily reinforced with conventional Grade 60 stirrups to prevent premature failure. The blocks were cast using wooden forms which were specially made to accommodate the anchored ends and to prevent stresses in the exposed bars before testing as shown in Figure 4.60.

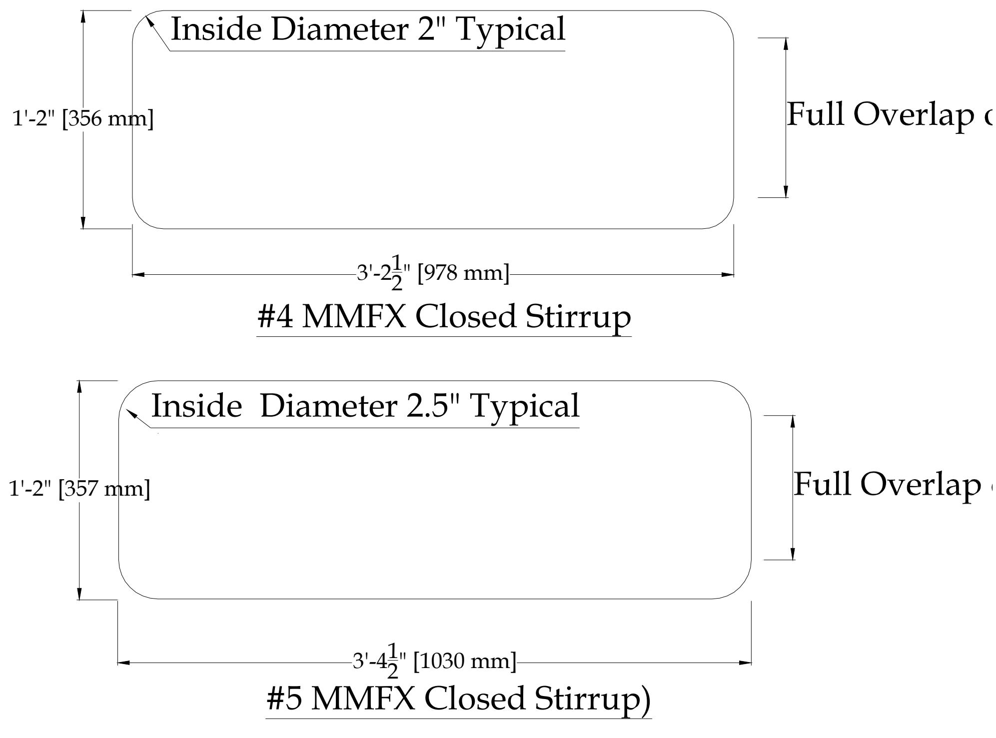

Figure 4.58: Dimensions of test stirrups

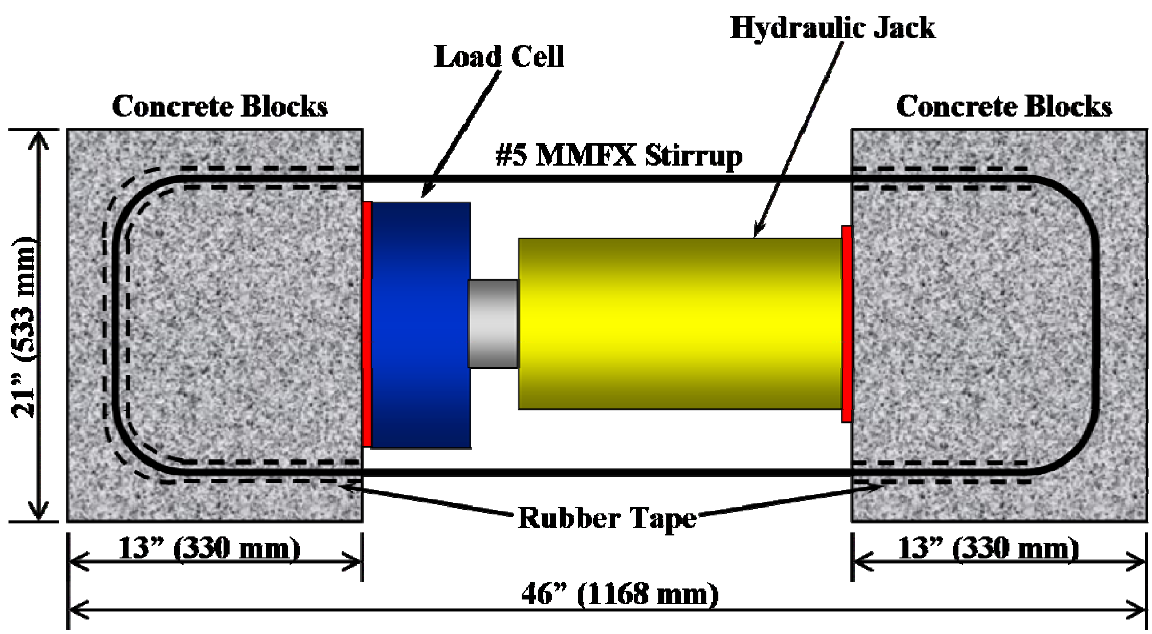

Figure 4.59: Schematic plan view of the test setup for #5 (No. 16) bent bars

Figure 4.60: Bent bars casting forms

The test setup shown in Figure 4.61, consists of a 120 kips (534 kN) hydraulic jack to apply the load between the two blocks, 150 kips (667 KN) load cell to measure the applied load, and four linear potentiometers to measure the relative displacement between the two blocks. The hydraulic jack and the load cell were centered between the two branches of the stirrup to ensure equal distribution of forces in each branch. An MTS axial mechanical extensometer of 2 in. (51 mm) gage length was mounted on the exposed length of the stirrup to measure the elongation during loading. An OPTIM Megadac data acquisition system was used to electronically record the readings of the load cell, the potentiometers, and the extensometer.

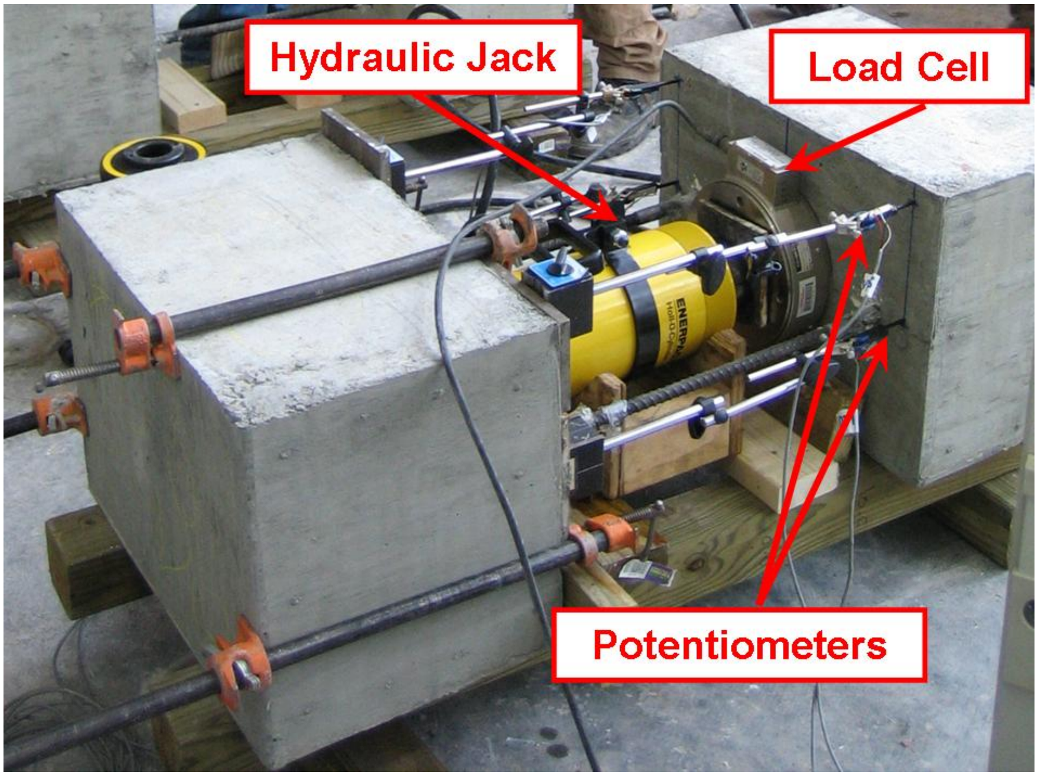

Figure 4.61: Isometric view of the bent bars test setup

4.3.2. Test Results

Failure of the four bent bars occurred inside the blocks at the end that was totally debonded from the concrete. The measured stress-strain relationships for #4 (No.13) and #5 (No.16) bent bars along with the data measured for straight bars are shown in Figure 4.62 and Figure 4.63, respectively. After testing, the concrete blocks of the four specimens used for #4 (No. 13) and #5 (No. 16) MMFX bars were cut using a concrete saw to inspect the location of failure. As expected, the four specimens failed at the bend location. Figure 4.64 through Figure 4.67 show the failure location of the four specimens after cutting the concrete blocks. The modes of failure of the four bars and the measured stress-strain characterizes of the bent bars indicate that their behavior are similar to the straight bars including the linear and the non-linear behavior up to strain value of 1.5 percent. Test results also indicate that bending of the MMFX bars induced residual strain affecting both the strength and the strain at ultimate. This strain reflects the well established phenomenon of the presence of stress concentration at the bend location resulting from the bending process. Based on the limited number of tests, the results suggest that bending of MMFX bars up to 90 degrees reduces their ultimate strength by 6 percent and their ultimate strain by 70 percent. Typically debonded bent bars are used in special applications, e.g. lifting hooks; therefore, in such applications the reduced strength should be considered. It should be noted that in concrete structures, the bent bars are bonded to the concrete which is expected to enhance their behavior. This is in agreement with the finding of a previous study conducted at the Constructed Facilities Laboratory, North Carolina State University, El-Hacha and Rizkalla (2002). In the previous study, the bent bars were bonded to the concrete and failure occurred in the exposed portion of the stirrup indicating that the behavior of bonded MMFX bent bars is similar to straight bars.

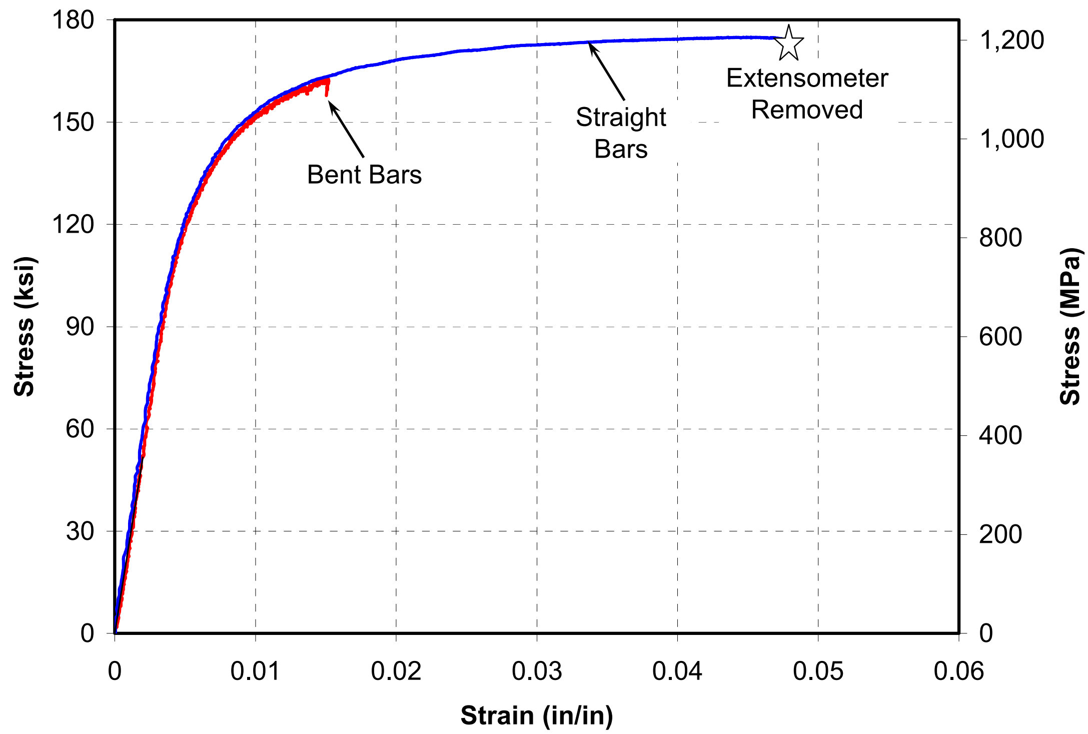

Figure 4.62: Stress-Strain relationship for #4 (N0. 13) bent and straight MMFX bars

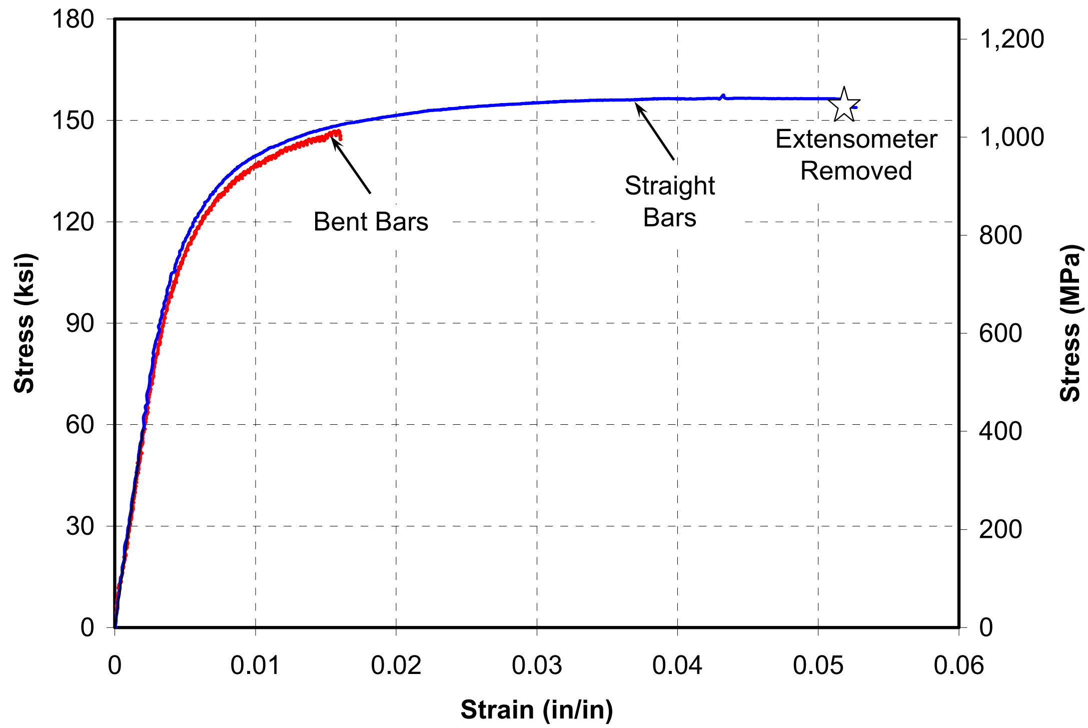

Figure 4.63: Stress-strain relationship for #5 (No. 16) bent and straight MMFX bars

Figure 4.64: Failure location of the first specimen of #4 (No. 13) MMFX bent bar

Figure 4.65: Failure location of the second specimen of #4 (No. 13) MMFX bent bar

Figure 4.66: Failure location of the first specimen of #5 (No. 16) MMFX bent bar

Figure 4.67: Failure location of the second specimen of #5 (No. 16) MMFX bent bar

4.4. Rate of Corrosion

MMFX Technologies Corporation, the manufacturer of MMFX steel, claims that MMFX steel exhibits improved corrosion performance when compared to conventional (ASTM A 615) steel. The company product bulletin, MMFX (2002) estimates the years of service life of concrete structures reinforced with MMFX steel to be 75+ years, in comparison to 15-30 years for structures reinforced with conventional steel, MMFX (2002). It was pointed out by CIAS report (2003) that this claim is supported by test results of a non-standard short-term Accelerated Chloride Threshold (ACT) test. The ACT test showed MMFX steel has lower corrosion rate than conventional reinforcing steel.

In order to investigate the rate of corrosion and the effect of corrosion on the tensile strength of MMFX steel bars, an accelerated corrosion test was conducted as described below. For comparison purposes conventional Grade 60 that has been used in reinforcing the second bridge deck model was included in the test.

4.4.1. Test Setup

MMFX and Grade 60 steel bars were immersed in salt-water solution (15% NaCl with PH of 7) at constant high temperature of 130 ^{o}F. High frequency wet-dry cycles were used for accelerated corrosion. One complete wet-dry cycle consisted of one week of wetting and one week of drying. #4 (No. 13) and #5 (No. 16) MMFX steel bars, and #5 (No. 16) Grade 60 steel bars were included in this study. Twelve specimens, 18 in. (457 mm) in length for each bar diameter, were immersed in the salt-water solution. After 6 weeks (3 wet-dry cycles) and 12 weeks (6 wet-dry cycles), three specimens of each bar diameter at each age were removed from the immersion tubs and then cleaned according to ASTM G1-03. The ASTM G1-03 provides a number of options for chemical cleaning of the rusted bars. After cleaning, the bars were weighted to determine the weight loss followed by testing in the MTS testing machine to obtain the stress-strain relationship of the corroded bars to evaluate the effect of corrosion on the tensile strength of MMFX Steel and Grade 60 steel.

The test setup shown in Figure 4.68 consists of two plastic tubs to accommodate the test specimens, where the MMFX steel was placed in one tub and the Grade 60 was placed in the other one. The tub accommodating the Grade 60 steel specimens was filled with salt-water while the other tub accommodating the MMFX steel specimens was empty at the beginning of the wet-dry cycles, which started on November 2nd, 2005. A submersible pump was used to transfer the salt-water solution between the tubs at the end of each week. A special salt-water heater with a built-in thermostat was used to maintain the water temperature and a submersible salt-water circulating-pump was used to ensure uniform salt concentration. The plastic tubs were wrapped up with "Styrofoam" to thermally insulate them and reduce the heat loss. The tub containing the salt-water solution was covered with a plastic lid to minimize the water evaporation as shown in Figure 4.69.

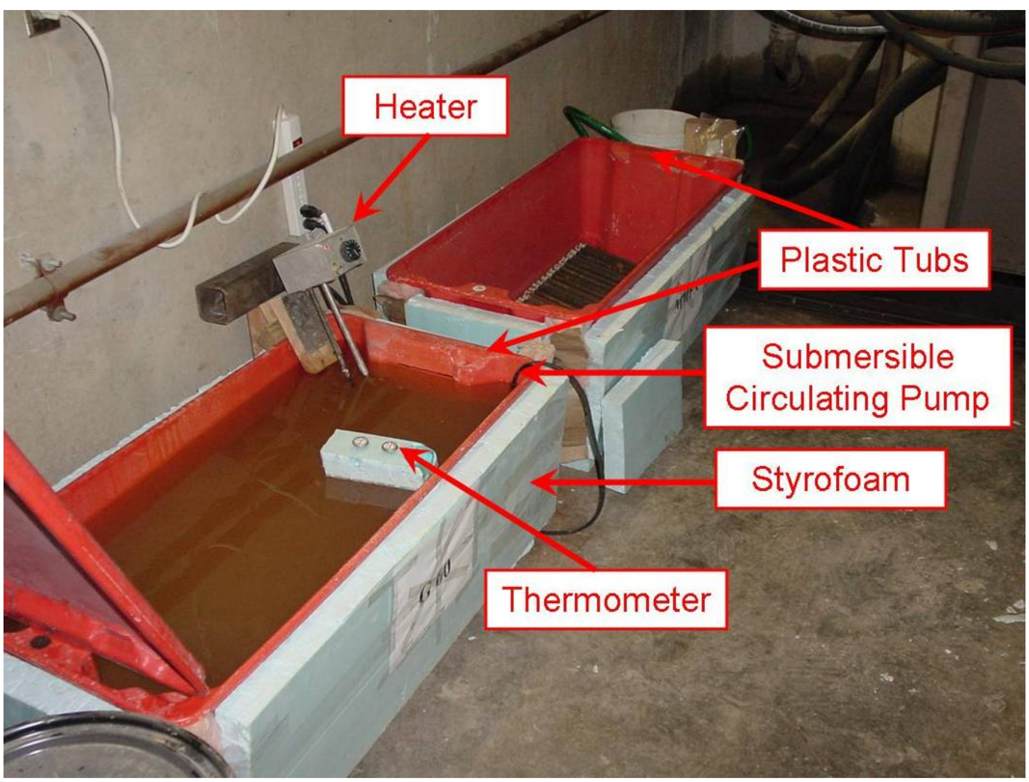

Figure 4.68: Corrosion test setup at the beginning of the cycles

Figure 4.69: Corrosion test setup during the first week

PH indicator papers were used for measuring the PH value of the salt-water solution. Those PH indicators are color-bonded paper strips with a PH range of 5-10 and a graduation unit of 0.5. Figure 4.70 shows the process of measuring the PH value of the salt-water solution. Salinity was checked with two methods, a quick one with direct observation which was conducted on daily basis and another more accurate method which was performed on longer intervals. At the beginning of the test, the initial water level was marked and water was added every two days to compensate for the effect of the evaporated water. The more accurate method was to take a sample of the water, determine the original weight, and after boiling the water to evaporate the salt concentration was determined by weight.

Figure 4.70: Measuring salt-water solution PH value

The specimens were cleaned by using a mixture of 1000 ml of hydrochloric acid (HCl), 7.0 grams of hexamethylene tetramine ($C_6H_{12}N_4$) and 1000 ml of reagent water to remove the corrosion products without removing any of the base metal. When soaked in this solution mixture, the bars would actually lose the majority of corrosion products to a chemical reaction with the liquid. This mixture was chosen based on the recommendations found in Cook (2004). The bars were soaked in the solution for 10-minutes cycles, while weighting after each cycle until no significant mass loss could be recorded. For this study, three cycles were found to provide the desired accuracy, as weight changes after 3 cycles diminished, as shown in the following section. Figure 4.71, Figure 4.72, and Figure 4.73 show the various steps in the mass loss measurement process.

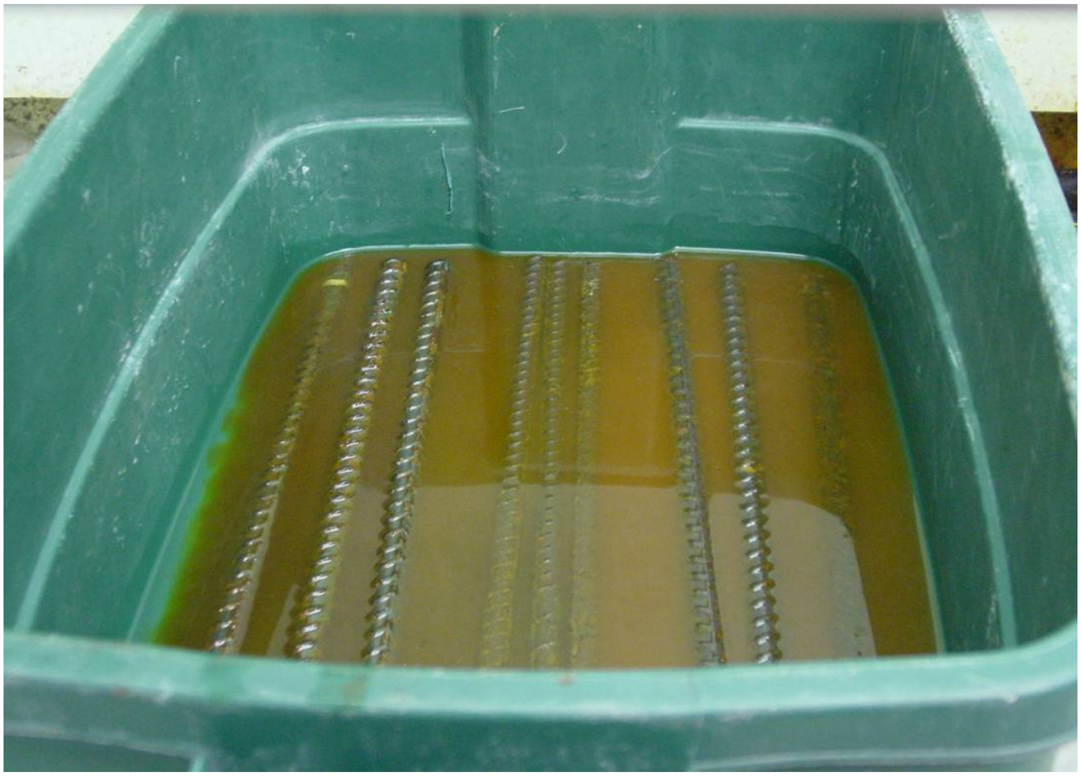

Figure 4.71: Bars submerged in chemical cleaning solution

Figure 4.72: Drying the bars after submerging in the chemical solution

Figure 4.73: Weighing a bars after the cleaning process

4.4.2. Test Results

- *<u>Results after 6 Weeks (3 Wet-Dry Cycles)</u>*

After completing 6 weeks (3 wet-dry cycles) of test on December 14th, 2005 the first three specimens of each bar diameter were removed and cleaned as discussed earlier. Figure 4.74 and Figure 4.75 show the specimens after 6 weeks (3 wet-dry cycles) before and after cleaning, respectively. The obtained results after 6 weeks of exposure are summarized in Table 2. Judging from Figure 4.74 and Figure 4.75 and considering the small values of the weight loss, it can be justified that the measured corrosion at 6 weeks was due to surface rust, which is expected for short period of testing. Despite the low values of the weight loss, the results seem to indicate that MMFX steel tends to have lower corrosion rate compared to conventional Grade 60 steel. Moreover, the results shown in Table 2 for #5 (NO. 16) bars demonstrate that MMFX steel has a corrosion rate of one-half that of conventional Grade 60 steel. However, results after longer period of exposure are needed to fully justify this conclusion.

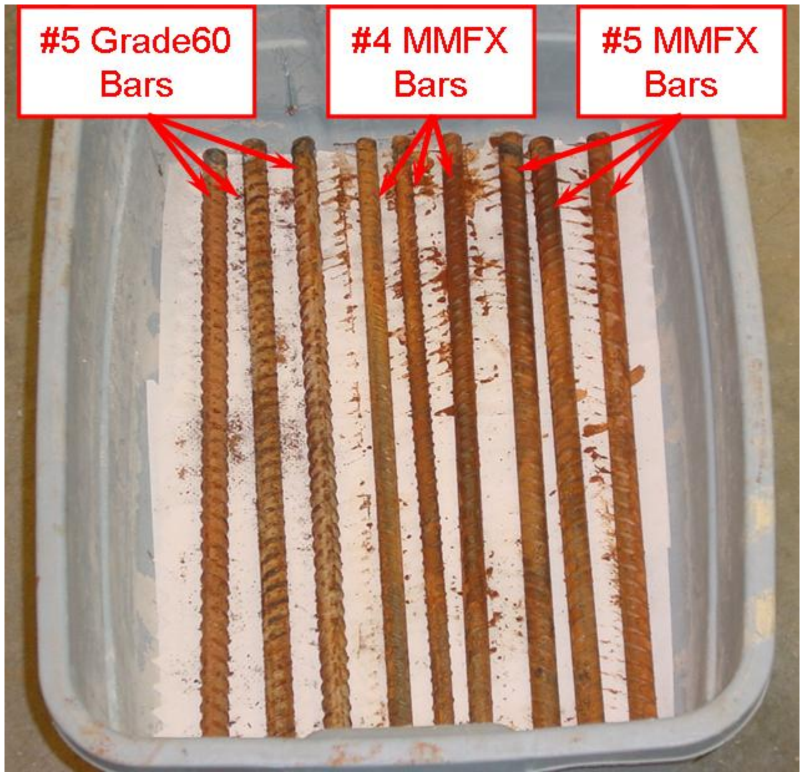

Figure 4.74: Corroded bars before cleaning at 6 weeks

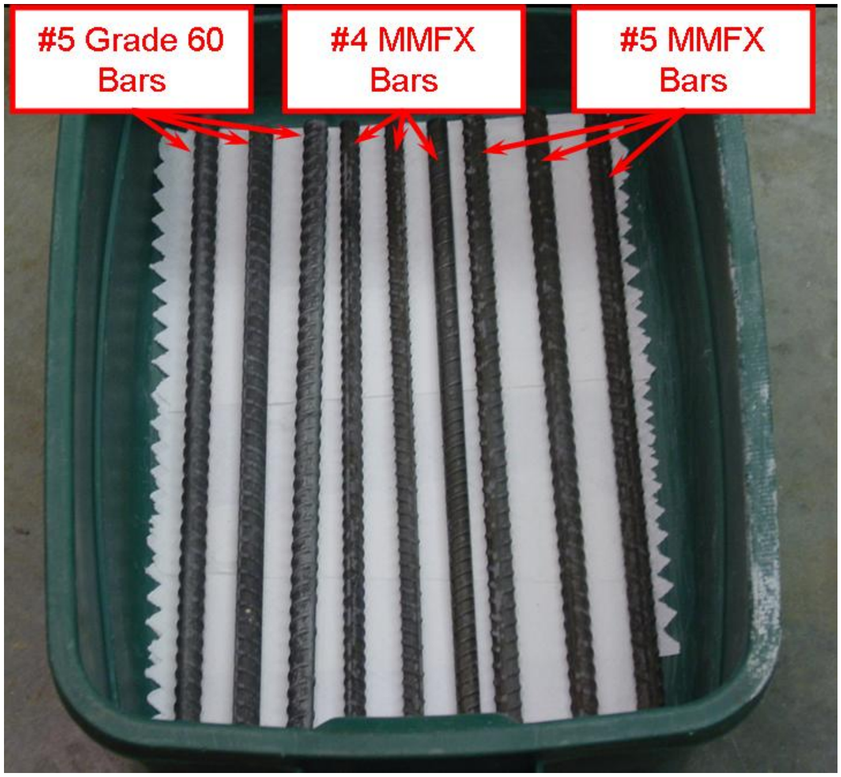

Figure 4.75: Corroded bars after cleaning at 6 weeks

Table 2: Weight of Corroded bars after 6 weeks (3 wet-dry cycles)

Bar	Steel	Bar Size	Weight (lbs)				Weight Loss (%)	Average Weight Loss (%)
			Original	First Cycle	Second Cycle	Third Cycle		
1	MMFX	#4 (No. 13)	0.9850	0.9775	0.9770	0.9765	0.86	0.86
2			0.9830	0.9755	0.9745	0.9745	0.86	
3			0.9820	0.9745	0.9735	0.9735	0.87	
1		#5 (No. 16)	1.5095	1.5020	1.5010	1.5010	0.56	0.57
2			1.5125	1.5045	1.5035	1.5035	0.60	
3			1.5095	1.5020	1.5010	1.5010	0.56	
1	Grade 60	#5 (No. 16)	1.5105	1.4925	1.4915	1.4915	1.26	1.23
2			1.5075	1.4895	1.4890	1.4890	1.23	
3			1.4975	1.4820	1.4795	1.4795	1.20	

Figure 4.76, Figure 4.77, and Figure 4.78 show the stress-strain characteristics of the corroded bars for #4 (No. 13) and #5 (No. 16) MMFX steel bars, and #5 (No. 16) Grade 60 steel bars, respectively, after 6 weeks (3 wet-dry cycles) of test. The results demonstrate the effect of corrosion on the tensile strength and the stress-strain relationship. It should be noted that the removal of the extensometer is not due to rupture of the specimen, but is due to the formation of the neck outside the MTS extensometer 2-in gage length. However, the neck occurred outside the extensometer gage length for all the corroded specimens except one specimen of #5 (No. 16) MMFX, as shown in Figure 4.79. The stress-strain relationship for the corroded bars indicates that there is no effect of corrosion on the tensile strength of #4 (No. 13) and #5 (No. 16) MMFX bars, and #5 (No. 16) Grade 60 steel bars after 6 weeks (3 wet-dry cycles) of exposure. However, this conclusion can not be extended to longer periods of testing.

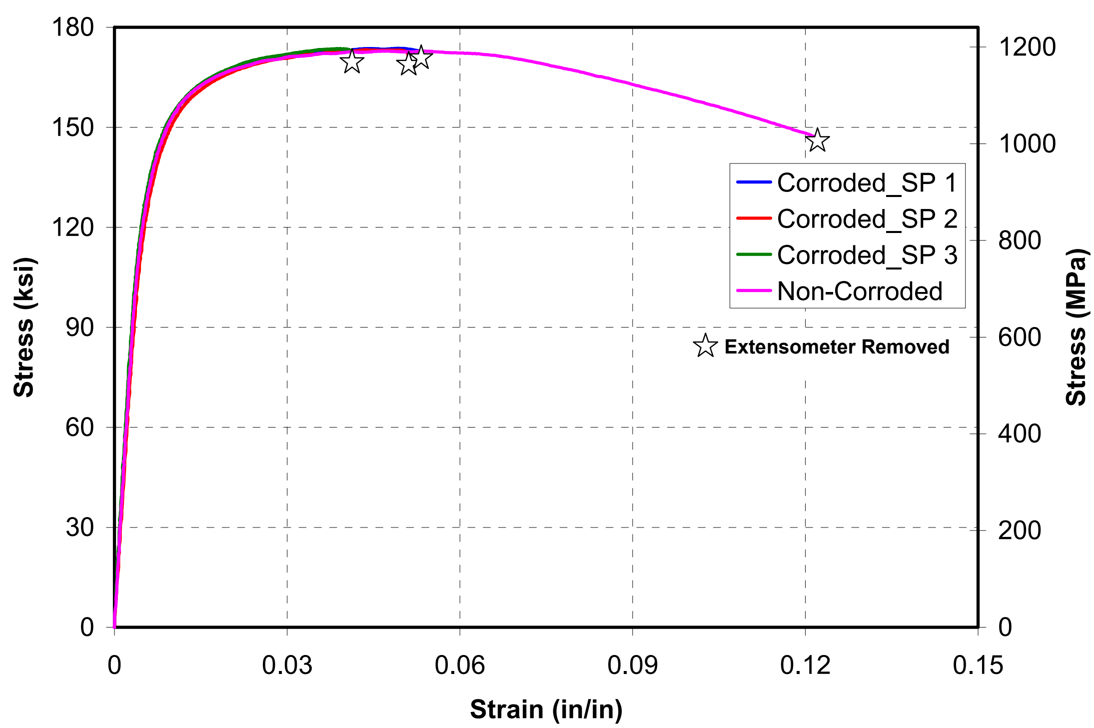

Figure 4.76: Stress-Strain relationship for #4 (No. 13) MMFX corroded bars at 6 weeks

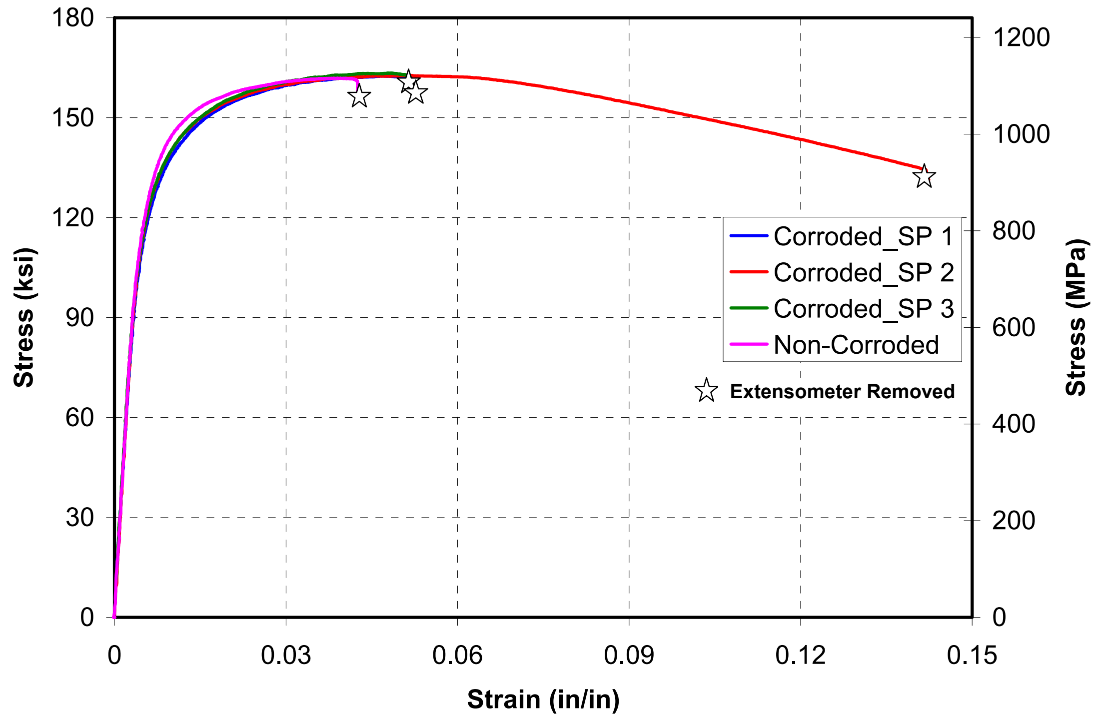

Figure 4.77: Stress-strain relationship for #5 (No. 16) MMFX corroded bars at 6 weeks

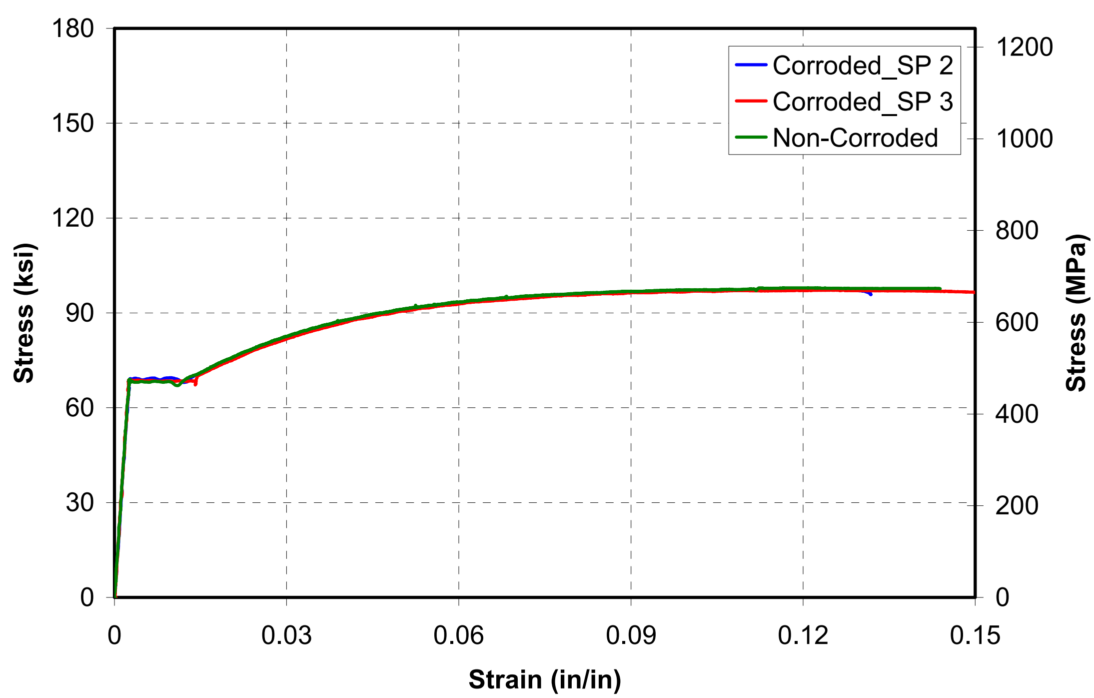

Figure 4.78: Stress-Strain relationship for #5 (No. 16) Grade 60 corroded bars at 6 weeks

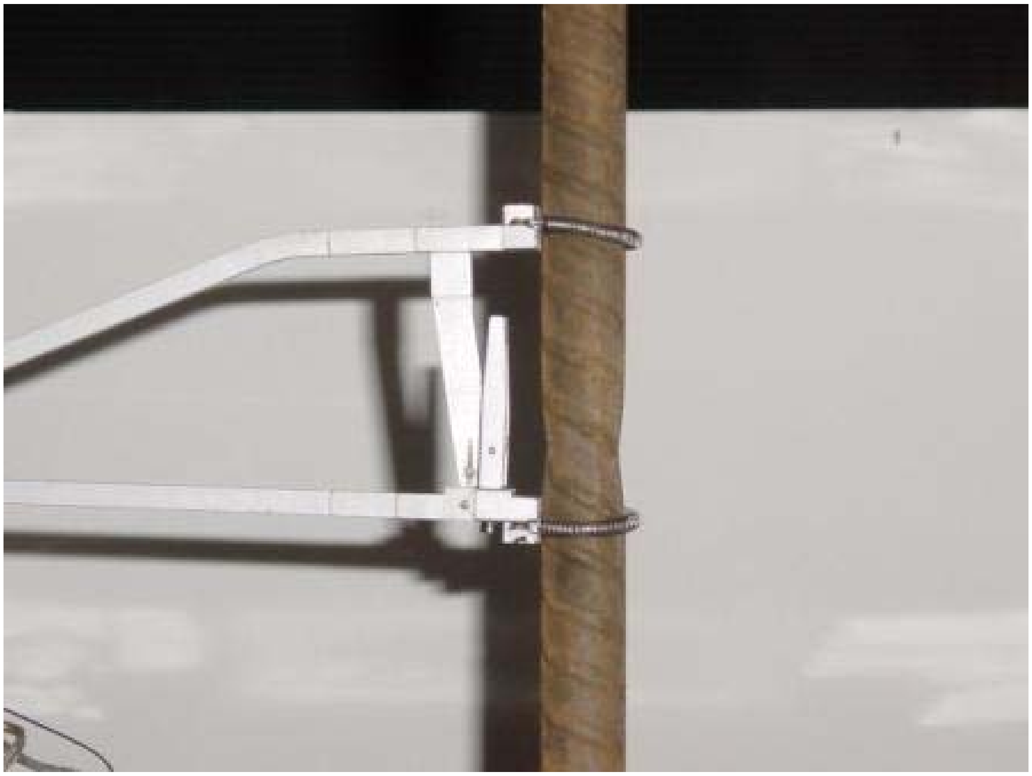

Figure 4.79: Necking occurring inside the MTS extensometer gage length

- *Results after 12 Weeks (6 Wet-Dry Cycles)*

After completing 12 weeks (6 wet-dry cycles) of test on January 25th, 2006 another three specimens of each bar diameter were removed and cleaned as discussed earlier. Figure 4.80 and Figure 4.81 show the specimens before and after cleaning, respectively. The obtained results after 12 weeks of exposure are summarized in Table 3. Similar to 6 weeks results, judging from Figure 4.80 and Figure 4.81 and considering the small values of the weight loss, it can be justified that the measured corrosion at 12 weeks was due to surface rust. However, pits were randomly distributed along the bars and were clearly seen on the surface of the bars as shown in Figure 4.82, Figure 4.83, and Figure 4.84. Pitting is a localized corrosion due to chloride ions found in the salt-water solution. Despite the low values of the weight loss, the results confirm that MMFX steel have a lower corrosion rate compared to conventional Grade 60 steel. Moreover, the results shown in Table 3 for #5 (NO. 16) bars demonstrate that MMFX steel has a corrosion rate of about one-third that of conventional Grade 60 steel. However, results after longer period of exposure are needed to fully justify this conclusion.

Figure 4.80: Corroded bars before cleaning at 12 weeks

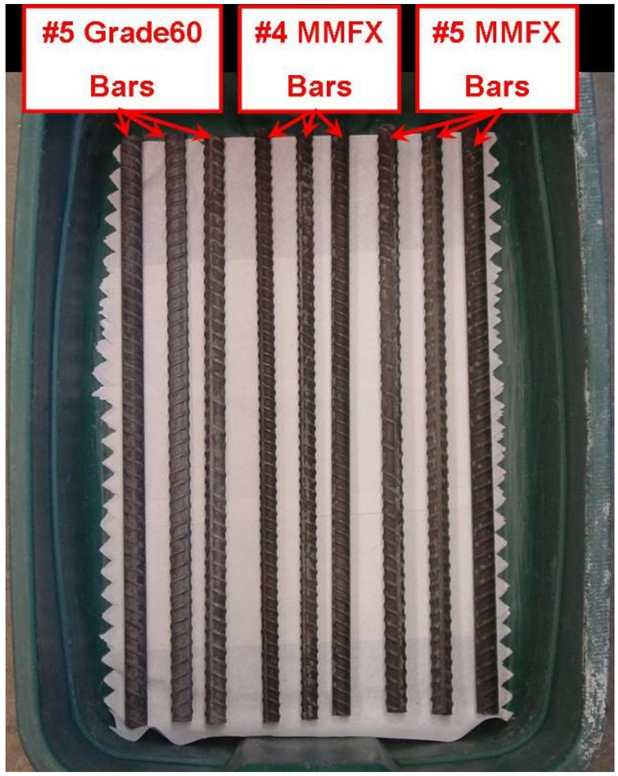

Figure 4.81: Corroded bars after cleaning at 12 weeks

Table 3: Weight of Corroded bars after 12 weeks (6 wet-dry cycles)

Bar	Steel	Bar Size	Weight (lbs)				Weight Loss (%)	Average Weight Loss (%)
			Original	First Cycle	Second Cycle	Third Cycle		
1	MMFX	#4 (No. 13)	0.9945	0.9825	0.9820	0.9820	1.26	1.30
2			0.9885	0.9765	0.9760	0.9755	1.32	
3			0.9835	0.9715	0.9710	0.9705	1.32	
1		#5 (No. 16)	1.5105	1.5000	1.4995	1.4990	0.76	0.75
2			1.5220	1.5115	1.5110	1.5105	0.76	
3			1.5220	1.5120	1.5110	1.5110	0.72	
1	Grade 60	#5 (No. 16)	1.5090	1.4795	1.4790	1.4790	1.99	2.04
2			1.5055	1.4750	1.4745	1.4740	2.09	
3			1.4995	1.4700	1.4690	1.4690	2.03	

Figure 4.82: Pits on the surface of #4 (No. 13) MMFX corroded bars at 12 weeks

Figure 4.83: Pits on the surface of #5 (No. 16) MMFX corroded bars at 12 weeks

Figure 4.84: Pits on the surface of #5 (No. 16) Grade 60 corroded bars at 12 weeks

Figure 4.85, Figure 4.86, and Figure 4.87 show the stress-strain characteristics of the corroded #4 (No. 13) and #5 (No. 16) MMFX steel bars, and #5 (No. 16) Grade 60 steel bars, respectively, after 12 weeks (6 wet-dry cycles) of exposure. The results demonstrate the effect of corrosion on the tensile strength and the stress-strain relationship. It should be noted that the removal of the extensometer is not due to rupture of the specimen, but is due to the formation of the neck outside the extensometer 2-in. gage length. The stress-strain relationship for the corroded bars indicates that still there is no effect of corrosion on the tensile strength of #4 (No. 13) and #5 (No. 16) MMFX bars, and #5 (No. 16) Grade 60 steel bars after 12 weeks (6 wet-dry cycles) of immersion in 15% salt-water solution. However, this conclusion can not be extended to longer periods of testing. Testing after 26 and 52 weeks (13 and 26 wet-dry cycles) will critically examine this conclusion.

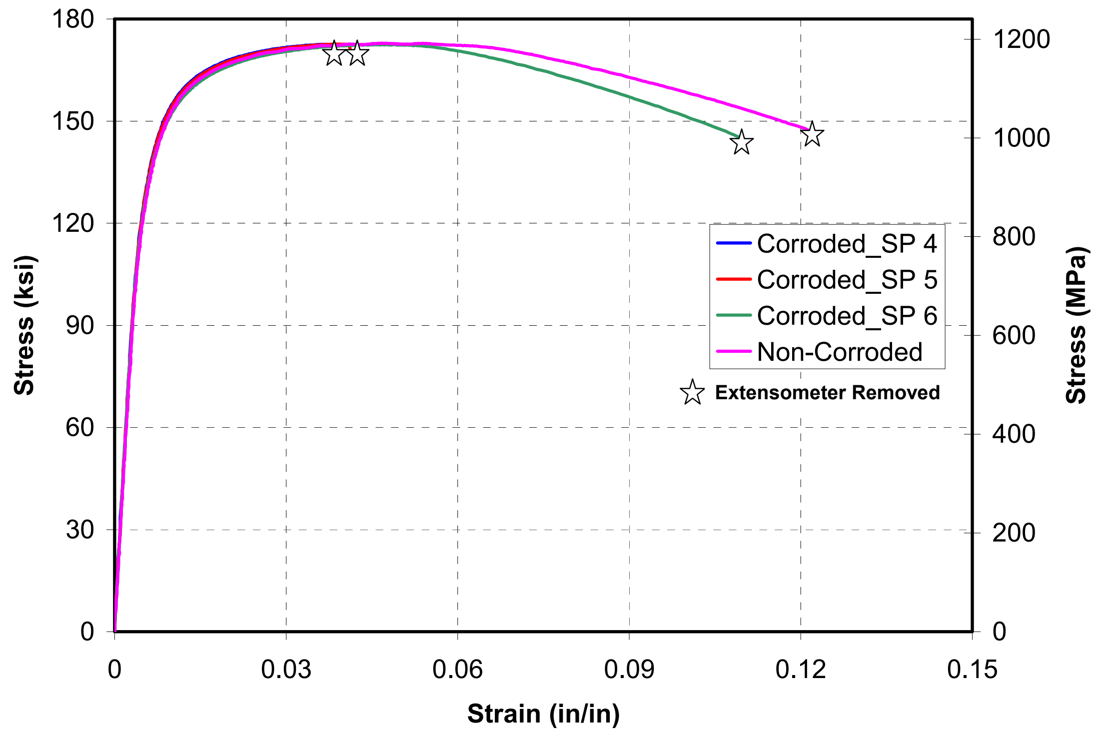

Figure 4.85: Stress-Strain relationship for #4 (No. 13) MMFX corroded bars at 12 weeks

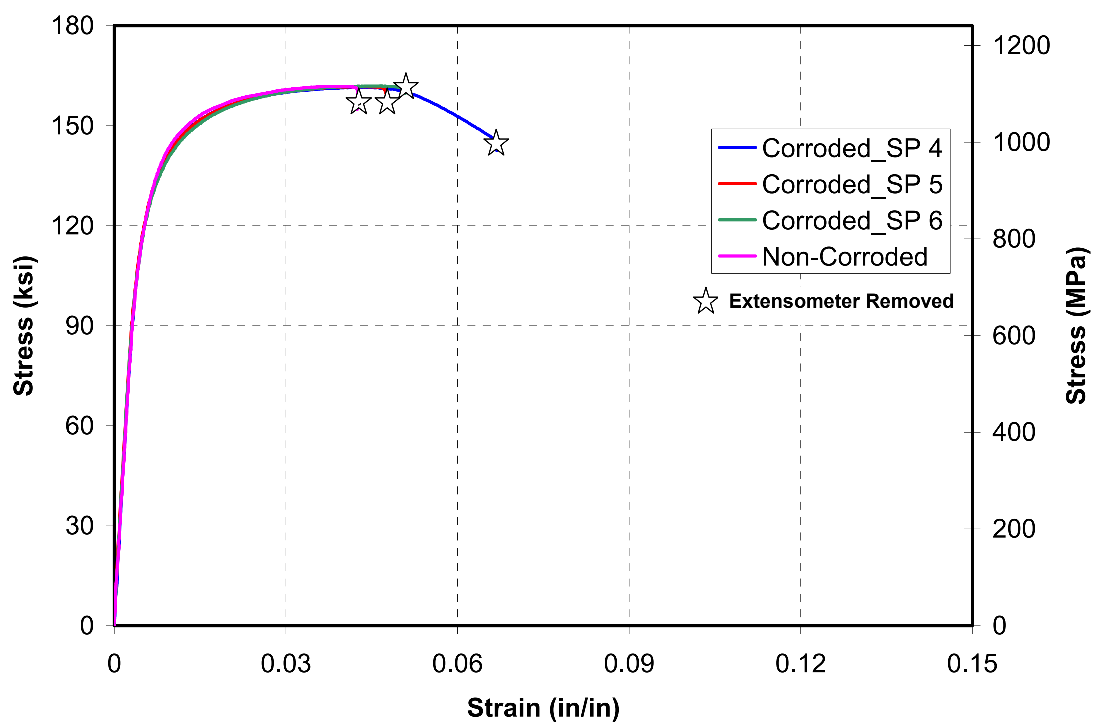

Figure 4.86: Stress-Strain relationship for #5 (No. 16) MMFX corroded bars at 12 weeks

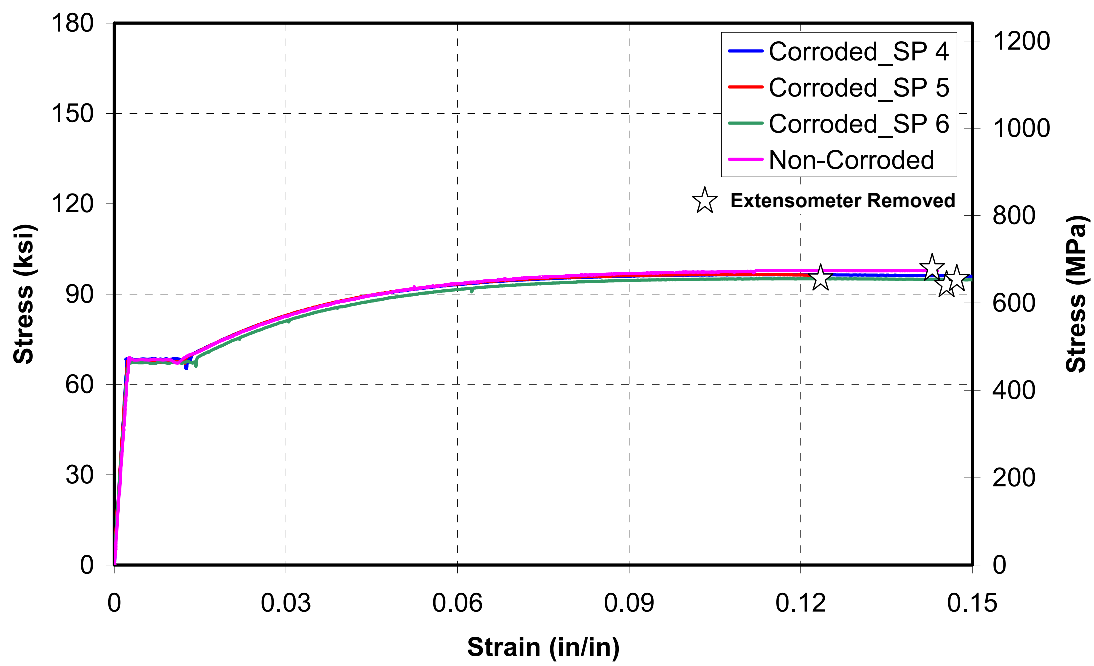

Figure 4.87: Stress-Strain relationship for #5 (No. 16) Grade 60 corroded bars at 12 weeks

- *Results after 26 Weeks (13 Wet-Dry Cycles)*

After completing 26 weeks (13 wet-dry cycles) of test on May 3rd, 2006 another three specimens of each bar diameter were removed and cleaned as discussed earlier. Figure 4.88 and Figure 4.89 show the specimens before and after cleaning, respectively. The obtained results after 26 weeks of exposure are summarized in Table 4. Despite the low values of the weight loss obtained after 26 weeks, the results firmly confirm the conclusion that MMFX steel has a much lower corrosion rate compared to conventional Grade 60 steel. Directly comparing the average weight loss of #5 MMFX and Grade 60 steel shown in Table 4, yields that corrosion rate of Grade 60 is five times that of MMFX steel.

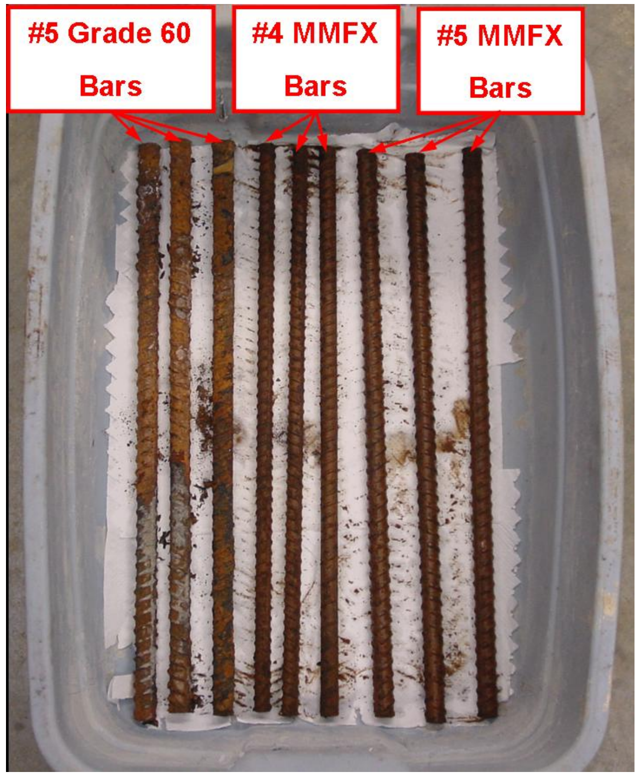

Figure 4.88: Corroded bars before cleaning at 26 weeks

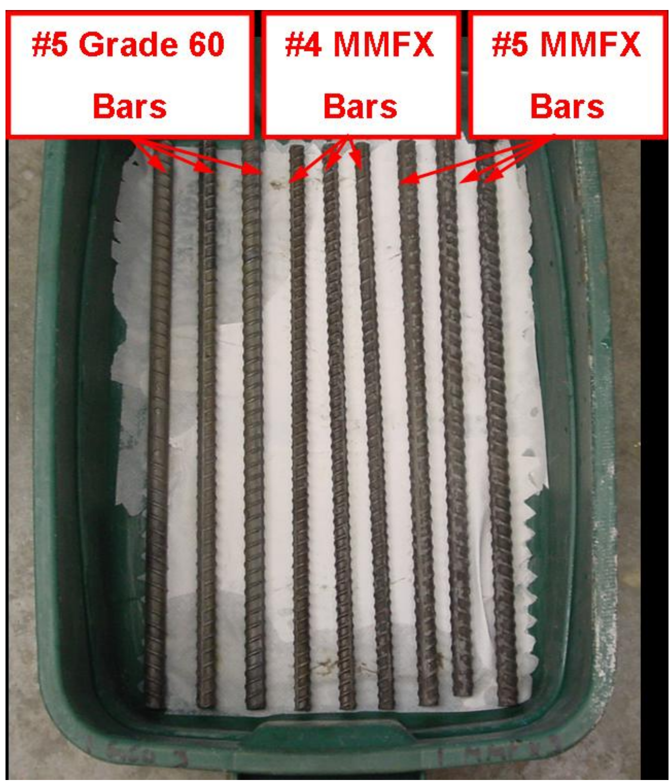

Figure 4.89: Corroded bars after cleaning at 26 weeks

Table 4: Weight of Corroded bars after 26 weeks (13 wet-dry cycles)

Bar	Steel	Bar Size	Weight (lbs)				Weight Loss (%)	Average Weight Loss (%)
			Original	First Cycle	Second Cycle	Third Cycle		
1	MMFX	#4 (No. 13)	0.9780	0.9635	0.9620	0.9620	1.64	1.62
2			0.9795	0.9645	0.9640	0.9640	1.58	
3			0.9795	0.9645	0.9640	0.9635	1.63	
1		#5 (No. 16)	1.5075	1.4920	1.4915	1.4915	1.06	1.11
2			1.5145	1.4965	1.4955	1.4950	1.29	
3			1.5180	1.5045	1.5040	1.5040	0.99	
1	Grade 60	#5 (No. 16)	1.5090	1.4270	1.4255	1.4250	5.57	5.61
2			1.5080	1.4250	1.4235	1.4230	5.64	
3			1.5115	1.4280	1.4265	1.4265	5.62	

Figure 4.90, Figure 4.91, and Figure 4.92, show the stress-strain characteristics of the corroded #4 (No. 13) and #5 (No. 16) MMFX steel bars, and #5 (No. 16) Grade 60 steel bars, respectively, after completing 26 weeks (13 wet-dry cycles) of exposure. The results demonstrate the effect of corrosion on the tensile strength and the stress-strain relationship. It should be noted that the removal of the extensometer is not due to rupture of the specimen, but is due to the formation of the neck outside the extensometer gage length. The stress-strain relationship for the corroded bars indicates that there is slight effect of corrosion on the tensile strength of #4 (No. 13) and #5 (No. 16) MMFX bars, and #5 (No. 16) Grade 60 steel bars after 26 weeks (12 wet-dry cycles) of immersion in the salt-water solution. Testing after 52 weeks (26 wet-dry cycles) should reflect significant effect on the tensile strength due to corrosion.

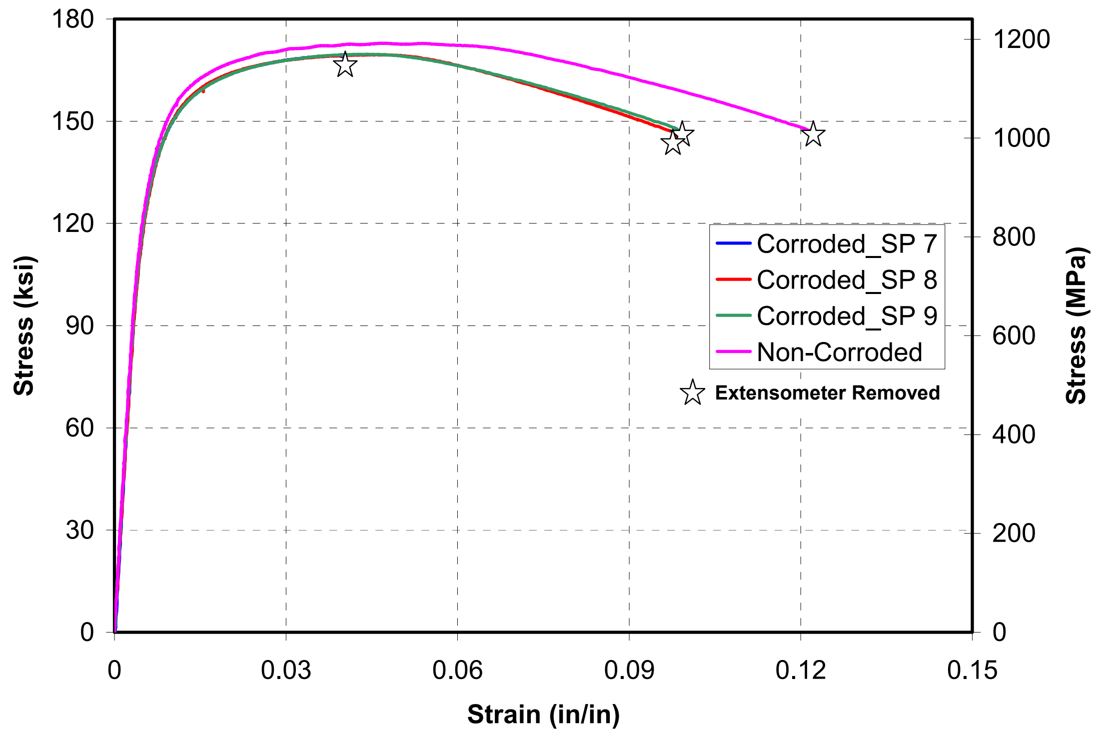

Figure 4.90: Stress-Strain relationship for #4 (No. 13) MMFX corroded bars at 26 weeks

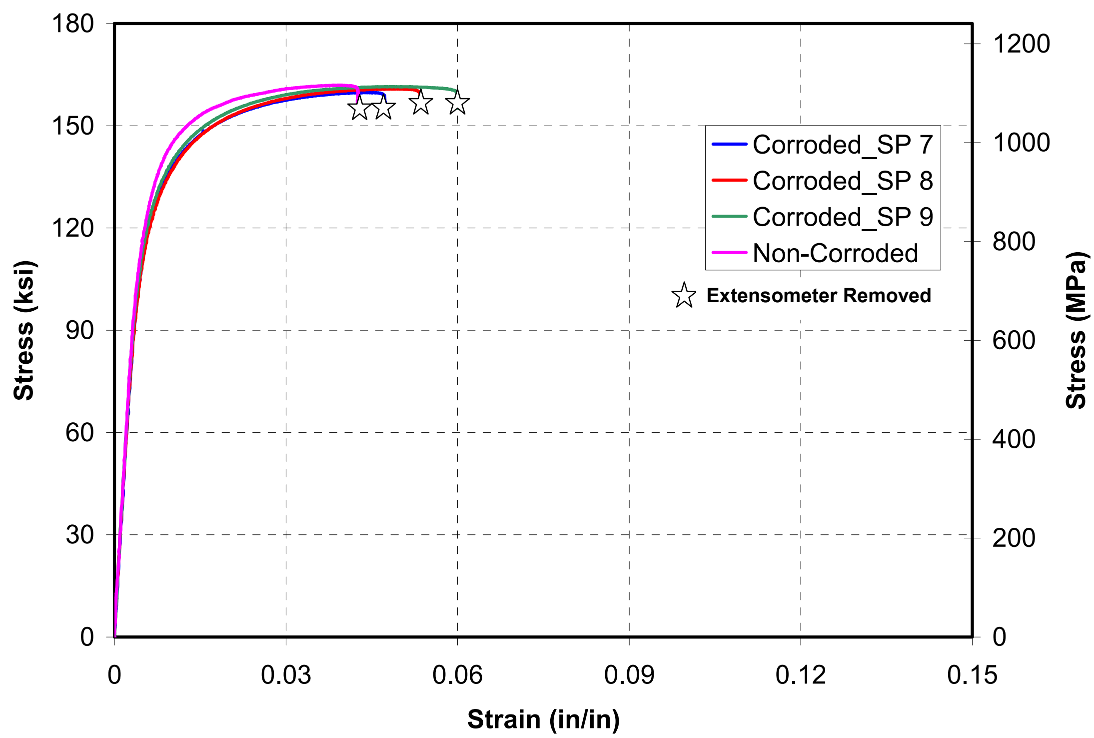

Figure 4.91: Stress-Strain relationship for #5 (No. 16) MMFX corroded bars at 26 weeks

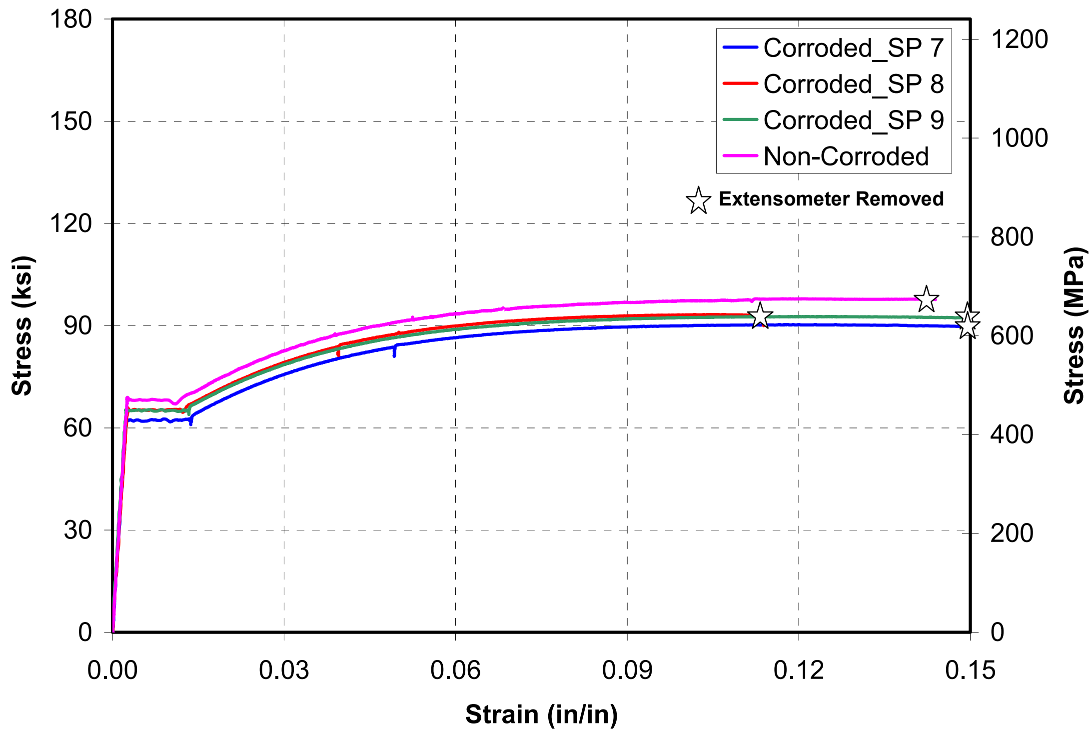

Figure 4.92: Stress-Strain relationship for #5 (No. 16) Grade 60 corroded bars at 26 weeks

5. ANALYTICAL MODELING

Finite element analysis (FEA) is one of the advanced and powerful computing techniques that can be used to predict the non-linear behavior of structures. However, it is imperative to investigate structural performance, experimental testing and analytical modeling be integrated in order to develop a deeper understanding of the inelastic structural behavior. Therefore, the experimental testing conducted in this study was deployed to verify and calibrate the analytical models developed.

5.1. General

The three bridge decks were modeled using the finite element analysis program "ANACAP" (Anatech Concrete Analysis Program) Version 3.0 (James 2004). The program can model 2D, axisymmetric, and 3D geometries and conducts static or dynamic analyses as well as failure analysis of reinforced and prestressed concrete structures. The concrete material model is based on smeared cracking methodology developed by Rashid (1960). Within the concrete constitutive model, cracking and all other forms of material non-linearity are treated at the finite element integration points. Cracks are assumed to form perpendicular to the principal tensile strain direction in which the criterion is exceeded and they are allowed to from at each material point. When cracking occurs, the normal stress across the crack is reduced to zero and distribution of stresses around the crack is recalculated. Cracks close or re-open under load cycles. Concrete modeling also included residual tension stiffness for the gradual transfer of load to the reinforcement during crack formation. In addition, the program accounts for the reduction in shear stiffness due to cracking and further decay as the crack opens. The reinforcement is modeled as individual sub-elements within the concrete elements. The stiffness of the bar sub-element is superimposed on the concrete element stiffness in which the bar resides. The anchorage loss is modeled as an effective stiffness degradation of the bar as a function of the concrete strain normal to the bar.

A 3-D analysis was conducted for the three bridge decks using 20-node hexahedral continuum elements. Only one quarter of the deck was modeled due to symmetry of geometry and loads about both axes. A convergence study was conducted including the mesh size (number and size of elements) and load increments. The depth of the deck was divided into five layers within its thickness with a total number of elements of 1040 for the deck and supporting beams, as shown in Figure 5.1.

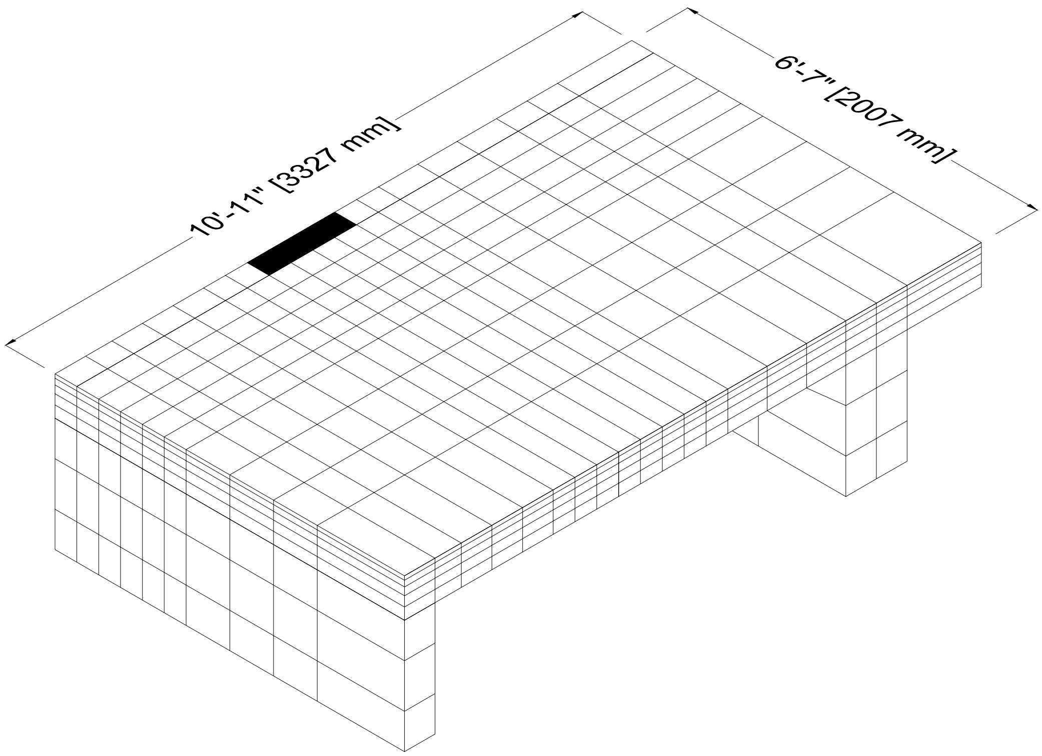

Figure 5.1: Mesh used for analytical model

5.2. Analytical Results

The predicted and experimental load-deflection curves for the three bridge decks are compared in Figure 5.2 through Figure 5.4, respectively. It can be seen that the predicted load-deflection behaviors of the three bridge decks compared very well to the measured values. The initial and post-cracking stiffnesses were very accurately predicted by the analytical model. In addition, the ultimate load was reasonably predicted considering the fact that the two spans of the second and third bridge decks failed in two different modes. However, the predicted ultimate deflection was slightly less than the experimental values; this is due to the nature of the smeared cracking methodology adopted by the program. For validation purposes, the contours of the principal strain at failure and the portion of the first bridge deck that failed due to punching failure are shown in Figure 5.5. The strain contours depict the punching shear cone that matches very well the observed shear cone at failure.

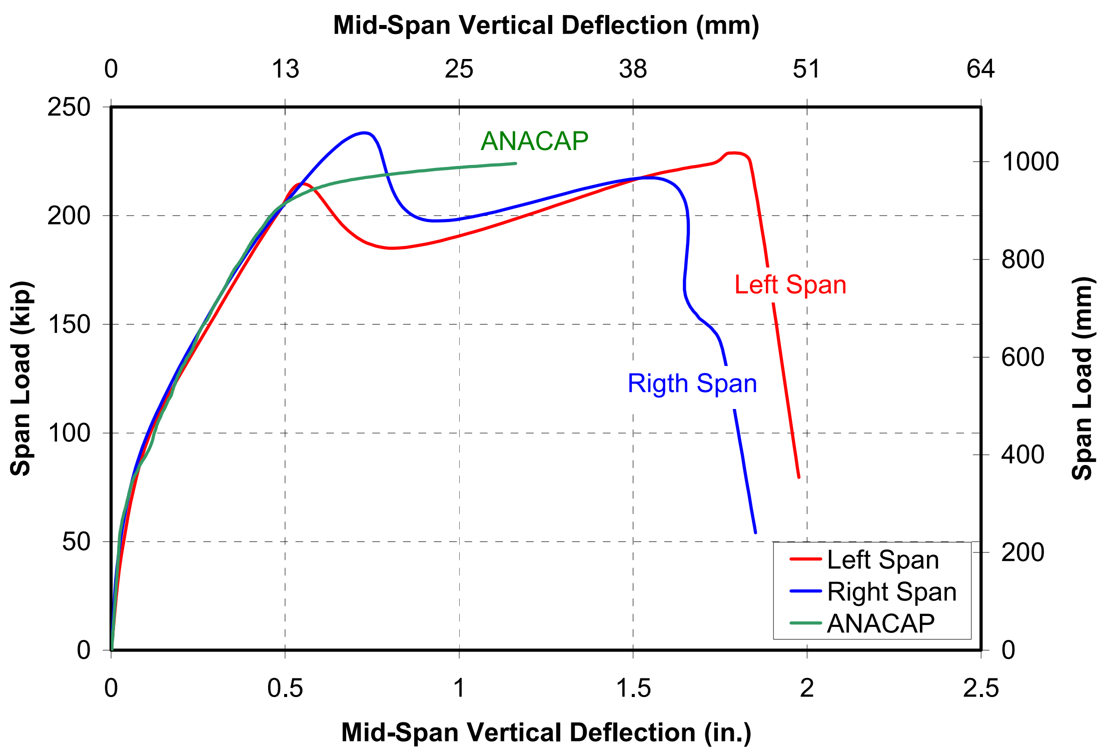

Figure 5.2: First bridge deck analytical and experimental load-deflection envelopes

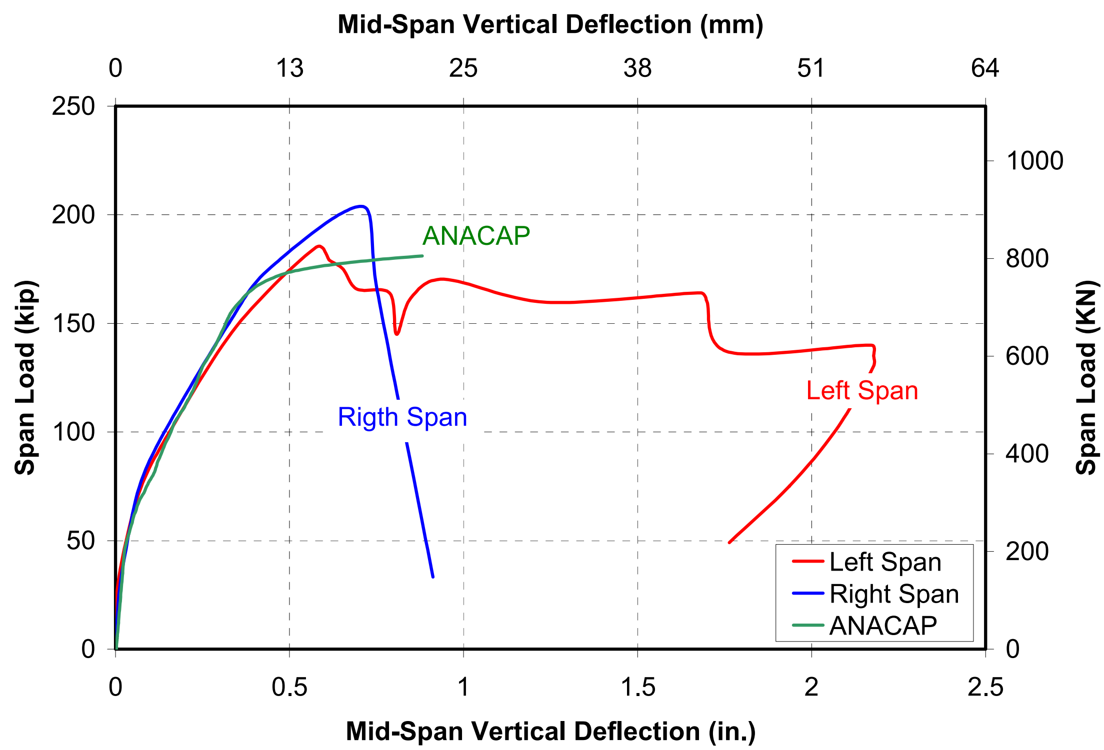

Figure 5.3: Second bridge deck analytical and experimental load-deflection envelope

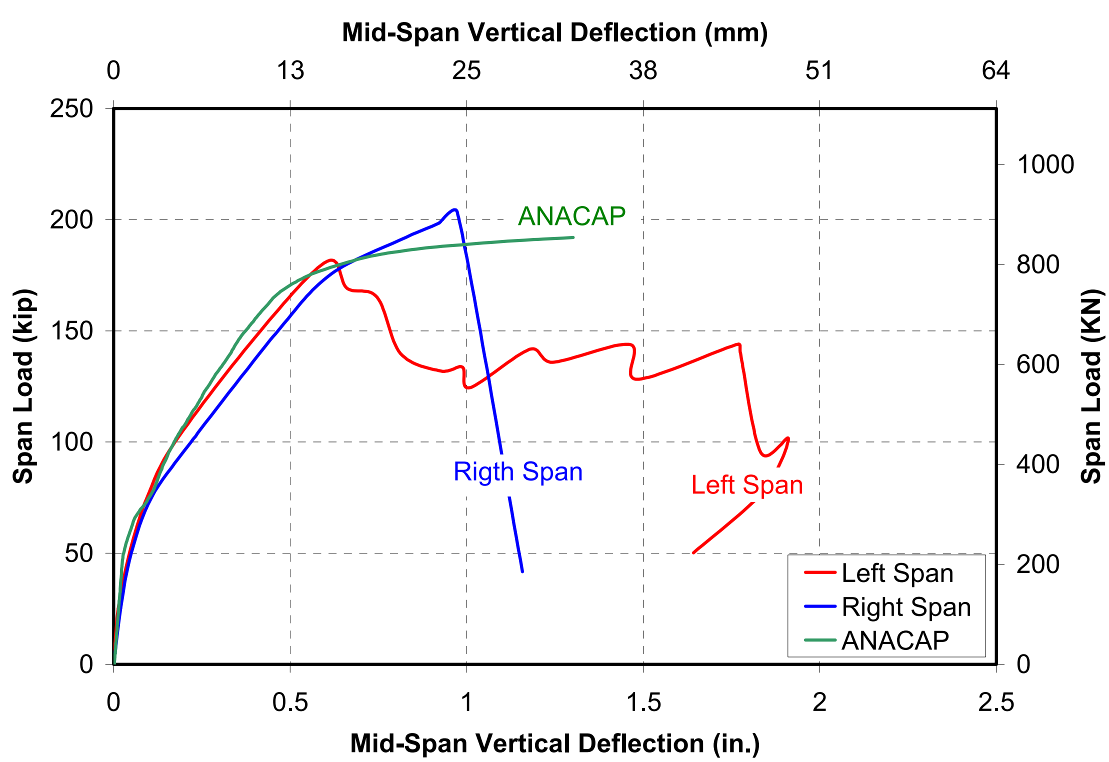

Figure 5.4: Third bridge deck analytical and experimental load-deflection envelopes

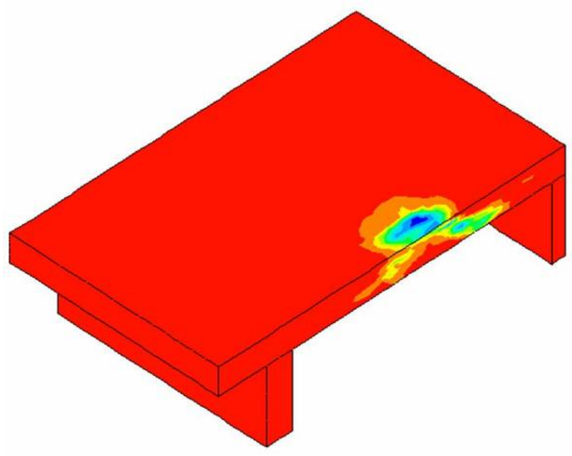

(a) ANACAP **(b) Experimental**

Figure 5.5: Principal strains contours at failure for the first bridge deck

6. FINDINGS, CONCLUSIONS, AND RECOMMENDATIONS

The potential use of MMFX steel for concrete bridge decks was demonstrated by the behavior of full-scale bridge decks continuously supported by three girders. The Micro-Composite Multi-Structural Formable steel, commercially known as MMFX steel, offers greatly enhanced corrosion-resistance and significantly higher strength when compared to conventional Grade 60 steel. The aim of the research was to evaluate the behavior of cast-in-place reinforced concrete bridge decks at different limit states including the mode of failure. The results demonstrate that the use of MMFX steel has the potential to enhance the service lives of newly constructed concrete decks due to its lower corrosion rate compared to conventional Grade 60 steel and reserved high strength. Results from this experimental program recommend effective use of MMFX steel by utilizing its high tensile strength which leads to significant reduction of the reinforcement ratio to achieve same serviceability and strength. Reduction of the reinforcing steel will alleviate reinforcement congestion, and improve concrete placement. In addition, the study confirmed that MMFX steel bars can be bent up to 90 degrees without affecting their ultimate strength given that the bent bars are bonded to the concrete.

The cost effectiveness of using MMFX steel versus conventional Grade 60 was investigated. The typical market cost of conventional Grade 60 steel is in the range of $0.35-0.40/lb and the cost of MMFX steel is $0.60/lb. Based on the research finding and the recommendation of this study to use a yield strength of 90 ksi, the amount of MMFX steel can be reduced by 33% than that required for Grade 60 steel. Therefore, the higher cost of MMFX steel can be compensated by the reduction of the amount of steel required. It should be noted that the prices are obtained from local suppliers in the Raleigh, NC area. In light of this comparison, it is evident that MMFX can be used without any additional cost in comparison to conventional Grade 60 steel considering the advantage of enhanced corrosion resistance, which would result in longer service life of a bridge and lower repair costs.

6.1. Findings

The findings of the research program presented in this report are summarized as follows:

1. The MMFX reinforcing bars exhibited a linear stress-strain relationship up to 100 ksi (689 MPa). This was followed by a nonlinear behavior up to an ultimate strength of approximately 173 ksi (1193 MPa). According to ASTM-A370 offset method (0.2% offset), the yield strength was determined to be 120 ksi (827 MPa). The initial modulus of elasticity was determined to be 29,000 ksi (200 GPa).

2. The ultimate load-carrying capacities of all three bridge decks investigated in this study were at least ten times the service load specified by the AASHTO Design Specifications (2004).

3. Punching shear was the primary mode of failure for all three of the bridge decks that were tested. Flexural-shear failure was observed as a secondary mode of failure.

4. Punching shear failure resulted in a sudden decrease of the load-carrying capacity, while flexural-shear failure resulted in gradual decrease of the load-carrying capacity.

5. The two bridge decks reinforced with MMFX steel exhibited the same deflections at service load as the deck reinforced with Grade 60 steel.

6. For the two bridge decks having the same reinforcement ratio, the bridge deck reinforced with MMFX steel developed more load-carrying capacity than the bridge deck reinforced with Grade 60 steel.

7. The bridge deck reinforced with 33-percent less MMFX steel developed the same ultimate load-carrying capacity as did the deck reinforced with Grade 60 steel.

This result is attributed to the higher tensile strength characteristics of MMFX steel.

8. The bridge deck reinforced with 33-percent less MMFX steel exhibited the same deflections at service load as did the deck reinforced with Grade 60 steel. These two decks also exhibited nearly identical ductility, as evidenced by their closely matching load-deflection plots.

9. The AASHTO and ACI codes can very accurately predict the shear strength of bridge decks reinforced with MMFX steel as well as Grade 60 steel.

10. Behavior of bonded bent MMFX bars is similar to straight bars including the linear and the non-linear behavior. Un-bonded bent MMFX bars have similar behavior up to strain of 1.5 percent; however, the ultimate strength and strain at failure are reduced by 6 and 70, respectively. This finding is important for the use of MMFX steel as lifting hooks. The bonded bent MMFX bars developed the same strength and strain at ultimate to those of straight bars.

11. Test results after 6, 12, and 26 weeks (3, 6, and 13 wet-dry cycles) indicate that MMFX steel has a much lower corrosion rate compared to conventional Grade 60 steel. Test results of tension tests indicate slight reduction of the tensile strength of MMFX and Grade 60 steel after 26 weeks of immersion in the salt-water solution. Test results after completion of the 52 weeks of exposure will be reported independently from this report.

6.2. Conclusions

Based on the research findings, the essence of this study can be concluded as follows:

1. Substituting MMFX steel directly for Grade 60 steel in a design, the case for the Johnston County Bridge, is an overly-conservative approach.

2. MMFX steel can be used as the main flexural reinforcement for cast-in-place concrete bridge decks at a reinforcement ratio corresponding to 33% less than that required for Grade 60 steel. Therefore, a design of reinforced concrete bridge decks using MMFX steel may utilize an equivalent yield stress of 90 ksi for the MMFX steel bars.

3. Design of concrete bridge decks utilizing the high tensile strength characteristics of the MMFX steel should satisfy all minimum reinforcement ratios required by the AASHTO LRFD Bridge Design Specifications as well as the serviceability requirements of the specifications.

4. MMFX steel has a much lower corrosion rate compared to conventional Grade 60 steel. Therefore, the use of MMFX steel could increase the service life of concrete bridges and lower repair costs.

5. Since the proportional limit of MMFX steel is 100 ksi (689 MPa), the potential exists to further reduce reinforcement ratios by increasing allowable design stresses to 100 ksi (689 MPa) or more. Further studies would be necessary to investigate this possibility.

6. MMFX steel bars can be bent up to 90 degrees without reducing its ultimate strength provided that the bend is fully bonded to the concrete.

6.3. Recommendations

The study recommends the following design guidelines for the North Carolina Department of Transportation (NCDOT):

1. MMFX steel can be used as flexural reinforcement for reinforced concrete bridge decks.

2. Design of bridge decks using MMFX steel as main flexural reinforcement should use a yield strength of 90 ksi (621 MPa) without impairing their ultimate load-carrying capacity.

3. Reduced MMFX reinforcement ratio must comply with all serviceability requirement specified by AASHTO LRFD Bridge Design Specifications.

4. MMFX steel bars can be bent up to 90 degrees without reducing their ultimate strength.

7. IMPLEMENTATION AND TECHNOLOGY TRANSFER PLAN

The research team is willing to offer a workshop to the bridge department at North Carolina Department of Transportation (NCDOT) for the design of concrete bridge decks using MMFX steel. The workshop is expected to be organized by NCDOT.

A technical paper entitled "Design Guidelines for Concrete Beams Reinforced with MMFX Microcomposite Reinforcing Bars" has been presented at "Housing and Building Research Center, Cairo, Egypt" and published in the proceedings of "International Conference of Future Vision and Challenges for Urban Development, December 2004". A copy of the abstract is given in Appendix A.

A technical paper entitled "Performance of Bridge Decks Reinforced with MMFX Steel" has been presented at the 7th International Conference on Short and Medium Span Bridges, Montreal, Canada, August, 2006 and published in the proceedings of the conference. A copy of the abstract is given in Appendix B.

A technical paper entitled "Behavior of Bridge Decks Reinforced with High Strength Steel" has been presented at the 2006 Concrete Bridge Conference, National Concrete Bridge Council, Reno, Nevada, May, 2006. A copy of the abstract is given in Appendix C.

Results of the study were presented to the project steering committee at the close out meeting that we held on May 23, 2006. The comments of the steering committee are included in this version of the report.

This project led to the development of a new idea for future research as listed in NCDOT 2008 research ideas. The new idea requesting proposal is to study the corrosion resistance of MMFX steel bars and compare it to the corrosion resistance of fusion bonded epoxy-coated bars.

8. FIELD APPLICATION: CONSTRUCTION OF JOHNSTON COUNTY BRIDGE

Johnston County Bridge is located over I-95 on SR 1178 interchange at Four Oaks, Johnston County, NC, as shown in the vicinity map given in Figure 8.1 and Figure 8.2. The bridge layout is shown in Figure 8.3 and Figure 8.4 gives a general drawing for the bridge. The bridge is 250'-10" (76450 mm) in total length with concrete deck slab supported in composite action by steel girders as shown in Figure 8.5. Cross-bracing was used on 21 ft (6400 mm) spacing for lateral stability of the steel girders.

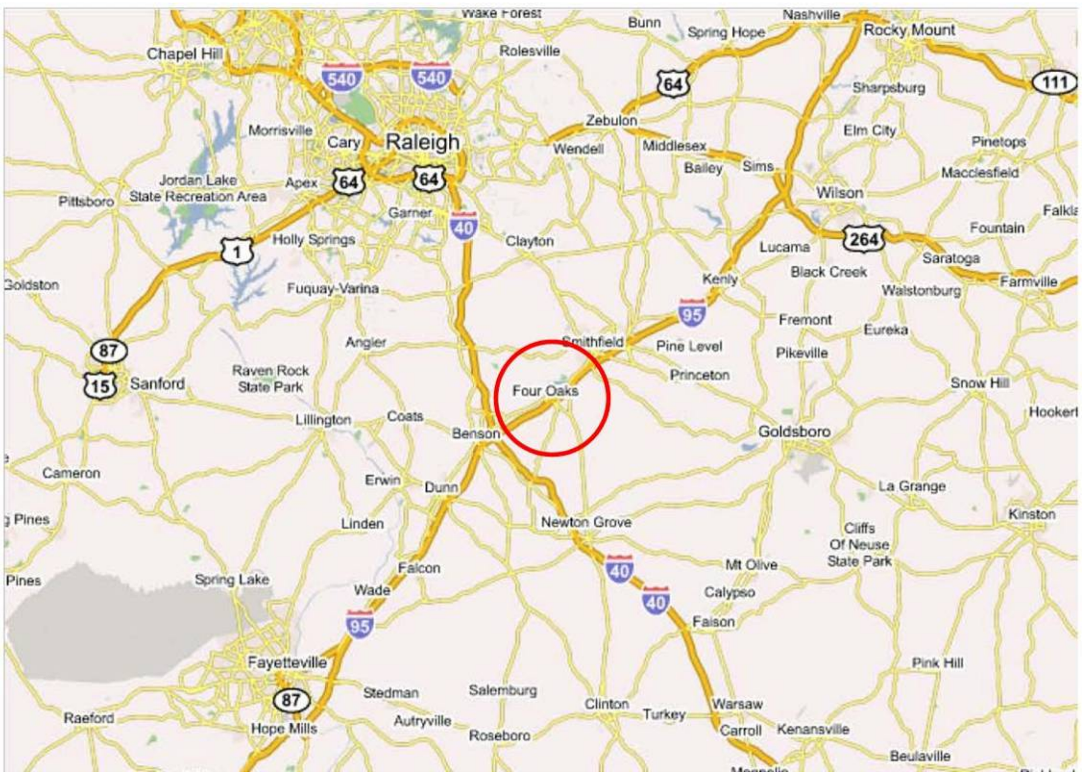

Figure 8.1: Vicinity map of the Johnston County Bridge

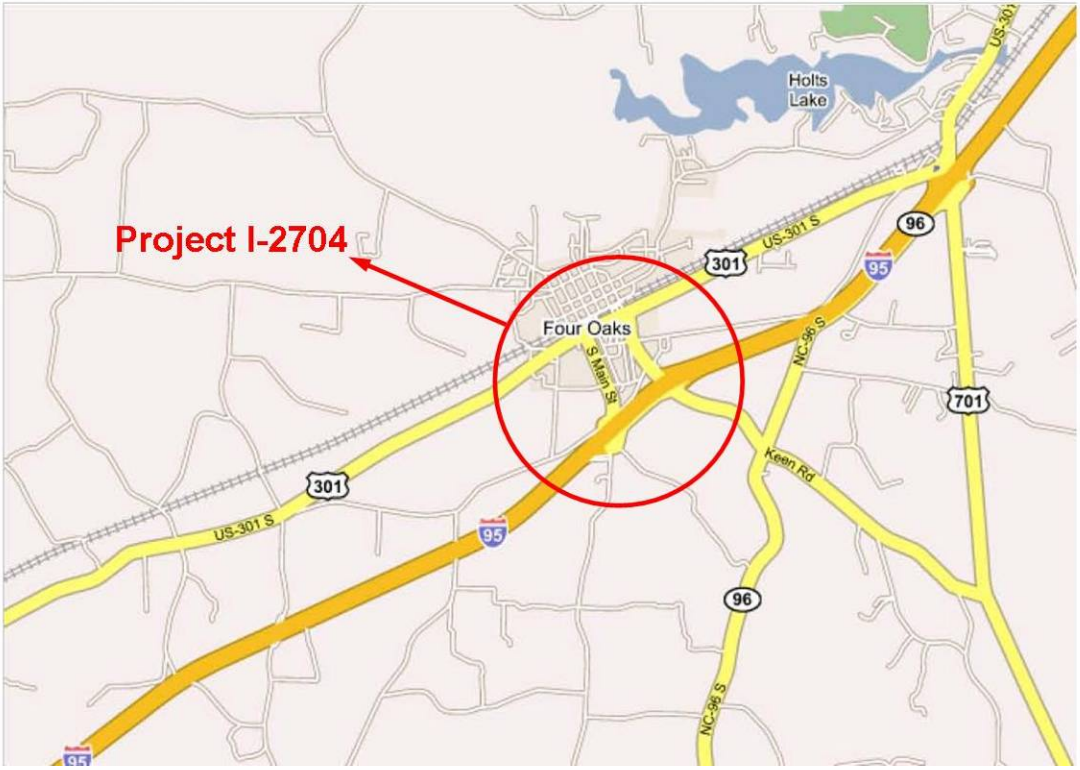

Figure 8.2: Close-up of the vicinity map of Johnston County Bridge

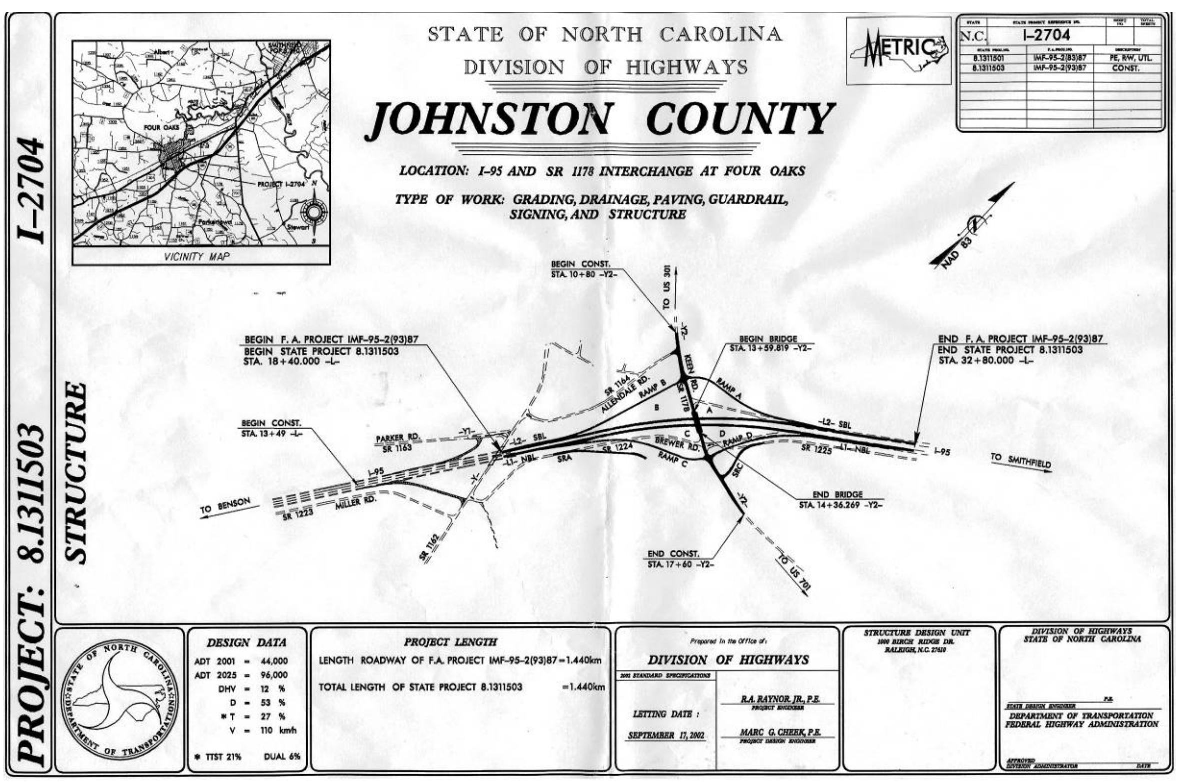

Figure 8.3: General layout for Johnston County Bridge

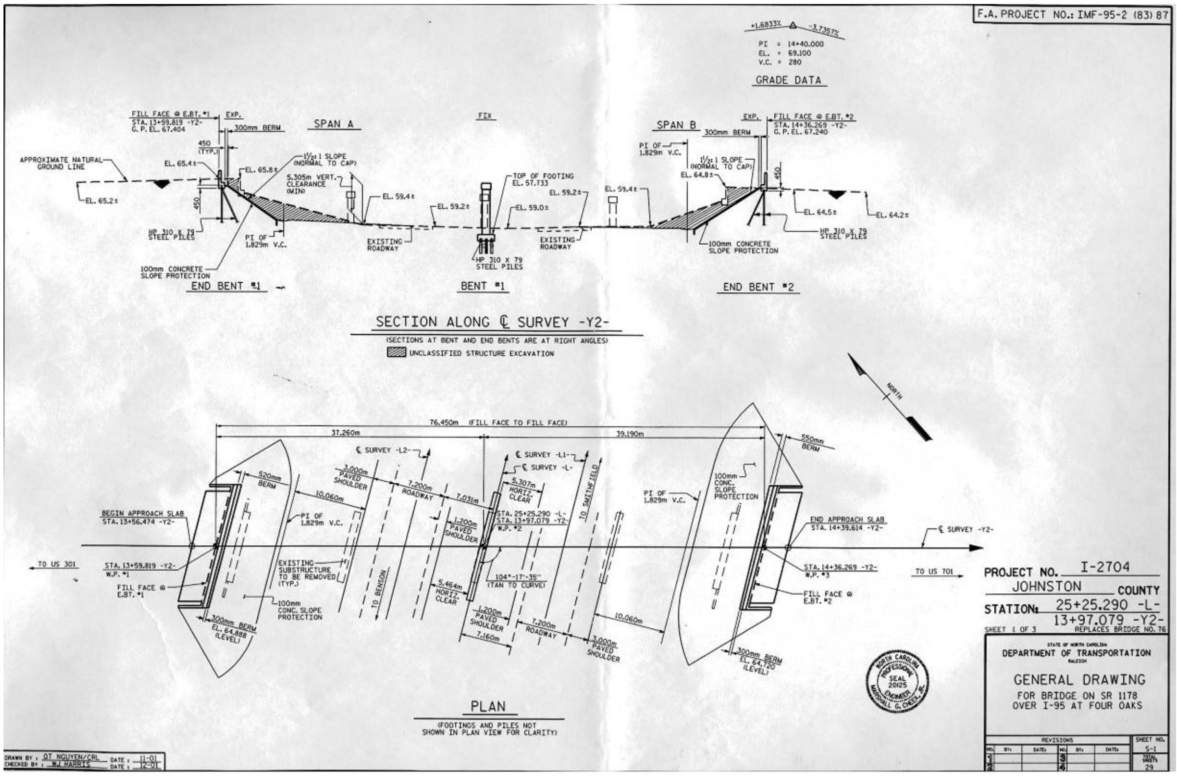

Figure 8.4: General drawing for Johnston County Bridge

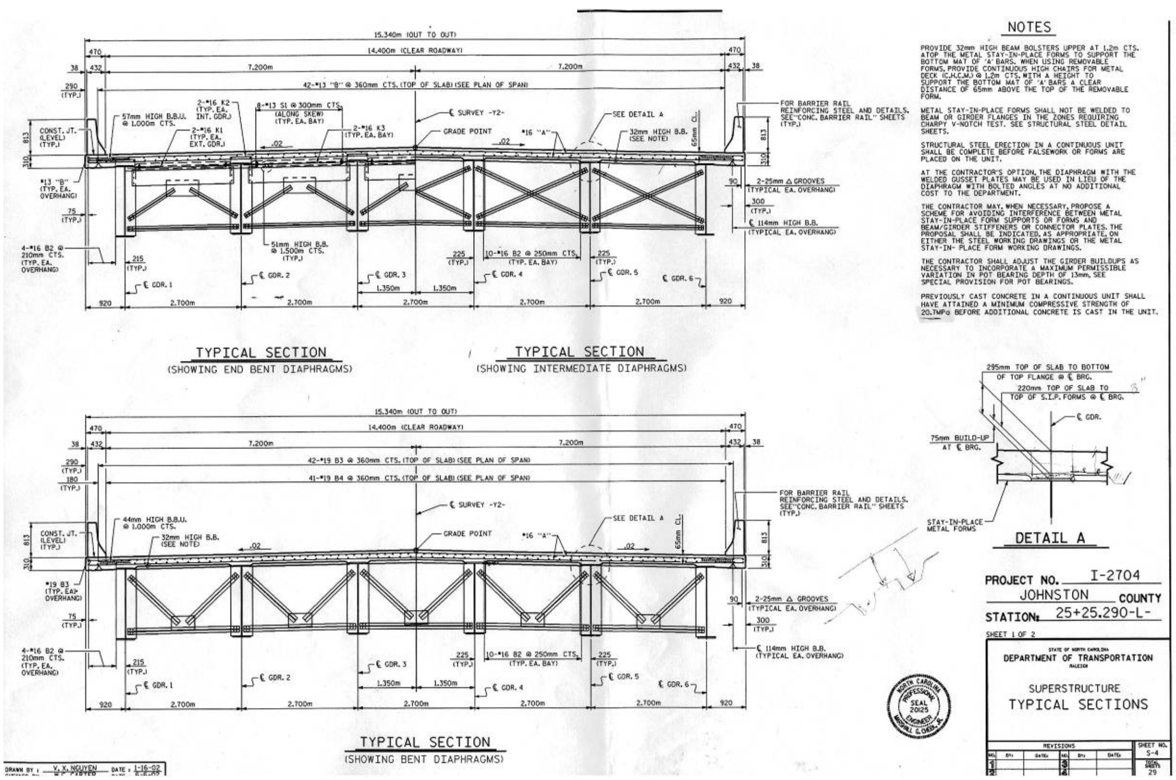

Figure 8.5: Superstructure typical sections for Johnston Country Bridge

The bridge site was visited by the Constructed Facilities Laboratory (CFL) research team to monitor the construction progress. The bridge deck slab reinforced with MMFX steel was cast on August 2005. The following is a brief description of the construction of the bridge according to the site visits dates.

- April 20th: Construction of the abutments and the forms for the double bent piers were completed, as shown in Figure 8.6 and Figure 8.7.
- May 18th: Concrete casting of the double bent bridge piers were completed, Figure 8.8.
- June 17th: Completed erection of the steel girders and the bracing system, as shown in Figure 8.9 and Figure 8.10.
- July 1st: Completed installation of the stay-in-place deck forms, as shown in Figure 8.11. All MMFX steel was shipped to the site, Figure 8.12 shows the engraved mark on the steel at the site.
- July 23rd: Placement of all the MMFX steel bars was completed as shown in Figure 8.13.
- July 27th: Visit by NCDOT and NCSU research team to the construction site prior to casting of the concrete deck, see Figure 8.14.
- August 5th: Casting concrete of the bridge deck started very early in the morning and the casting was completed before noon; see Figure 8.15 and Figure 8.16.

Figure 8.6: East abutment's wall

Figure 8.7: Bridge piers forms

Figure 8.8: Double bent bridge pier

Figure 8.9: Steel girders after erection

Figure 8.10: Transverse cross-bracing

Figure 8.11: Stay-in-place forms after installation

Figure 8.12: Type of reinforcement at the site

Figure 8.13: Bridge deck prior to casting concrete

Figure 8.14: NCDOT and NCSU teams at the bridge site

Figure 8.15: placing deck concrete early in the morning

Figure 8.16: Near the end of concrete placement

REFERENCES

1. American Association of State Highway and Transportation Officials, "AASHTO LRFD Bridge Design Specifications," Washington, D.C, 2004.

2. American Concrete Institute (ACI), "Building Code Requirements for Structural Concrete," ACI 318-05, Farmington Hills, Michigan, 2005.

3. ASTM A 370-03, "Standard Test Methods and Definitions for Mechanical Testing of Steel Products," West Conshohocken, PA, American Society for Testing and Materials, 2003.

4. ASTM G1-03, "Standard Practice for Preparing, Cleaning, and Evaluating Corrosion Test Specimens," West Conshohocken, PA, American Society for Testing and Materials, 2003.

5. CAN/CSA-S6-00, "Canadian Highway Bridge Design Code," Canadian Standard Association, Rexdale, Ontario, Canada, 2000, 706 pp.

6. Cook, A. K., "Evaluation of the Effectiveness of Surface Applied Corrosion Inhibitors for Concrete Bridges," M.Sc. Thesis, Department of Civil, Construction, and Environmental Engineering, North Carolina State University, Raleigh, NC.

7. Concrete Innovations Appraisal Service (CIAS), "High Corrosion Resistance MMFX Micorcomposite Reinforcing Steels," May, 2003, 42 pp.

8. Darwin, D., Browning, J., Nguyen, T. V., and Locke, C. Jr., "Mechanical and Corrosion Properties of a High-Strength, High Chromium Reinforcing Steel for Concrete," Report No. SD2001-05-F, South Dakota Department of Transportation, March 2002, 142 pp.

9. Dilger, W., Birkle, G., and Mitchell, D., “Effect of Flexural Reinforcement on Punching Shear Resistance,” ACI SP-232, 2005, pp. 57-74.

10. El-Hacha, R. and Rizkalla, S. H., “Fundamental Material Properties of MMFX Steel Bars,” Research Report RD-02/04, North Carolina State University, Constructed Facilities Laboratory, Raleigh, North Carolina USA, 2002, 62 pp.

11. Hallagren, M., “Punching Shear Capacity of Reinforced High Strength Concrete Slabs,” Ph.D. Thesis, KTH Stockholm, TRITA-BKN. Bulletin No 23, 1996, 150 pp.

12. Hassan, T., Abdelrahman, A., Tadros, G., and Rizkalla, S., “Fibre Reinforced Polymer Bars for Bridge Decks,” Canadian Journal of Civil Engineering, V. 27, 2000, pp. 839-849.

13. Hon, A., Taplin, G., and Al-Mahaidi, R. S., “Strength of Reinforced Concrete Bridge Decks Under Compressive Membrane Action,” ACI Structural Journal, V. 102, No. 3, May-June 2005 pp. 393-401.

14. Hunkler, F., “Corrosion in Reinforced Concrete: Process and Mechanisms,” Corrosion in Reinforced Concrete Structures, Hans Böhni, Woodhead Publishing Limited, 2005, 248 pp.

15. James, R.G., “ANACAP Concrete Analysis Program Theory Manual,” Version 3.0, Anatech Corporation, San Diego, CA, 2004.

16. Khanna, O. S., Mufti, A. A., and Bakht, B., “Experimental Investigation of the Role of Reinforcement in the Strength of Concrete Deck Slabs,” Canadian Journal of Civil Engineering, V. 27, 2000, pp. 475-480.

17. Kinnunen, S., and Nylander, H., “Punching of Concrete Slabs without Shear Reinforcement,” Transactions of the Royal Institute of Stockholm, Sweden, 1960.

18. Kuang, J. S. and Morely, C. T., “Punching Shear Behavior of Restrained Reinforced Concrete Slabs,” ACI Structural Journal, V. 89, No. 1, January-February 1992, pp. 13-19.

19. Marzouk, H. and Hussein, A., “Punching Shear Analysis of Reinforced High-Strength concrete Slabs,” Canadian Journal of Civil Engineering, V. 18, 1991, pp. 954-963.

20. Marzouk, H. and Hussein, A., “Experimental Investigation on the Behavior of High-Strength Concrete Slabs,” ACI Structural Journal, V. 88, No. 6, November-December 1991, pp. 701-713.

21. MMFX Steel Corporation of America, “MMFX Steel Product Bulletin,” February, 2002.

22. Mufti, A. A., Jaeger, L. G., Bakht, B., and Wegner, L. D., “Experimental Investigation of Fibre-Reinforced Concrete Deck Slabs Without Internal Steel Reinforcement,” Canadian Journal of Civil Engineering, V. 20, 1993, pp. 398-406.

23. Mufti, A. A., and Newhook, J. P., “Punching Shear Strength of Restrained Concrete Bridge Deck slabs,” ACI Structural Journal, V. 95, No. 4, July-August, 1998, pp. 375-381.

24. Mufti, A. A., Bakht, B., and Newhook, J., “Precast Concrete Decks for Slab-on-Girder Systems: A New Approach,” ACI Structural Journal, V. 101, No. 3, 2004, pp. 395-402.

25. Rashid, Y. R., “Ultimate Strength Analysis of Prestressed Concrete Pressure Vessels,” Nuc. Eng & Design, 1960, pp. 334-344.

26. Richart, F. E., “Reinforced concrete Wall and Column Footings, Part 1,” Journal of the American Concrete Institute, V. 45, No. 2, October 1948, pp. 97-127.

27. Richart, F. E., “Reinforced concrete Wall and Column Footings, Part 2,” Journal of the American Concrete Institute, V. 45, No. 2, October 1948, pp. 237-260.

28. Taylor, R. and Hayes, B., “Some Tests on the Effect of Edge Restraint on Punching Shear in Reinforced Concrete Slabs,” Magazine of Concrete Research, V. 17, 1965, pp. 39-44.

29. Thomas, M. “Review of Report SD2001-05-F by Darwin et al. 2002,” Presentation made to South Dakota DOT on June 20, pp. 1-34.

30. Trejo, D., “Evaluation of the Critical Chloride Threshold and Corrosion Rate for Different Steel Reinforcement Types,” Texas Engineering Experimental Station Interim Report, Texas A&M University, College Station, TX, USA, 2002, 38 pp.

31. Vanderbilt, M. D., “Shear Strength of Continuous Plates,” Journal of Structural Division, ASCE, V. 98, No. ST5, May 1972, pp. 961-973.

Appendix A

DESIGN GUIDELINES FOR CONCRETE BEAMS REINFORCED WITH MMFX MICROCOMPOSITE REINFORCING BARS

M. Dawood , H Seliem, Dr. T. Hassan, Dr. S. Rizkalla
Department of Civil, Construction and Environmental Engineering, NCSU
2414 Campus Shore Dr., Raleigh, NC, 27695-7533, USA, Sami_Rizkalla@ncsu.edu

ABSTRACT:

Corrosion of steel reinforcement in concrete structures and bridges is a major problem facing the departments of transportation worldwide. In the United States, maintenance and replacement costs are measured in billions of dollars. Salt environment in hot climate and the use of deicing salts in cold regions have resulted in steady deterioration of bridge decks due to corrosion. These concerns have initiated continual development of protective measures including the use of corrosion-resistant MMFX Microcomposite reinforcing bars.

This paper provides design guidelines for the use of MMFX steel as flexural reinforcement for concrete beams and slabs. The behavior of concrete beams reinforced with MMFX reinforcing bars is evaluated and characterized using cracked section analysis. Principles used for the design of MMFX-reinforced concrete beams are discussed. The behavior of concrete beams reinforced with MMFX is compared to the behavior of the beams reinforced with conventional Grade 60 steel. Using the principles of equilibrium and compatibility, the effect of reinforcement ratio on the strength of concrete beams reinforced with MMFX is examined. The ductility of concrete sections reinforced with MMFX steel throughout the entire loading range is evaluated and design limits for tension and compression controlled failure modes are proposed. In addition to the concrete bridges constructed recently using MMFX steel, this paper discusses the construction procedures of a new bridge at North Carolina where the concrete deck is totally reinforced with MMFX steel.

APPENDIX B

International Conference on Short and Medium Span Bridges, Montreal, Canada, August 23-25, 2006

Performance of Bridge Decks Reinforced with MMFX Steel

Hatem Seliem, Gregory Lucier, Sami Rizkalla, and Paul Zia

Constructed Facilities Laboratory

Department of Civil, Construction, and Environmental Engineering

North Carolina State University

2414 Campus Shore DR., Raleigh, NC, 27695-7533, USA, sami_rizkalla@ncsu.edu

Theme: Advanced Materials in Bridges

Keywords: Bridge, Bridge deck, Concrete, Corrosion-resistant, MMFX, Strength

Abstract

Corrosion of steel reinforcement is undoubtedly a leading cause for deterioration of concrete bridges. Many technologies have been developed in an effort to control this problem including corrosion-resistant steel.

The new, commercially available, Microcomposite Multistructural Formable (MMFX) steel is corrosion-resistant steel that offers a promising alternative to conventional steel without the use of coating technologies. In addition, the control of MMFX steel's morphology of its microstructure has resulted in higher strength. Use of the new steel could lead to potential savings through lower reinforcement ratios and longer service life due to its high corrosion resistance. Recently MMFX steel has been utilized by several state transportation departments as reinforcement in concrete bridge decks. Therefore, there is a need for more information on the performance of bridge decks constructed with this novel type of steel.

This paper describes an experimental program of three full-scale bridge decks tested to failure. The structural performance of MMFX as main flexural reinforcement is evaluated. The three decks are identical in all aspects except for the type and amount of steel used. Each deck consists of two spans and two cantilevers, supported in composite action by three post-tensioned concrete girders. The overall nominal dimensions of the bridge decks are 6600 x 4000 x 220 mm. The first and second bridge decks, having a top and bottom reinforcement ratio of 0.54 percent, are reinforced with MMFX and conventional steel, respectively. The third bridge deck is reinforced with MMFX, having a reinforcement ratio 33.3 percent less than that of the first two decks.

This paper discusses test results along with the general behavior of the bridge decks, including the failure mode in each case. Test results are compared to analytical results

APPENDIX C

National Concrete Bridge Council, 2006 Concrete Bridge Conference, Reno, Nevada, May 7-9, 2006

Behavior of Bridge Decks Reinforced with High Strength Steel

H. Seliem, G. Lucier, S. Rizkalla, and P. Zia

Constructed Facilities Laboratory

Department of Civil, Construction, and Environmental Engineering

North Carolina State University

ABSTRACT

Corrosion of steel reinforcement is one of the primary causes for deterioration of concrete bridges. Various technologies have been developed to mitigate this problem. Such technologies include cathodic protection systems, chemical corrosion inhibitors, high-performance concretes, epoxy coated rebars, and non-metallic reinforcement.

The commercially available Microcomposite Multistructural Formable (MMFX) steel has a higher strength in addition to its higher corrosion resistance in comparison to conventional steel without the use of coating materials. Potential savings could be achieved with MMFX steel through using lower reinforcement ratio due to its higher strength and longer service life because of its improved corrosion resistance. Many state transportation departments have begun to use MMFX steel for reinforcing bridge decks. However, there is insufficient information about the behavior of such concrete bridge decks utilizing MMFX steel as reinforcement.

This paper describes an investigation of three full-scale bridge decks to evaluate the performance of MMFX steel as main flexural reinforcement. The three bridge decks are identical in all aspects except the type and amount of steel used. The bridge decks consist of two spans and two cantilevers, supported in composite action by three post-tensioned concrete girders. The overall nominal dimensions of the bridge decks are 6600 x 4000 x 220 mm. The first and second bridge decks, having a top and bottom reinforcement ratio of 0.54 percent, are reinforced with MMFX and conventional steel, respectively. The third bridge deck is reinforced with MMFX steel, having a reinforcement ratio 33 percent less than that of the first two decks to utilize the higher tensile strength characteristic of the steel.

The test results and the behavior of the bridge decks using the three reinforcement configurations, including the failure mode in each case are discussed. A comparison is made between flexural, arch action, and punching shear mechanisms for bridge decks. The test results are also compared to analytical results based on the finite element analysis program, "ANACAP" (Anatech Concrete Analysis Program version 3.0, 2004). Finally design guidelines for using MMFX steel as reinforcement for bridge decks are proposed.